Process Intensification in Removal of Pollutants from Waste Water

Thesis submitted by

Anup Pralhadrao Pardey

Doctor of Philosophy

(Engineering)

Chemical Engineering Department

Faculty of Engineering and Technology

Jadavpur University

Kolkata – 700032

2024

PROCESS INTENSIFICATION IN REMOVAL OF POLLUTANTS FROM WASTE WATER

Thesis submitted for

Doctor of Philosophy (Engineering)

of

Jadavpur University

by

Anup Pralhadrao Pardey

Under the guidance

of

Dr. Avijit Bhowal
Professor
Chemical Engineering Department
Jadavpur University
Kolkata – 700032
&

Dr. Papita Das
Professor
Chemical Engineering Department
Jadavpur University
Kolkata – 700032

J A D A V P U R U N I V E R S I T Y

KOLKATA – 700032, INDIA

INDEX NO. 76/19/E and REF. NO. D-7/E/225/19

1. **Title of the Thesis:** Process Intensification in Removal of Pollutants from Waste Water
2. **Name, Designation and Institution of Supervisors:**

Dr. Avijit Bhowal

Professor,

Chemical Engineering Department,

Jadavpur University, Kolkata – 700032, India.

&

Dr. Papita Das

Professor,

Chemical Engineering Department,

Jadavpur University, Kolkata – 700032, India.

3. **List of Publications in Referred Journals:**
    1. Anup P. Pardey, Avijit Bhowal, Papita Das, Sudhanya Karmakar, Performance of slurry contact adsorber operating under high gravity for removal of fluoride, Chemical Engineering & Processing: Process Intensification 191 (2023) 109463.
4. **List of Patents:** Nil
5. **List of Conference Presentations:**
    1. 'Process Intensification in removal of phenol from wastewater', Anup P. Pardey, Avijit Bhowal, Papita Das, International Conference on Chemical Engineering, Innovations & Sustainability (ICEIS 2023), organized by the Department of Chemical Engineering, Jadavpur University, Kolkata, India, on the

auspicious occasion of Centenary Celebration Program, during February, 25-27, 2023, held at Jadavpur University, Kolkata, India.

2. 'Removal of fluoride from wastewater using Alum and Lime' Anup P. Pardey, Avijit Bhowal, Papita Das, Sudhanya Karmakar, Indian Chemical Engineering Congress & 74th Annual session of Indian Institute of Chemical Engineers (CHEMCON-2021) - organized by CSIR - Institute of Minerals and Materials Technology, Bhubaneswar, India, In association with Indian Institute of Chemical Engineers, Kolkata, India, during December, 26th – 30th, 2021.
3. 'Adsorption of fluoride from aqueous solution by activated charcoal', Anup P. Pardey, Avijit Bhowal, Papita Das, Sudhanya Karmakar, 11th International Conference on Sustainable Waste Management towards Circular Economy (11th IconSWM-CE 2021) Jadavpur University, Kolkata organized by International Society of Waste Management, Air and Water (ISWMAW) center for sustainable development & resource Efficiency Management, Jadavpur University, Kolkata, India, during December, 1st – 4th, 2021.
4. 'Adsorptive removal of fluoride by activated charcoal and comparative study between Packed bed and CSTR', Anup P. Pardey, Avijit Bhowal, Papita Das, Sudhanya Karmakar, International Chemical Engineering Conference 2021 (ICHEEC 2021), organized by Department of Chemical Engineering, Dr. B. R. Ambedkar National Institute of Technology, Jaladhar, India, during September, 16th – 19th, 2021.
5. 'Removal of fluoride from wastewater by Precipitation and Coagulation in continuously Fed Stirred Tank Reactor', Anup P. Pardey, Avijit Bhowal, Papita Das, Sudhanya Karmakar, 10th International Conference on Sustainable Waste Management towards Circular Economy (10th IconSWM-CE 2020) Jadavpur University, Kolkata organized by International Society of Waste Management, Air and Water (ISWMAW) center for sustainable development & resource Efficiency Management, Jadavpur University, Kolkata, India, during December, 2nd – 7th, 2020.

PROFORMA – 1

Statement of Originality

I Anup Pralhadrao Pardey registered on 30th April, 2019 do hereby declare that this thesis entitled "PROCESS INTENSIFICATION IN REMOVAL OF POLLUTANTS FROM WASTE WATER" contains literature survey and original research work done by the undersigned candidate as part of Doctoral studies.

All information in this thesis have been obtained and presented in accordance with existing academic rules and ethical conduct. I declare that, as required by these rules and conduct, I have fully cited and referred all materials and results that are not original to this work.

I also declare that I have checked this thesis as per the "Policy on Anti Plagiarism, Jadavpur University, 2019", and the level of similarity as checked by iThenticate software is 8%.

Anup Pralhadrao Pardey

Date:18/09/2025

Certified by Supervisor(s):

1. Dr. Avijit Bhowal

Professor,

Chemical Engineering Department,

Jadavpur University, Kolkata – 700032,

India

Professor
CHEMICAL ENGINEERING DEPARTMENT
JADAVPUR UNIVERSITY
Kolkata-700 032

2. Dr. Papita Das

Professor,

Chemical Engineering Department,

Jadavpur University, Kolkata – 700032,

India.

Professor
CHEMICAL ENGINEERING DEPARTMENT
JADAVPUR UNIVERSITY
Kolkata-700 032

PROFORMA – 2

CERTIFICATE FROM THE SUPERVISORS

This is to certify that the thesis entitled **"PROCESS INTENSIFICATION IN REMOVAL OF POLLUTANTS FROM WASTE WATER"** submitted by Anup Pralhadrao Pardey, who got the name registered on 30.04.2019 (Index No. 76/19/E and Ref. No. D-7/E/225/19) for the award of Ph.D. (Engineering) degree of Jadavpur University is absolutely based upon his own work under the supervision of Dr. Avijit Bhowal and Dr. Papita Das and that neither his thesis nor any part of the thesis has been submitted for any degree/diploma or any academic award anywhere before.

Avijit Bhowal 18/9/25

Dr. Avijit Bhowal

Professor,

Chemical Engineering Department,

Jadavpur University, Kolkata – 700032,

India

Professor
CHEMICAL ENGINEERING DEPARTMENT
JADAVPUR UNIVERSITY
Kolkata-700 032

Papita Das 18/9/25

Dr. Papita Das

Professor,

Chemical Engineering Department,

Jadavpur University, Kolkata – 700032,

India.

Professor
CHEMICAL ENGINEERING DEPARTMENT
JADAVPUR UNIVERSITY
Kolkata-700 032

Dedicated to my beloved mother and father, All my teachers, my dear brothers, my precious daughters, and my loving wife.

Acknowledgment

My deepest gratitude is to my supervisors, Dr. Avijit Bhowal, Professor, and Dr. Papita Das, Professor, Department of Chemical Engineering, Jadavpur University, Kolkata. I have been amazingly fortunate to have them as advisors who gave me the freedom to explore on my own and at the same time the guidance to recover when my steps faltered in crises. They taught me how to question thoughts, express ideas, and analyse results which were required for publications. Their patience and consistent support helped me finish this dissertation.

I am grateful to Dr. Papita Das, Professor, Chemical Engineering for extending Laboratory facilities which was necessary for my research work. I am also grateful to the Heads of the Department, Chemical Engineering for their timely cooperation in administrative formalities. I am also thankful to the supporting staff of the department who maintained all the machines in the central analysis laboratory of the department. Extended cooperation by Dr. B. Bhattacharya, QIP coordinator, Jadavpur University is deeply appreciated. I am also thankful to The Secretary, Faculty of Engineering and Technology, Jadavpur University for their cooperation and support.

I would like to express my profound gratitude to Mr. Rajesh Raool, my former Head of the Department of Packaging Technology at Government Polytechnic Nagpur, for his unwavering support and invaluable guidance. His consistent encouragement and insightful direction helped me stay focused on my research goals, even in the most challenging times. His leadership and belief in my potential have been instrumental in shaping the course of my academic journey.

I am also deeply thankful to Dr. Chandrashekhar Thorat, the former Principal of Government Polytechnic Nagpur, for his remarkable support and belief in my abilities. His vision and dedication to fostering academic excellence created an environment where I could pursue my research with confidence. Both of these mentors have left an indelible mark on my career, and I will always be grateful for their encouragement and wisdom.

I am deeply indebted to my friends Dinesh Alaspure, Rahul Meshram, Dr. Vivek Bhange, and Sevakram Kumbhare, whose unwavering support has carried me through the most challenging years of my research. Their encouragement and understanding kept me focused and motivated in moments of doubt. I also extend my heartfelt gratitude to my esteemed colleagues, Dr. Sudhanya Karmakar and Dr. Moumita Sharma, from the Mass and Heat Transfer Research Laboratory. Their invaluable insights and assistance during the experimental phases of my work were instrumental in my progress. Additionally, I am sincerely thankful to my lab mates, Dr. Shondipan, Subhashish, Sayan, and Aakash, whose timely help and camaraderie made the long hours of research more bearable and productive.

None of this journey would have been possible without the unwavering love, care, and patience of my family my mother, father, uncle Mr. Vilasrao Karale, my younger brothers Chetan and Gaurav, and my sister Damayanti. My wife, Rupali, has stood by me through every challenge, offering endless support and encouragement. Her strength and understanding have been my anchor, allowing me to pursue my goals with confidence. My daughters, Ishwari and Pruthvi, have been a constant source of joy, reminding me daily of the importance of perseverance and love. Their laughter and innocence have given me the strength to keep moving forward, even in the most difficult times. I am deeply grateful for the sacrifices they have made and the time they have allowed me to dedicate to my work.

I am deeply grateful to the Government of Maharashtra for providing me with the opportunity to pursue advanced studies through the Quality Improvement Programme of AICTE. Their support has been pivotal in enabling me to focus on my research and professional development. This initiative reflects their commitment to enhancing the quality of technical education in the state. I would also like to extend my sincere thanks to the Director of the Directorate of Technical Education, Mumbai, (M.S.) for recommending my name for this prestigious programme. Their confidence allowed me to contribute my knowledge more meaningfully to the field of technical education and to the entire environment. Finally, I appreciate All India Council for Technical Education (AICTE) for selection under Quality Improvement Programme (QIP) and providing financial assistance.

Anup Prālhadrao Pardey

Department of Chemical Engineering

Jadavpur University

Kolkata-700032

I N D E X

ABSTRACT

Industries are obligated to maintain pollutant level below specified threshold when discharging effluent into water bodies. Some of the commonly used waste water treatment techniques to remove pollutants from waste water are adsorption, precipitation-coagulation, and liquid-liquid extraction. The removal in these processes involve chemical reaction and mass transfer. These are carried out in equipment wherein the solution containing the pollutants flows under terrestrial gravity. Low rate of reaction due to poor micro-mixing, low values of mass transfer rates due to high diffusional resistance result in equipment of large size to provide more residence time for removal to meet the regulatory standards. The aim of this work is to implement Process Intensification strategy though use of equipment operating under high gravity to increase process efficiency within reduce the equipment size and bring about reduction in capital and operating cost. In these equipment, the liquid flows under centrifugal acceleration hundreds of times the terrestrial gravity by rotating the equipment about its axis. Three different design of high gravity equipment has been studied, namely Rotating Packed Bed, Rotating Zigzag contactor and rotating spiral contactor. The liquid flows through the void space in the packing in the former and over a spiral baffle as thin film in the latter. In Rotating zigzag contactor, the liquid flows zigzag's its way across a series of rotating baffles, splashing and flowing as film/rivulets on their surface and flowing as rivulets and drops in the space between the baffles. The objective of the experimental studies has been to determine whether the conventional contactor can be replaced by this high gravity equipment towards obtaining higher removal efficiency.

Chemical species such as fluoride and phenol have a detrimental effect on humans as well as on aquatic life and animals. Fluoride removal has been studied by adsorption with powdered activated carbon, and precipitation-coagulation technique based on Nalgonda method using lime and alum.

Phenol has been studied by liquid-liquid extraction using Aliquat 336 as the extractant with kerosene as the solvent.

Removal of Fluoride by Adsorption

Solution flowing under terrestrial gravity through adsorbent packed in a fixed bed is the conventional equipment in industrial practise of this process. Investigators noted that the mass transfer rates can be improved by ~2.5 times by rotating packed bed adsorber. However, the limitations of liquid mal-distribution in the rotating adsorbent bed among others limited further improvement in mass transfer rates. In this experimental investigation, the effectiveness of slurry contact adsorption in rotating contactors for the continuous removal of fluoride was studied. Powdered activated charcoal was dispersed into the solution and pumped through the high gravity contactors. This approach can avoid the disadvantages of high pressure drop associated with fine adsorbents, high diffusion resistance with granular adsorbents in fixed bed adsorption. In the rotating contactors, the percentage removal increased with rotational speed and slurry concentration. The percentage removal decreased with increase of feed flow rate though the amount of fluoride removed increased. The percentage utilization of adsorbent capacity for fluoride in the contactors is higher at large adsorbate dosage and low feed concentration. The rotating spiral contactor is the most efficient among the rotating contactors for removal of fluoride by this technique. Use of high gravity makes the process more efficient compared to the conventional contactors, like continuous stirred tanks and fixed bed. The mass transfer rates in slurry adsorption in rotating contactors is much faster than in rotating packed bed adsorber. The reported values of the overall volumetric mass transfer coefficient in this study serve as a useful reference for designing this contactor.

Removal of Fluoride by Precipitation-coagulation

Alum serves as the source of aluminium ions that initiate coagulation, while calcium hydroxide supplies calcium ions responsible for fluoride removal through precipitation as calcium fluoride. The overall process is governed by both chemical reaction and mass transfer phenomena. The chemistry of this system is influenced by the pH and concentration dependent speciation of aluminium and

fluoride ions. In industrial practice, the process is typically carried out in two stages using continuous stirred tank reactors.

Experiments were carried out by simultaneously introducing saturated lime solution, alum and fluoride solution into the same reactor. The rotating spiral reactor exhibited the highest removal efficiency among the three high gravity equipment studied. The percentage removal in this reactor closely approached the maximum value obtained in batch studies within a radial distance of 0.08 m of the equipment and estimated residence time (flow rate = 1.0 L/min) of about a second at the optimal pH 7.0 (alum concentration = 7 gm/L). The performance of the high gravity reactors compared to traditional reactors (continuous stirred tank reactor and fixed bed) due to efficient micromixing and higher values of mass transfer coefficient in the former.

Removal of Phenol by liquid-liquid extraction

The present work focuses on intensifying liquid–liquid extraction by employing advanced rotating contactors such as rotating packed bed, rotating zigzag contactor, and rotating spiral contactor operating under centrifugal force. Phenol removal from aqueous solution was investigated using Aliquat-336 dissolved in kerosene, with decanol as a phase modifier. A wide range of operating parameters was examined, including rotational speed (300–1100 rpm), aqueous and organic phase flow rates (0.5–1.5 L/min and 0.5–1.25 L/min, respectively), feed concentration (25–200 mg/L), and extractant concentration (0.25–1.5 vol%). The results demonstrated that phenol extraction efficiency increased with rotational speed, feed concentration, extractant dosage, and solvent phase flow rate, but decreased with aqueous flow rate. Among the contactors studied, the rotating spiral contactor exhibited superior performance, achieving up to 78.8% phenol removal and higher overall volumetric mass transfer coefficient ($K_{oc}a$) than RZC, RPB, and conventional contactors such as fixed beds and stirred tank reactors.

Keywords: Defluoridation, Phenol, Alum, Lime, Aliquat 336, rotating packed bed, rotating zigzag bed, rotating spiral contactor.

Chapter 01

INTRODUCTION

Water is a basic building block to maintain the quality of life. Only 3% of total water is available as fresh water and only a third part of that is available as surface water or groundwater. From ancient times, surface water has played a very important role in day-to-day life as this is the only source of drinking water because of its easy availability in comparison with the other sources of water. The need for fresh and good-quality water is on the increase in urban as well as rural areas because of the growth of population, economic development, and urbanization.

Water is used for most activities in domestic and industrial sectors [1.1]. The harmful ions in water such as arsenic, iron, manganese, selenium, radioactive materials, chloride, toxic metals, nitrate, and fluoride originate from both natural and anthropogenic sources. This occurs when wastewater from industries as well as from domestic households discharges pollutants into the nearby rivers, lakes, and oceans without treatment [1.2] creating health hazards to human beings and living animals.

Various countries have established their water quality standards. All the standards are generally in accordance with the Guidelines of Drinking Water Quality (GDWQ) and issued by the World Health Organization (WHO). Table 1.1 states the permissible limit for the presence of various ions in drinking water.

1.1 Fluoride

Fluorine is the 13th most abundant, reactive, and electronegative chemical compound found in nature [1.3]. It plays a very important role for both humans and animals in the production and growth of teeth enamels, and bones [1.4 – 1.5], but becomes a major public health problem when high concentrations of fluoride are ingested. Table 1.2. mentioned range the fluoride concentration, and its influence human health [1.6 - 1.7].

Table 1.1. WHO guidelines for drinking water

S. No.	Parameter	Desirable Limit (ppm)	Permissible Limit (ppm)	Maximum Allowable concentration (ppm)
1	Chlorides (Cl)	250	1000	250
2	Calcium (Ca)	75	200	------
3	Sulphate (SO_4^{2-})	200	400	400
4	Nitrate (NO_{3-})	45	100	10
5	Fluoride (F^-)	1.0	1.5	1.5
6	Phenolic compounds (C_6H_5OH)	0.001	0.002	------
7	Zinc (Zn)	5.0	15	5.0
8	Iron (Fe)	0.3	1.0	0.3
9	Manganese (Mn)	0.1	0.3	0.1
10	Copper (Cu)	0.05	1.5	1.0
11	Arsenic (As)	0.05	Not Permissible	0.05
12	Cyanide (CN)	0.05	Not Permissible	0.1
13	Lead (Pb)	0.05	Not Permissible	0.05
14	Chromium (Cr^{6+})	0.05	Not Permissible	0.05
15	Aluminium (Al)	0.03	0.2	0.2
16	Cadmium (Cd)	0.01	Not Permissible	0.005
17	Selenium (Se)	0.01	Not Permissible	0.01
18	Mercury (Hg)	0.001	Not Permissible	0.001

Table 1.2. Health Effects in Humans with a range of fluoride concentration

Level of fluoride (mg/L)	Human health disorders
Less than 0.5	Teeth diseases
0.5 to 1.5	Favorable for teeth growth
1.5 to 4.0	Dental fluorosis
4.0 to 10	Skeletal & dental fluorosis, cancer, etc.

1.2 Environmental Sources and Mobility of Fluoride

1.2.1 Natural Sources

Fluoride contamination in groundwater mainly arises due to the breakdown of rocks containing fluoride ions. The natural source of fluoride in nature is fluorine which originated in sedimentary phosphate rock deposits and minerals [1.8]. The host minerals like amphiboles (chain silicates), tourmaline, apatite, mica (layer silicates), kaolinite, montmorillonite, and bentonite also contain inorganic fluoride [1.9]. The naturally found limestone has fluoride concentration in the range of 0.4% – 1.2%. The fluoride content in various types of rock [1.10] is shown in Table 1.3.

Table 1.3. The fluoride content in different rocks

Rocks	Fluoride Conc. (mg/L)	Average Conc. (mg/L)
Basalt	20–1060	360
Granites and gneisses	20–2700	870
Sandstones	10–880	180
Limestones	0–1200	220
Phosphorite	24000–41500	31000
Shales and clays	10–7600	800
Coal (ash)	40–480	80

1.2.2 Anthropogenic Sources

The various anthropogenic sources of fluoride are from industries such as oil refining, coal burning, chemical production, steel manufacturing, aluminium smelting, clay production, glass and enamel manufacturing, fertilizers and pesticides industries, brick and ceramic manufacturing, wastes, sewage and sludge from industries [1.8] [1.10]. Table 1.4 illustrates the fluoride emission from the various manufacturing industries [1.11].

Table 1.4. Fluoride emission (ton/year) from various industries

Manufacturing Source	Product/Process Type	Fluoride Emission, Tons/Year
Aluminium	------	16000
Phosphate Fertilizer	Normal superphosphate	9700
	Triple super phosphate	300
	Diammonium phosphate	100
Steel	Open-hearth furnace	16800
	Basic oxygen furnace	8400
	Electric furnace	14900
Phosphoric Acid	Wet Process	3000
Elemental Phosphorus	------	5500
Nonferrous Metal Foundries	------	4000
Brick & Tiles	------	18500
Glass and Frit	------	2700
Coal Combustion	------	16000

1.3. Phenol

Phenol commonly known as hydroxybenzene (C_6H_5OH) consists of one hydroxyl group attached to the benzene ring. It has popular names such as phenic acid, carbolic acid, phenylic acid oxybenzene, and phenyl hydroxide. At room temperature, phenol is a carbolic corrosive, colorless crystalline hygroscopic solid and has a sweet smell. It is highly soluble in water and various organic solvents like chloroform, ether, polar solvent, and alcohol. Phenol and phenolic compounds act as a precursor in manufacturing techniques such as crude oil and plastics processing and are also useful in the manufacturing of paints, textiles, explosives, pharmaceuticals, fertilizers, paper, rubber, wood preservatives, soap, and adhesives. It is evaluated that, the phenolic compounds release from these industries near about 10 million tons in the environment [1.12]. Table 1.5 states the phenol concentration present in waste water of various industries [1.13].

Table 1.5. Phenol concentration from various industries

Industry	Phenol Concentration (mg/L)
Oil refineries	6–500 mg/L
Coking operations	28–3900 mg/L
Coal processing	9–6800 mg/L
Petrochemicals manufacturing	2.8–1220 mg/L
Pharmaceutical, plastics, paint & wood products, pulp and paper	0.1–1600 mg/L

Phenol compounds are listed as the top 20 hazardous compounds by the International Maritime Organization (IMO) due to their high sensitivity and creating high risks to aquatic life [1.14]. The US Environmental Protection Agency (EPA) and the Canadian National Pollutant Release Inventory (NPRI) listed as phenol is a priority pollutant out of 129 pollutants due to its harmful effects at low concentration. Phenol is toxic even at low concentrations and can form other substituted compounds when it is present in natural water. Phenol concentration of 1.0 mg/L can have fatal consequences in humans, 2.0 mg/L can be toxic to fish and when this concentration ranges between 10.0 and 100.00 mg/L can be a death threat to aquatic life. The adverse effects of phenol on human health are due to the incorporation of phenol in the food chain as it gets induced in plants and by bioaccumulation in birds and fish [1.15 - 1.16]. Phenol-contaminated drinking water can cause serious health effects such as paralysis of the central nervous system, nausea, dark urine, diarrhea, mouth sores, liver and kidney, and other effects [1.17- 1.18].

1.4 Wastewater treatment techniques

Various techniques are used for the removal of pollutants from wastewater. This includes distillation, adsorption, extraction, biodegradation, electrochemical oxidation, chemical oxidation, enzymatic treatment, reverse osmosis, nanofiltration, pervaporation, membrane distillation, and extractive membrane bioreactor. All these techniques have advantages and some disadvantages like the

requirement of high energy, fouling, scaling, restrictions in pH level, pretreatment requirement, selectivity constraint, and use of hazardous chemicals. Other constraints include the volume of waste water and concentration of pollutants to be treated, and operational and maintenance costs. The present trend is to use environmentally sustainable, safe, compatible techniques, combined with low operational costs for wastewater treatment [1.19 - 1.20].

1.5 Techniques used for fluoride and phenol removal

1.5.1 Adsorption

Adsorption is a simple and energy-efficient method which remove low as well as high concentrations of various types of pollutants [1.21]. This is a surface phenomenon in which selected ions or molecules get attached to the surface of the solid. The material on which the adsorption occurs is known as adsorbent and the molecules that get attached are referred to as adsorbate. The adsorption process occurs by two mechanisms - one by physical adsorption (Physisorption), and the second by chemical adsorption (Chemisorption). In physisorption, the adsorbate is attached to the surface of the adsorbent by weak Van der Waals forces. In contrast, chemical adsorption occurs through the formation of a strong covalent bond between adsorbent and adsorbate [1.22].

In the adsorption process, there are three main steps involved. In the initial step, the adsorbate moves from the bulk phase (either gas or liquid) to the surface of the adsorbent material through diffusion process. In the second step, molecules attach on the surface by either physical adsorption or chemical adsorption. In the last step, the molecules diffuse into the interior of the particle. The kinetics and capacity of the adsorption process depend on temperature, pH, nature and particle size of adsorbate and adsorbent, contact time, pressure, adsorbent surface area, the concentration of reactant, presence of other substances and ionic strength, etc.

1.5.2 Liquid-Liquid Extraction

Liquid-liquid extraction is a unit operation wherein the pollutant present in a liquid is removed by the addition of a solvent in which the pollutant is soluble. The operation produces two product

streams i.e. the raffinate phase and the extractant phase. The raffinate phase is that from which solute is extracted and the extract phase is the solvent-rich phase.

The selection of a suitable solvent plays a significant role in maximizing extraction efficiency. Liquid-liquid extraction is associated with ease of operation, automation, high loading, high purity effluent, and high efficacy in removing organic pollutants, dyes, and heavy metals from the wastewater [1.23]. Extractants are often added to the solvent phase to increase the solubility of solutes having low solubility in this phase.

1.5.3 Coagulation / Flocculation

Coagulation and flocculation are essential stages in the wastewater treatment. Coagulation involves the addition of chemicals, are called as coagulants into the wastewater. These coagulants neutralize the charges of particles suspended in the water, enabling them to adhere together and form larger clusters called flocs. This process destabilizes and aggregates small particles, facilitating their removal in later treatment processes, such as sedimentation or filtration.

The various coagulants used in industrial wastewater treatment are categorized as organic and inorganic. The organic coagulants are poly-DADMAC, polyamines, polyvinyl alcohols, polyacrylamides, melamine-formaldehyde, etc. The inorganic coagulants are ferric and ferrous salts, lime, aluminium salts (alum), aluminium chloride, aluminium sulfate, calcium/magnesium oxide, polyaluminium sulfate, ferric chloride/sulfate, poly-aluminium chloride, etc. [1.24].

Flocculation is a process which combined the fine particles into larger flocs. This process typically follows coagulation, where coagulant added to destabilize particles. During flocculation, gentle mixing encourages destabilization of particles to come together and form larger, more easily removable masses. The flocs can then be removed from the water through settling or filtration, improving water clarity and quality. This process can remove suspended solids, bacteria, and other contaminants from water. The flocculation helps development of flocs of optimal size, density, and strength making them easier to remove from the water by sedimentation or filtration [1.25 - 1.26].

1.5.4 Electrochemical Method

The electrochemical (EC) method is a promising alternative to classic coagulation as it reduces the need for chemicals. The coagulants are generated by electrolytic oxidation of an appropriate anode material such as $Al, Fe, Zn, Pb,$ and stainless steel. The ionic species, metals, and other pollutants are removed from the wastewater due to a reaction with opposite charge ions and metallic hydroxide flocs produced within the effluents.

The technique comprises physical and chemical stages like cathodic reduction, anodic oxidation, electron migration, discharge, adsorption, and coagulation. The newly developed modern techniques of this method are electro-coagulation, electro-oxidation, electro-floatation, electro-reduction, electro-ionization, and electro-kinetic. This method can be used to treat effluents containing organic dyes, organic pollutants, suspended solids, oil and greases, algae and microorganisms, and heavy metals [1.25]. The electrochemical method can remove high concentrations of pollutants and also can be used as a pretreatment method. The high energy cost required to run the electrochemical technique is a major disadvantage [1.27].

1.5.5 Chemical oxidation technique

It involves the application of oxidizing agents in the treatment operation to oxidize organic pollutants. In this technique, the most common oxidants used are oxygen, chlorine, chlorine dioxide, peroxide, ozone, chloramines, permanganate, and ferrate [$Fe\ (VI)$] [1.28]. These oxidants create radicals that quickly and non-selectively react with organic compounds leading to their degradation. The advantages of the chemical oxidation process are low energy requirements, low-temperature needs, low requirement of reagents, and mild pH conditions [1.19].

1.5.6 Advanced Oxidation Process (AOP)

The advanced oxidation technique is popularly known for non-waste-generating technology. This technique is applied for the removal of organic compounds and microorganisms from wastewater.

The process involves the in-situ generation of hydroxyl radicals. The hydroxyl radical is an extremely reactive free radical which consist strong oxidants. [1.29]. Hydroxyl radical has a high redox potential so it is strongest of all the oxidants.

$$HO^{\bullet} + H^{+} + e^{-} \rightarrow H_2O, \qquad E^0 = 2.33V \qquad (6)$$

The hydroxyl radicals react with the organic molecules at the rate of 10^6–$10^9\ M^{-1}S^{-1}$ by hydrogen abstraction, combination or addition of radicals, and electron transfer. The organic compounds are converted into organic radicals by the removal of hydrogen atoms from the hydroxyl radicals. The organic radical proceeds through consecutive reactions and finally mineralized to H_2O and CO_2 [1.30]. The process of advanced oxidation has a high oxidation rate and needs very less time to remove the contaminants from the wastewater. Due to the high reactivity of hydroxyl radicals, it can react with all kinds of organics (lipid, ethylenic, aliphatic, aromatic) and inorganics (cations and anions) [1.31].

1.5.7 Ion-Exchange method

The ion exchange process is used to separate and remove contaminants, heavy metals, nitrogen, total dissolved solids, acidic species, and organic matter from aqueous solution by use of zeolites, soil humus, some clay, and some ion exchange resins. The ion exchanger can be a cations exchanger which exchanges positively charged ions, or an anion exchanger which exchange negatively charged ions. After saturation is reached, the resins are regenerated by treatment with chemicals.

1.5.8 Biological treatment

Biological treatment depends on the presence of roundworms, bacteria, and small organisms for decomposing organic waste and various kinds of chemicals. Biological treatment is advantageous over the other wastewater treatment methods, due to its environmentally friendly, energy-efficient, and requires less investment cost. The biological technique is classified into various types like bio-reduction, bioremediation, bio-sorption, bio-transformation, bio-accumulation, bio-augmentation,

etc [1.32]. The two mechanisms involved in this process are adsorption onto microorganisms and biodegradation through microorganisms. The microorganisms used are living or dead forms. The bacteria used like Acetobacter sp., Bacillus sp., Ochrobactrum sp., and Staphylococcus sp. The fungi used like Aspergillus sp., Trichoderma sp., etc., and algae used such as red algae, Spirogyra, blue-green algae, Spirulina, etc. Also, parasites, yeasts, some plants, etc. are also used in this technique. The microorganisms process the various contaminants by enzymatic conversion and transform them into biomass, methane, carbon dioxide, and water. The main limitation of this technique is the low removal rate in comparison with the other treatment methods.

1.5.9 Membrane separation

The different modern techniques of membrane separation such as nanofiltration (NF), microfiltration (MF), reverse osmosis (RO), electrodialysis (ED), and ultrafiltration (UF) are categorized based on separation method, driving forces, the pore size of the membrane, and the material used for the membrane systems [1.33]. All these techniques are efficient techniques for dealing with a variety of water pollutants. Membrane separation techniques have some advantages over conventional methods such as low energy consumption, compact installation, requiring less amount of chemicals, fully automatic process, eventuality in the small and large treatment system, and simultaneous removal of other species from the wastewater, etc. [1.34].

1.5.10 Reverse Osmosis (RO)

In this process, a semipermeable membrane is placed between two mediums to act as the barrier. When the pressure applied is above the osmotic pressure, water molecules permeate through the membrane while the contaminants cannot. Generally, the earliest material used for manufacturing of RO membrane is Cellulose Acetate. Nowadays very popular material used for membrane manufacturing is the Thin-Film Composite (TFC). The TFC is made from the layers of polysulfone, polyamide (Nylon), and other types of polymers which have very good resistance from chemical degradation and a high rate of rejection of salt content and comparatively give better performance

than cellulose acetate membrane [1.35]. In reverse osmosis, mostly spiral-wound-type membrane module configuration is used. The hollow fibre membrane module is especially limited for seawater purification. Tubular module and Plate-and-frame are generally used for industrial wastewater and food process industries [1.36].

Fouling is a major concern in membrane separation and rejection of water in high quantities typically between 35% and 65% is not suitable in regions where there is water scarcity. The highly concentrated brine water discharge coming from the reverse osmosis plant requires further treatment. This technique involves impurities plugging, high investment, and maintenance costs. Onyango et al [1.34] noted that it required highly configured technology so this is not suitable in developing countries.

1.5.11 Membrane Distillation

Membrane distillation (MD) is used for the separation of components from water. Membrane distillation consists of a microporous hydrophobic membrane where the aqueous phase is in contact with it. Mass transfer occurs between the two phases through the membrane pores because of the temperature gradients and initiation of pressure gradient across the membrane. Due difference in pressure, the volatile components get evaporated. The hydrophobic nature of the membrane prevents liquid molecules from passing through it, while only water vapor molecules can move through its pores and condense on the other side [1.37 - 1.38].

1.5.12 Emulsion Liquid Membrane (ELM)

The emulsion liquid membrane process is efficient for removal of metal ions, hydrocarbons, and organic and inorganic acids from wastewater in comparison with conventional methods. In this technique, the extraction and striping process occur simultaneously in a single step. The process reduces the need for high-cost extractants, high fluxes, and selectivity during the operation. A preliminary emulsion of water in oil is prepared by emulsifying immiscible phases of stripping and organic liquid membrane with a surfactant to generate the emulsion. This is then dispersed in a

solution that needs to be treated. Pollutant diffuses from the feed solution into the internal droplets of the stripping phase through the organic membrane phase. Despite the advantages, there are some disadvantages like leaking and swelling of liquid membrane. Swelling reduces the driving force responsible for the separation making the membrane weak causing emulsion breakage leakage of extracted solute, thereby decreasing the percentage of extraction [1.39].

References:

1.1 Y. Liu, L. Yang, W. Jiang, Qualitative and quantitative analysis of the relationship between water pollution and economic growth: a case study in Nansi Lake catchment, China, *Environ. Sci. Pollut. Res.,* 27 (2020) 4008 – 4020.

1.2 G. Wu, J. Hong, Z. Tian, Z. Zeng, C. Sun, Assessing the total factor performance of wastewater treatment in China: A city-level analysis, *Sci. Total Environ.,* 758 (2021) 143324.

1.3 M. G. García, L. Borgnino, Fluoride in the Context of the Environment, RSC, 2015.

1.4 P. E. Petersen, R. J. Baez, Oral Health Surveys, Basic Methods, (2013) 5th Edition, World Health Organization (WHO).

1.5 D. M. O'Mullane, R. J. Baez, S. Jones, M. A. Lennon, P. E. Petersen, A. J. Rugg-Gunn, H. Whelton, G. M. Whitford, Fluoride and Oral Health, *Community Dent. Health,* 33 (2016), 69 – 99.

1.6 M. Mohapatra, S. Anand, B. K. Mishra, D. E. Giles, P. Singh, Review of fluoride removal from drinking water, *J. Environ. Manage.,* 91 (2009) 67–77.

1.7 J. Fawell, K. Bailey, J. Chilton, E. Dahi, L. Fewtrell, Y. Magara, Fluoride in Drinking-Water; World Health Organization (WHO) and IWA Publishing: London, UK, 2006.

1.8 R. Fuge, M. J. Andrews, Fluorine in the UK environment, Environ. Geochem. Health, 10(3/4) (1988) 96 -104.

1.9 C. Reimann, P. d. Caritat, Chemical elements in environment, Fact sheets for the geochemist and environmental scientist. (1998) Springer, New York, NY.

1.10 S. K. Jha, V. K. Mishra, D. K. Sharma, T. Damodaran, Fluoride in the Environment and Its Metabolism in Humans, *Rev Environ Contam. Toxicol.,* 211 (2011) 121- 42.

1.11 H. C. Hodge, F. A. Smith, Occupational Fluoride Exposure, *J. Occup. Health,* 19 (1) (1977) 12-39.

1.12 M. Alshabib, S. A. Onaizi, A review on phenolic wastewater remediation using homogeneous and heterogeneous enzymatic processes: Current status and potential challenges, *Sep. Purif. Technol.,* 219 (2019) 186 – 207.

1.13 G. Busca, S. Berardinelli, C. Resini, L. Arrighi, Technologies for the removal of phenol from fluid streams: A short review of recent developments, *J. Hazard. Mater.,* 160 (2008) 265–288.

1.14 N. Panigrahy, A. Priyadarshini, M. M. Sahoo, A. K. Verma, A. Daverey, N. K. Sahoo, A comprehensive review on eco-toxicity and biodegradation of phenolics: Recent progress and future outlook, *Environ. Technol. Innov.,* 27 (2022) 102423.

1.15 S. Garg, P. Kumar, S. Singh, A. Yadav, L. F. Dumée, R. S. Sharma, V. Mishra, Prosopis juliflora peroxidases for phenol remediation from industrial wastewater — An innovative practice for environmental sustainability, *Environ. Technol. Innov.,* 19 (2020) 100865.

1.16 Mandeep, A. Gulati, R. Kakkar, Graphene-based adsorbents for water remediation by removal of organic pollutants: Theoretical and experimental insights, *Chem. Eng. Res. Des.,* 153 (2020) 21 – 36.

1.17 H. B. Senturk, D. Ozdes, A. Gundogdua, C. Durana, M. Soylak, Removal of phenol from aqueous solutions by adsorption onto organomodified Tirebolu bentonite: Equilibrium, kinetic and thermodynamic study, *J. Hazard. Mater.,* 172 (2009) 353–362.

1.18 W. W. Anku, M. A. Mamo, P. P. Govender, Phenolic Compounds in Water: Sources, Reactivity, *Toxicity and Treatment Methods*, (2017) 420 – 443.

1.19 A. Bibi, S. Bibi, M. A. Dieyeh, M. A. Al-Ghouti, Towards sustainable physiochemical and biological techniques for the remediation of phenol from wastewater: A review on current applications and removal mechanisms, *J. Clean. Prod.,* 2023, 137810.

1.20 K. A. M. Said, A. F. Ismail, Z. A. Karim, M. S. Abdullah, A. Hafeez, A review of technologies for the phenolic compounds recovery and phenol removal from wastewater, *Process Saf. Environ. Prot.,* 151 (2021) 257 – 289.

1.21 D. R. Rout, H. M. Jena, O. Baigenzhenov, A. H. Bandegharaei, Graphene-based materials for effective adsorption of organic and inorganic pollutants: Acritical and comprehensive review, *Sci. Total Environ.,* 863 (2023) 160871.

1.22 O. K. Akeremale, O. T. Ore, A. A. Bayode, H. Badamasi, J. A. Olusola, S. S. Durodola, Synthesis, characterization, and activation of metal organic frameworks (MOFs) for the removal of emerging organic contaminants through the adsorption-oriented process: A review, *Results Chem.,* 5 (2023) 100866.

1.23 W. Wei, C. W. Cho, S. Kim, M. H. Song, J. K. Bediako, Y. S. Yun, Selective recovery of Au (III), Pt (IV), and Pd (II) from aqueous solutions by liquid–liquid extraction using ionic liquid Aliquat-336, *J. Mol. Liq.,* 216 (2016) 18 – 24.

1.24 R. Shrestha, S. Ban, S. Devkota, S. Sharma, R. Joshi, A. P. Tiwari, H. Kim, M. K. Joshi, Technological trends in heavy metals removal from industrial wastewater: A review, *J. Environ. Chem. Eng,* 9 (2021) 105688.

1.25 D. Ghernaout, B. Ghernaout, Sweep flocculation as a second form of charge neutralisation—a review, *Desalin. Water Treat.,* 44 (2012) 15–28.

1.26 S. Ayoob, A. K. Gupta, V. T. Bhat, Conceptual Overview on Sustainable Technologies for the Defluoridation of Drinking Water, *Crit. Rev. Environ. Sci. Technol.,* 38 (2008) 401–470.

1.27 C. A. M. Huitle, S. Ferro, Electrochemical oxidation of organic pollutants for the wastewater treatment: direct and indirect processes, *Chem. Soc. Rev.,* 35 (2006) 1324 – 1340.

1.28 Y. Liang, Y. Ning, L. Liao, B. Yuan, Special Focus on Produced Water in Oil and Gas Fields: Origin, Management, and Reinjection Practice, Formation Damage During Improved Oil Recovery, (2018), 515–586.

1.29 W. H. Saputera, A. S. Putrie, A. A. Esmailpour, D. Sasongko, V. Suendo, R. R. Mukti, Review Technology Advances in Phenol Removals: Current Progress and Future Perspectives, *Catalysts,* 11 (2021) 998.

1.30 J. M. Herrmann, Heterogeneous photocatalysis: fundamentals and applications to the removal of various types of aqueous pollutants, *Catal. Today,* 53 (1999) 115–129.

1.31 B. K. Hordern, M. Ziółek, J. Nawrocki, Catalytic ozonation and methods of enhancing molecular ozone reactions in water treatment, *Appl. Catal. B.,* 46 (2003) 639 – 669.

1.32 D. Bhatia, N. R. Sharma, J. Singh, R. S. Kanwar, Biological methods for textile dye removal from wastewater: A review, *Crit. Rev. Environ. Sci. Technol.,* 47 (19) (2017) 1836–1876.

1.33 A. Nqombolo, A. Mpupa, R.M. Moutloali, P.N. Nomngongo, Wastewater treatment using membrane technology, *Wastewater Water Qual.,* 29 (2018).

1.34 M. S. Onyango, H. Matsuda, Fluoride Removal from Water Using Adsorption Technique, Fluorine and the environment, Vol (2), 2006.

1.35 K. P. Lee, T. C. Arnot, D. Mattia, A review of reverse osmosis membrane materials for desalination—Development to date and future potential, *J. Membr. Sci.,* 370 (2011) 1–22.

1.36 R. W. Baker, Membrane Separation, Membrane Technology and Applications, John Wiley & Sons. (2023) 189-210.

1.37 A. Jafari, M. R. S. Kebria, A. Rahimpour, G. Bakeri, Graphene quantum dots modified polyvinylidenefluride (PVDF) nanofibrous membranes with enhanced performance for air Gap membrane distillation, *Chem. Eng. Process.: Process Intensif.,* 126 (2018) 222 – 231.

1.38 M. R. S. Kebria, A. Rahimpour, Membrane Distillation: Basics, Advances, and Applications, Advances in Membrane Technologies, Intech Open, (2020).

1.39 L. Zeng, L. Yang, Q. Liu, W. Li, Y. Yang, Influences of axial mixing of continuous phase and polydispersity of emulsion drops on mass transfer performance in a modified rotating disc contactor for an emulsion liquid membrane system, *Ind. Eng. Chem. Res.,* 54 (40) (2015) 9832–9843.

Chapter 02

LITERATURE REVIEW

The various sources of fluoride and phenol and their detrimental effects on humans as well as on aquatic life and animals have been discussed in Chapter 1. Industries are obligated to maintain pollutant levels below specified threshold when discharging effluent into water bodies. Compliance with these established standards is a fundamental aspect of water quality management and public health protection [2.1 - 2.2].

Various general techniques for treating contaminated wastewater were discussed in Chapter 1. In this chapter, the present status of research on a few techniques for removal of fluoride and phenol finds mention.

2.1 Removal of Fluoride by adsorption

Over the years, the adsorption technique has been a prime area of research for the removal of fluoride and used in many industrial treatment processes [2.3]. Activated carbon/charcoal and other types of adsorbents remove fluoride from wastewater by the combination of adsorption and ion exchange processes [2.4]. Activated charcoal (also called activated carbon) is widely favored as an adsorbent in various industries due to its high porosity, availability of significant surface area, nonpolar nature, and cost-effectiveness [2.5] and adaptable surface chemistry [2.6]. It can be sourced from a range of agricultural (including waste rice husk, rubber wood, apricots, coconut shells, rice straw, sawdust, sugar beet bagasse, molasses, bamboo, rattan sawdust, and oil palm fiber) and industrial waste materials, making it a versatile and environmentally friendly choice. Bio based material are preferred for activated carbon production due to their cost-effectiveness and renewable nature [2.7].

Many researchers used modified activated carbon for de-fluoridation of wastewater by adsorption. The oxides and hydroxides of metals were blended with the carbon material to form modified adsorbents. Pang et al. [2.8] studied the removal of fluoride by using modified adsorbent Zirconium (Zr-ACF). The highest adsorption capacity of the modified adsorbent was found to be 28.50 mg/g. Iwar et al. [2.9] conducted a study using a packed column to examine the effectiveness of raffia palm shell-activated carbon blended with aluminum oxide composite for fluoride removal.

In addition to the mentioned adsorbents, various other materials were used for adsorption processes. These include activated carbon derived from bone [2.10], ceramic materials [2.11], hydroxides [2.12], nanocomposites [2.13], carbon nanotubes [2.14 - 2.15] and graphene oxide [2.16]. Some of the adsorbents used for removal of fluoride and the adsorption isotherm model in which best fitting was observed is given in Table 2.1.

Various equipment has been studied for the adsorption process and is discussed below.

Table 2.1. Different adsorbents used for fluoride removal with adsorption isotherms

Adsorbent	Adsorption Isotherm Model			References
Tetra metallic oxide adsorbent Fe-Al-Ce-Ni (FACN)	Freundlich Isotherm			[2.17]
	$\frac{1}{n}$	K_f $(mg^{1-1/n}/gL)$	R^2	
	0.52	3.22	0.99	
Sugarcane Bagasse	Langmuir Isotherm			[2.18]
	q_{max} (mg/g)	K_L (L/mg)	R^2	
	2.443	1.818	0.998	
Bone char (BC)	Freundlich Isotherm			[2.19]
	$\frac{1}{n}$	K $(mg^{1-1/n}/gL)$	R^2	
	0.39	1.06	0.998	
Activated Charcoal (AC)	Freundlich Isotherm			[2.19]
	$\frac{1}{n}$	K $(mg^{1-1/n}/gL)$	R^2	
	0.53	0.08	0.999	
Titanium Dioxide (TiO_2)	Langmuir Isotherm			[2.20]
	q_{max} (mg/g)	b (L/mg)	R^2	
	4.1900	2.0400	0.9826	
Pyrophyllite	Langmuir Isotherm			[2.21]
	q_{max} (mg/g)	b (L/mg)	R^2	
	3.79	0.34	0.99	
Modified Zeolite (Rice husk ash zeolite)	Freundlich Isotherm			[2.22]
	$\frac{1}{n}$	K_f $(mg^{1-1/n}/gL)$	R^2	
	0.3553	2.6184	0.9916	
Nanocellulose/polyvinyl alcohol composite	Langmuir Isotherm			[2.23]
	q_{max} (mg/g)	K_L $(L\ /\ (mg)$	R^2	
	0.263	0.4681	0.982	

2.1.1 Packed Bed Adsorption Column

Industrial adsorption processes typically use fixed-bed adsorption columns. It consists of a vertical column that is packed with the adsorbent. Packed bed columns have ports or fittings at the top and bottom to allow the introduction of the fluid and discharge the treated fluid (referred to as effluent) respectively. At the bottom of the column, there is often a support grid or distributor that help to distribute the incoming fluid evenly across the cross-section of the column. The fluid that needs to be treated enter in the column from the top and flow downward through the packed bed under gravity. Alternatively, in some applications, the flow may be upward. Mass transfer takes place between the fluid and the adsorbent as the fluid percolates through the column in contact with the packing bed.

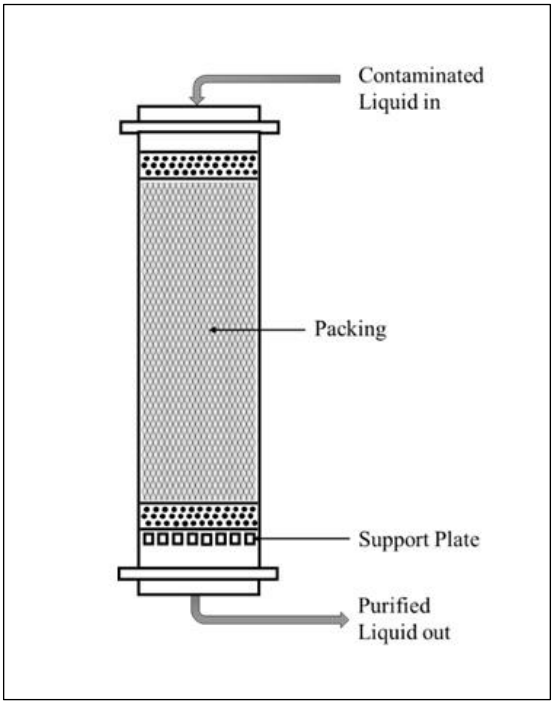

Figure 2.1: Schematic Diagram of a Packed Column

The effectiveness of this procedure depends on several factors, such as the selection of the adsorbent material, wastewater flow rate, feed concentration, and the duration of contact between the wastewater and the adsorbent. These variables can be fine-tuned and optimized to attain the targeted degree of removal. As time progresses the adsorbent becomes loaded with the pollutant and

eventually the concentration in the effluent reaches the breakthrough point. Analyzing the breakthrough data allows for the assessment of the adsorbent column's performance and its operational lifespan in practical scenarios.

Numerous studies have been carried out for removal of fluoride in fixed bed adsorber. Few of them are outlined in this chapter. Talat et al. [2.24] used activated carbon generated from coconut husk which was further treated with KOH solution. It was observed that the specific surface area and the pore volume of the adsorbent increased at higher KOH concentration. The adsorption capacity was found to be 6.5 mg/g at pH=5, feed concentration = 10 mg/L and adsorbent dose = 1.4 g/L. They analyzed the breakthrough curve by applying Bed Depth Service Time (BDST), Thomas and Yoon–Nelson model. The adsorption rate constant K_a was found to be 0.00027 and 0.0032 L/mg min^{-1} at flow rate of 1.66 mL/min and 3.32 mL/min respectively.

Jayashree et al. [2.25] studied the removal of fluoride in batch and continuous process in packed columns using activated carbon made from the seed pods of Bauhinia variegate. One type of adsorbent was thermally treated or physically treated Bauhinia (PTB), whereas the other was Chemically Treated Bauhinia (CTB). They latter showed higher efficiency at optimum pH = 3.0 for the removal of fluoride. The maximum adsorption capacity of the prepared adsorbents obtained in the column studies was 1.176 mg/g at bed depth of 5 cm and the flow rate of 5 mL/min.

Amberlite XAD-4 resin impregnated with Aliquat-336 was used by Arya et al. [2.26] as an adsorbent for continuous removal of fluoride in fixed bed adsorption column. The percentage removal of fluoride increased from 22% to 74% on varying resin dosage from 2.5 g/L to 25 g/L. Higher removal of fluoride (76%) was observed at pH 6.04.

Bera et al. [2.27] studied a novel adsorbent synthesized by the combination of aluminum hydroxyapatite $(Al - HAp)$ and calcium aluminium hydroxyapatite $(Al - HApC)$ on commercial granular charcoal made from wood for removal of fluoride. The experimental column studies reveal that the adsorption capacity of $Al - HApC$ increased with temperature from 105 mg/g at 303 K to

127 mg/g at 323 K. The author claimed that the highest fluoride adsorption capacity was 105 mg/g. Sarkar et al. [2.28] investigated fluoride removal in a packed column using geological material Laterite as an adsorbent. The adsorption capacity was obtained to be 0.3473 mg/g.

Ghorai et al. [2.29] studied the performance of activated alumina having particle size 2–5 mm for removal of fluoride in batch and in fixed bed. The adsorption capacity of activated alumina was 1450 mg/kg at pH 7.0. In the column study, lower fluoride removal was observed at high feed concentrations and high feed flow rate. Roy et al. [2.30] in their study on removal of fluoride by calcium-impregnated activated charcoal in fixed bed noted that breakthrough time increased at higher bed depth. The removal efficiency was higher at low flow rate due to increased residence time. Mulugeta et al. [2.31] examined the removal of fluoride employing a variety of adsorbent materials including aluminium hydroxide (AO), activated alumina (AA), and pseudoboehmite (PB). The results of their continuous study revealed that the fluoride adsorption capacity was 10.6 mg/g for AO, 1.9 mg/g for AA, and 2.4 mg/g for PB at feed concentration of 20 mg/L and up flow controlled at 10 empty bed volume per day.

Chen et al. [2.32] reported the adsorption performance of kanuma mud for the removal of fluoride in a batch process and fixed bed column. Continuous studies carried out in a packed column showed that on increasing the column flow rate from 3 to 7 mL/min, the breakthrough time reduced from 39 to 9 hours. Steeper breakthrough curve was obtained at lower bed depth. Breakthrough time was observed to increase at lower fluoride concentration.

Bishayee et al. [2.33] carried out continuous adsorption experiments in a packed bed column using an activated mixture of soil and clay as the adsorbent. The fluoride removal efficiency reached 97% after 20 hours of operation in a column of bed height 15 cm, feed concentration of 10 mg/L, feed flow rate of 4 mL/min, and feed pH 4.5. Sánchez et al. [2.34] performed experimental studies for the removal of fluoride by adsorption using corrosion products modified by aluminum. The authors studied synthetic fluoride solution having 4 mg/L concentration at pH 6.5, and also drinking water

having fluoride concentration of 4 mg/L and pH = 7.4. The adsorption capacity was found to be 0.509 mg/g at 3.5 cm bed depth for synthetic fluoride solution and 0.296 mg/g for drinking water at the same column bed depth.

Rodriguez et al. [2.35] reported the removal of fluoride using a synthetic solution as well as natural fluoride water in a packed column filled with either chitin or a chitin-based bio composite. The most effective bio composite was achieved by combining chitin and polyurethane prepolymer during the polymerization process. At the saturation point (feed concentration = 3.9 mg/L), the bio composite exhibited a fluoride adsorption capacity of 1.7 mg/g, while for chitin it was 3.4 mg/g at 300-bed volumes of feed solution. The fluoride removal efficiency achieved was approximately 85%. Ma et al. [2.36] performed batch and column adsorption studies for the removal of fluoride using granular acid-treated bentonite (GHB) bentonite. Breakthrough time decreased on increasing flow rate and the breakthrough curve becomes steeper. The time required for breakthrough decreased on increasing the feed concentration and breakthrough curve became steeper.

Brunson et al. [2.37] assessed the fluoride removal capabilities of different materials such as bone char, aluminum oxide-coated wood char, aluminum oxide-coated bone char, aluminum oxide-impregnated wood char, and activated alumina as reference material. The column experiments were performed at feed pH 8.2 in a glass column having 2.5 cm internal diameter having 7.1 cm bed height. The adsorption capacity for activated alumina, bone char, aluminum-coated bone char and aluminum-impregnated wood char was 5.9 mg/g, 5.7 mg/g, 6.3 mg/g and 8.3 mg/g respectively at feed fluoride concentration 8.6 mg/L with feed flow rate 1.2 L/min.

Mayorga et al. [2.38] carried out fluoride adsorption study in a fixed bed micro-column packed with the adsorbent metal-modified bone char. The experimental investigation showed that on increasing feed concentration from 10 mg/L to 100 mg/L (pH 7, flow rate = 0.18 L/h) adsorption capacity increased from 3.3 to 14.2 mg/g. Artificial neural network (ANN) showed the best correlation and offered the best data fitting. Sinha et al. [2.39] evaluated through both batch and column

methodologies activated carbon produced from the plant, Eichhornia crassipes that present a substantial global challenge for its disposal. At breakthrough, the capacity of the column for fluoride uptake was calculated to be 4.4 mg/g in a bed containing 10 grams of activated carbon having particle size 50-200 mesh with a bed height of 18 cm, influent concentration of 10 mg/L, solution pH 5.5 and flow rate at 1.7 mL/min.

Mohan et al. [2.40] conducted continuous flow fixed-bed column investigation using hydroxyapatite (HAp)-coated limestone for fluoride removal from water. The adsorbent was formulated by reacting limestone with sodium dihydrogen phosphate. The sorbent displayed defluoridation capacity of 3.86 mg/g in a column packed with 40 g adsorbent with particle size ranging from 0.1 cm to 0.2 cm, feed flow rate of 8 mL/min, and feed concentration of 5 mg/L. Ghosh et al. [2.41] evaluated the effectiveness of agglomerated nanoparticles of Ce (IV)–Zr (IV) mixed oxide (CZO) in removing fluoride from groundwater. Fixed bed column results showed that the adsorption capacity at breakthrough point (q_b) increased from 304 to 424 mg/g as the bed depth was varied from 4.0 to 8.0 cm. On increasing the feed concentration from 3.0 to 7.0 mg/L, $q_b$increased from 304 to 458 mg/g.

Fang et al. [2.42] conducted studies in fixed bed employing various synthetic cation exchange resins and natural adsorption gels loaded with lanthanum (III). The fluoride removal capacity of 200CT resin loaded with lanthanum (III) at pH of 6.0 at the breakthrough point was determined to be 1.05 mol/kg, which is slightly less than the maximum adsorption capacity (1.34 mol/kg) obtained from batch adsorption process. Table 2.2 summarizes the performance reported in a few of the studies.

Table 2.2. Operating Specifications and Adsorption Efficiency for Various Fixed Bed Adsorbents

Adsorbent Used	Operating Conditions	Adsorbent / Volume of Liquid	Adsorption Rate	References
Coconut Husk Activated Carbon	D = 1.0 cm; H = 30 cm; Q = 1.66 mL/min; C_i = 10 mg/L	1.4 g/L	0.0425 mg/L.min	[2.24]
Chemically Treated Activated carbon of seed pods of Bauhinia variegates	D = 3.0 cm; H = 20 cm; Q = 10 mL/min; C_i = 10 mg/L	0.15 g/L	0.1637 mg/L.min	[2.25]
Calcium Impregnated Activated Charcoal	D = 2.5 cm; H = 10 cm; Q = 5.5 mL/min; C_i = 50 mg/L	0.75 g/L	1.246 mg/L·min	[2.30]
Kanuma Mud	D = 5.0 cm; H = 15 cm; Q = 5.0 mL/min; C_i = 20 mg/L	20.0 g/L	0.0123 mg/L·min	[2.32]
Activated Soil-Clay Mixture (laterite soil with silica enriched clay)	D = 1.0 cm; H = 35 cm; Q = 4.0 mL/min; C_i = 10 mg/L	3.4375 g/L	0.00808 mg/L·min	[2.33]
Activated Carbons derived from E. Crassipes.	D = 1.2 cm; H = 18 cm; Q = 1.7 mL/min; C_i = 10 mg/L	10.0 g/L	0.00938 mg/L·min	[2.39]
Hydroxyapatite (HAp)-Coated Limestone	D = 4.0 cm; H = 30 cm; Q = 8.0 mL/min; C_i = 5.0 mg/L	40 g/L	0.001073 mg/L·min	[2.40]

D = diameter of column (cm); H = height of column (cm); Q = feed flow rate (cm^3/min);

C_i = feed concentration (mg/L)

2.1.2 Rotating packed bed

In 1981, Ramshaw and Mallinson pioneered a water oxygen absorption system using a rotating packed bed (RPB) and discovered that its mass transfer coefficient was 27 to 44 times greater than that of traditional packed columns [2.43]. This allows for reduction in the equipment's physical size as well as lower capital and operating expenses [2.44].

A rotating packed bed (Figure 2.2) typically consists of a cylindrical shaped rotor packed with structured packing material, which could be in the form of randomly packed spheres or specially designed structured packing elements. The entire bed is set into motion using a drive mechanism. The axis of rotation could be horizontal or vertical. The centrifugal force generated by the rotation causes the liquid phase to flow as a thin film on the packing surface. This thin film reduces the resistance to mass transfer. The ability to achieve efficient mass transfer in a smaller footprint makes rotating packed beds an attractive option for certain industrial applications.

The flow pattern of liquid within the rotating packed bed (RPB), was investigated by various researchers. Burns and Ramshaw et al. [2.119] reported visual observations on liquid distribution in rotating bed with metal foam as packing material. They noted an inner region of relatively uniform distribution followed by liquid maldistribution. Liquid flowed over the packing as rivulets and droplets rather than film flow. Liquid rivulets extended radially outward leaving large section of the packing dry. The liquid flow through the bulk zone of the packing can be classified into three modes: pore flow, droplet flow, and film flow. In this process, the liquid travels along the inner surfaces of the packing while liquid droplets intermittently cross the void spaces

Guo et al. [2.120] conducted a detailed visual investigation to understand the liquid flow behaviour and residence time distribution of wire mesh and foam metal packing within RPB. The liquid holdup remains below 5%, while the average liquid residence time (depending on the flow rate and rotational speed) typically ranges between 200 and 800 milliseconds. Their observations revealed that as the liquid enters the equipment, it strikes the surface of metal foam packing, undergoes

significant deformation, and experiences intense mixing throughout the bed. They found that apart from the initial impingement zone, the liquid predominantly flows as a thin film coating the surface of the packing while also traversing the void spaces as droplets or jets. This film-like flow pattern enhances contact between phases and promotes efficient mass transfer. Additionally, the study demonstrated that the average residence time of the liquid inside the RPB is strongly influenced by both the liquid flow rate and the rotational speed of the rotor.

Zhang et al. [2.121] employed high-speed stroboscopic photography to examine the liquid flow behaviour on metal foam packing in a rotating packed bed (RPB). Their observations demonstrated that when the rotational speed exceeds 600 rpm, the liquid predominantly takes the form of a thin, continuous film spreading over the surface of the packing material. Simultaneously, a portion of the liquid is dispersed into fine droplets and filaments that move through the void spaces between the packing. This results in an intricate flow regime where both film flow and dispersed liquid particles coexist, with the film and droplets becoming increasingly fine at higher speeds, thereby maximizing the interfacial area for mass transfer. Yan et al. [2.122] carried out a hydrodynamic study to further understand the liquid distribution within an RPB. They also reported that the liquid partially travels as a thin film adhering to the packing surfaces while the remaining fraction is dispersed as small droplets and thread-like filaments that are propelled through the open spaces in the packing.

Micromixing refers to the diffusive mixing of chemical species at the molecular scale, plays a critical role in chemical reactors, especially for fast and complex reactions. Micromixing occurs through laminar stretching, turbulent erosion, shrinking, and molecular diffusion [2.123]. These processes reduce segregation and facilitate reactions at the molecular level. Rotating packed beds (RPBs) improve micromixing performance significantly. The efficiency of micromixing is characterized by the Segregation index (X_s), [2.124]. The value of X_s is between 0 to 1. The segregation index X_s = 0, indicates maximum micromixing, and X_s = 1 suggest total segregation [2.125].

Chu et al. [2.128] studied micromixing in rotating packed beds (RPBs) with different packings. A novel surface-modified nickel foam packing (SNP) showed superior performance over non-modified nickel foam (NNP) and stainless-steel wire mesh (SWP), as indicated by lower segregation index (X_s). For SNP, X_s decreased from 0.011 to 0.008 with speed (200–1600 rpm) and from 0.011 to 0.003 with flow rate (200–800 mL/min).

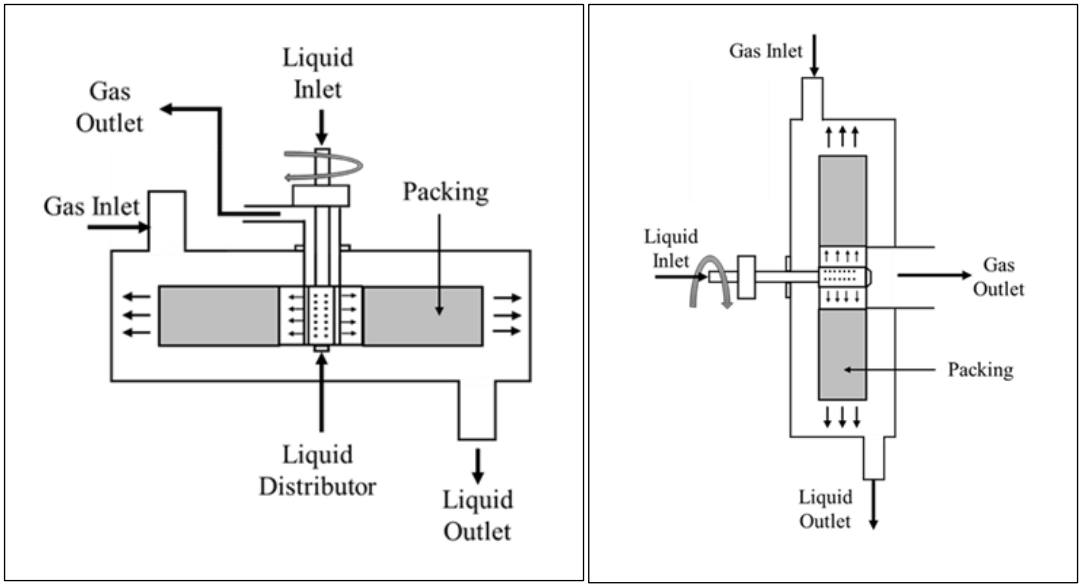

(a) Horizontal axis **(b)** Vertical axis

Figure 2.2: Schematic Diagram of Rotating packed Bed

Munjal et al. [2.45] reported the volumetric solid-liquid mass transfer coefficient in this equipment using naphthalene-water system. The bed was packed with naphthalene beads. The values were 4-6 times higher compared to gravity flow in conventional packed bed at centrifugal acceleration of 50g – 150g.

2.1.3 Rotating packed bed adsorber

Various investigators carried out studies by packing adsorbent into the rotating bed. Das et al. [2.46] studied the removal of Cu (II) with scales of *Catla - Catla* fish in a rotating packed bed adsorber (RPBA). These studies were carried out by recirculating a fixed volume of feed solution through the bed packed with fish scales. They noted the possibility of bed compaction under the influence of

centrifugal force. High flow rate had a negative effect on adsorption efficiency. The study determined that mass transfer per unit volume increases by ~ 2.4 times compared to fixed bed adsorber. The amount of Cu (II) adsorbed per mass of adsorbent increased with rotational speed and flow rate.

Lin et al. [2.47] studied the removal of a dyestuff, Basic Yellow 2 using activated carbon in this equipment with continuous re-circulation of feed solution through the bed. They used pseudo first order kinetic rate equation to represent the experimental data and also determined the apparent diffusion coefficient. The equilibrium uptake was ~16.25 mg/g at feed concentration of 205 mg/L (rotational speed = 1600 rpm). Kundu et al. [2.48] studied the application of rotating packed bed adsorber for removal of dyestuff Direct Red 23 by activated carbon. Pseudo first order model gave better fit to the experimental data. They noted that rotor speed and flow rate significantly influence removal efficiency.

Chang et al. [2.49] reported the breakthrough curve in RPBA for removal of pesticide methomyl with activated carbon and also compared the performance of rotating packed bed adsorber and batch adsorption. The time required to reach the feed concentration at the outlet in breakthrough studies increased with rotational speed, and decreased with increase of flow rate. Panda et al. [2.50] studied the removal of Cr (VI) using crude tamarind fruit shell in RPBA. They noted that the removal occurs due to reduction of Cr (VI) to Cr (III). The removal rate of Cr (VI) increased with decrease in particle size and at lower pH. Modak et al. [2.51] developed a mathematical model for analyzing the removal of methylene blue using rice husk. The volumetric mass transfer coefficient was assumed to decrease with radial distance. They also noted that the removal efficiency of a RPBA divided into smaller beds and operated in series is higher.

Li et al. [2.52] used Artificial Neural Network to model the adsorption in RPBA. They noted that ANN gave better prediction than multiple nonlinear regression. Hasim et al. [2.53] used Taguchi method to optimize the removal of Arsenic by activated carbon. The optimum conditions were

rotating speed of 1600 rpm, packing density of 510 kg/m^3, initial concentration of 150 mg/L and pH 3. Decolorization of Reactive Red 2 using nanoscale zero-valent iron was studied in RPBA. A pseudo first order model was used to describe the adsorption process during the initial period.

2.2 Precipitation and Coagulation for Fluoride Removal

Precipitation and coagulation are extensively utilized techniques for eradicating impurities such as heavy metals and specific inorganic ions from wastewater. The selection of precipitants and coagulants relies on considerations like the quality of the water, pH levels, fluoride concentrations, and the existence of accompanying ions and impurities. Numerous substances and agents are employed for the removal of fluoride, which includes:

1) Precipitants involving Calcium**:** Calcium compounds like calcium chloride and calcium hydroxide find application in fluoride removal utilizing precipitation.
2) Coagulants with Aluminum: Aluminum-based coagulants, including aluminum sulfate (alum), poly aluminum chloride (PAC), and aluminum chloride, are frequently employed in coagulation-flocculation procedures for fluoride removal.
3) Coagulants containing Iron: Coagulants based on iron, including ferric sulfate and ferric chloride, are applied to eliminate fluoride from water.
4) Zirconium Salts: Zirconium compounds, like zirconium chloride, have been explored for their coagulation potential in the context of fluoride removal.
5) Coagulants with Titanium: Poly aluminum-titanium chloride (PATC) serves as an illustration of a coagulant that incorporates both aluminum and titanium elements.
6) Lime: In specific instances, calcium hydroxide (lime) can be employed to jointly precipitate fluoride along with other contaminants.

Reardon et al. [2.54] examined the elimination of fluoride in a dual-column limestone reactor. The reactor operated by dissolution of calcite ($CaCO_3$) and the precipitation of fluorite (CaF_2). In

laboratory trials, the effluent fluoride concentration from feed containing initial fluoride levels of 109 mg/L was successfully reduced to meet the maximum contaminant level threshold of 4 mg/L within a 2-hour residence time inside the column.

Chang et al. [2.55] explored the removal of fluoride from waste water of semiconductor manufacturing industries using calcium-based chemical precipitation. The researchers carried out experiments using a Jar test with the primary goal of examining the coagulation and flocculation of calcium fluoride (CaF_2) precipitates. Under specific conditions with a calcium-to-fluoride (Ca^{2+}/F^-) molar ratio of 0.5 and a pH ranging from 6.5 to 8.5, the residual fluoride concentration in the effluent was reduced to less than 15 mg/L. The fine CaF_2 precipitates were subsequently subjected to flocculation using polyaluminum chloride (PAC) and an anionic polyelectrolyte called polyacrylic acid (PAA). The experimental results of the investigation indicated that both PAC and low to medium molecular weight PAA effectively removed CaF_2 precipitates.

Dubey et al. [2.56] determined the most effective dosage of aluminum sulfate (alum) and poly aluminum chloride ($PACl$) for removing fluoride from drinking water. The experimental investigation revealed that after treating water with alum, the remaining fluoride, turbidity, and total dissolved solids (TDS) were measured at 1.3 mg/L, 7 NTU, and 280 mg/L, respectively, for initial fluoride concentration of 4 mg/L. The corresponding values using $PACl$ were lower at 0.48 ppm, 4 NTU and 200 mg/L respectively. Aoudj et al. [2.57] focused on defluoridation employing two types of coagulants-ferric sulfate and aluminum sulfate using jar test. The author noted that aluminum sulfate yielded the highest fluoride removal.

Batch study for removal of fluoride was performed by Wang et al. [2.58] using nano-scale aluminum oxide hydroxide ($AlOOH$). Fluoride removal was over 90% for pH levels between 6 to 8. The efficiency decreased as pH value rose to 11. Nano- $AlOOH$ exhibited a peak fluoride capacity of 3259 mg/kg at approximately pH 7, indicating that nano- $AlOOH$ has the potential to serve as an adsorbent for treating drinking water.

Ozairi et al. [2.59] conducted defluoridation employing coagulation and flocculation methods. They used aluminum sulfate, poly aluminium chloride, and ferric chloride as coagulants. The experimental study was performed in the Jar tester with initial fluoride concentration ranging from 4 to 20 mg/L. This jar test comprised of three stages: coagulation, flocculation, and sedimentation. The results indicated that the highest fluoride removal achieved was 57% for Alum, and 50% for $PACl$ at pH 4, and 53% for Fe^{3+}at pH 8. The most efficient removal (83%) was achieved with 30 mg/L of aluminum sulfate with minimal turbidity.

Zhang et al. [2.60] investigated removal of fluoride using aluminium sulphate as coagulant. Sodium hydroxide was used to supply hydroxide ions for pH adjustment. Removal efficiency of ~75% was achieved in optimal pH range between 6 and 6.7. Gong et al. [2.61] explored the impact of aluminum fluoride complexation on fluoride removal. This study involved a comparison between coagulation with $Al-F$ complexation and adsorption using $Al(OH)_3$ flocs without complexation. Coagulation studies were performed at pH 6.0, 7.0 and 8.0. Experimental observations suggested that complexation was formed between Al and fluoride at acidic condition. On increasing pH to 7, the complexes dissociated into free fluoride. The highest removal of fluoride was observed at 7 pH condition. They also noted that removal of fluoride was faster with coagulation compared to adsorption onto flocs.

In recent years, extensive research has explored the use of zirconium Zr salts as coagulants in water treatment. Among them, inorganic Zr salts particularly zirconium chloride ($ZrCl_4$) have demonstrated high efficiency in removing both organic matter and fluoride [2.62–2.65].

Their study included coagulation using a programmable jar test device to assess the efficiency of $ZrCl_4$ coagulation for fluoride removal. Additionally, they compared the results with those obtained using the commonly used $Al_2(SO_4)_3$ as a reference. The optimal pH range was determined to be 4.0 to 6.0 for $ZrCl_4$ and 8.0 to 10.0 for $Al_2(SO_4)_3$. The researcher noted that $ZrCl_4$ out performed

$Al_2(SO_4)_3$ in terms of fluoride removal when the initial fluoride concentration was below 30.0 mg/L.

Zhang et al. [2.66] studied the effectiveness of fluoride elimination using two coagulants, namely poly aluminum-titanium chloride *(PATC)* and poly aluminum chloride ($PACl$). *PATC* displayed notably superior efficiency in removing fluoride compared to $PACl$. In the case of PATC, fluoride removal efficiency steadily increased with dosage, peaking at 73.4% with a dosage of 0.8 mmol/L and then stabilizing. The removal efficiency with $PACl$ also increased with dosage, reaching values of 53.2% and 65.1% at dosages of 0.8 mmol/L and 1.0 mmol/L, respectively. The inclusion of titanium offered additional attachment sites for fluoride making it more efficient.

Ayoob et al. [2.67] conducted a comprehensive review of various methods employed in eliminating fluoride. In the precipitation and coagulation process, the author discussed the utilization of lime $\left(Ca(OH_2)\right)$ or alternative calcium salts (like $CaSO_4$, $CaCl_2$) for precipitation of fluoride in the form of insoluble CaF_2. The effectiveness of lime-based fluoride removal can be enhanced by incorporating $CaCl_2$-lime mixture. This combination benefits from the high solubility of $CaCl_2$, which supplies more calcium than lime while maintaining a stable pH. Magnesium oxide and calcium phosphate compounds were also employed in the precipitation technique to eliminate fluoride. Furthermore, the author discussed the utilization of alum for co-precipitating fluoride.

2.2.1 Nalgonda Technique

The first community defluoridation facility designed to eliminate fluoride from drinking water was established in the Nalgonda district of Andhra Pradesh, specifically in Kadri town based on the precipitation and coagulation technique. This technology was innovated by the National Environmental Engineering Research Institute (NEERI), located in Nagpur in 1961. The Nalgonda technique became famous because of its low-cost operation. In this technique, the required quantity of alum, lime, and bleaching powder was mixed in the fluoride-containing water to remove fluoride. The whole mixture was rapidly mixed followed by flocculation, sedimentation, filtration, and

disinfection [2.67]. In this process, the concentration of alum and lime to be added depends on the concentration of fluoride that need to be removed. Aluminium sulfate ($Al_2(SO_4)_3 18H_2O$) was used as a source of Al ions and Calcium hydroxide $Ca(OH)_2$ as a source of calcium ions.

Lime facilitates the precipitation of fluoride and the forming insoluble calcium fluoride (CaF_2). After the addition of aluminium sulphate (Alum) into water, entire solution becomes acidic. The acidic nature of the solution is minimized by the adding Calcium hydroxide (Lime), which helps to increase the pH and neutralize the solution. Aluminium sulphate (Alum) on addition of calcium hydroxide (Lime) forms microflocs of gelatinous aluminium hydroxide [$Al(OH)_3$] in the water by hydrolysis. These micro-flocs attract negatively charged ions through electrostatic forces. In sweep coagulation, fluoride ions get adsorbed onto the surface of sticky, gelatinous aluminium hydroxide [$Al(OH)_3$] flocs, and subsequently removed through coprecipitation with the flocs [2.67].

The following equations represent the process of removal of fluoride [2.68].

Dissolution of Alum:

$$Al_2(SO_4)_3 18H_2O = 2Al^{3+} + 3SO_4^{2-} + 18H_2O \quad (2.1)$$

Precipitation of Aluminium (Acidic):

$$2Al^{3+} + 6H_2O = 2Al(OH)_3 + 6H^+ \quad (2.2)$$

Co-precipitation:

$$F^- + Al(OH)_3 = Al - F\ complex + undefined\ product \quad (2.3)$$

Adjustment of pH:

$$6Ca(OH)_2 + 12H^+ = 6Ca^{2+} + 12H_2O \quad (2.4)$$

Formation of calcium fluoride

$$Ca(OH)_2 + 2F^- \rightarrow CaF_2 + 2OH^- \quad (2.5)$$

Industrially, continuous defluoridation is based on Nalgonda technique and is performed in two separate continuous stirrer tank reactors. Figure 2.3 shows the industrial process of Nalgonda technique. In the first continuous stirrer tank reactor (CSTR-1), lime and the fluoride contaminated

water is mixed. The fluoride ions are removed by precipitation reaction between Ca^{2+} ions with the fluoride (F^-) ions through the formation of CaF_2 precipitates.

The stream then passes into a second continuous stirrer tank reactor (CSTR-2), where aluminum salt is added. The addition of alum results in the formation of gelatinous aluminium hydroxide $Al(OH)_3$ flocs on to which fluoride ions are adsorbed.

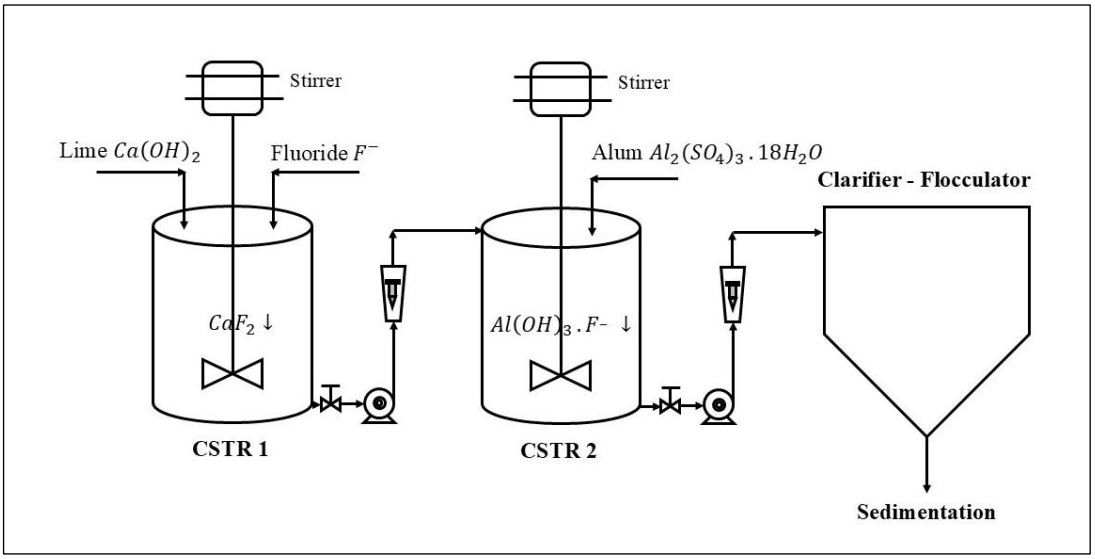

Figure 2.3: Industrial process of Defluoridation by Nalgonda technique

Process modification of the Nalgonda technique was done by Zewge et al. [2.69]. In their investigation, the authors prepared aluminum hydro(oxide), AO from aluminum sulfate found in the local area. This AO was then employed to eliminate fluoride from water. The efficiency of fluoride removal through this combined method was examined through a series of batch experiments. The combined approach achieved roughly 93% removal efficiency when utilizing an ideal mixture of alum and AO (80 mg alum/mg F, 5 mg AO/mg$F$), with lime making up 35% of the alum dose, and an initial fluoride concentration of 15 mg/L. The optimal pH range for effective fluoride removal was identified to be within 5 to 9.

2.3 Liquid-Liquid Extraction of Phenol removal

Phenolic compounds are commonly produced as secondary products in different industrial procedures. These substances represent a noteworthy hazard to the well-being of land-based and water-based ecosystem [2.70]. Scientists have employed diverse methods to eliminate phenol from wastewater. The operational ease, elevated efficacy, and loading capabilities render liquid-liquid extraction superior to other purification approaches [2.71].

Jiang et al. [2.72] carried out liquid-liquid extraction batch studies for removing phenol from wastewater using alcohols, amines, and organic acids. For the experimental study, the authors used wastewater having an initial phenol concentration of 6000 mg/L, 5% salt content, and a COD_{Cr} of 18200 mg/L, originating from chemical plants. The research indicated that the effectiveness of alcohol was much more than amines or organic acids. Among the alcohols, those with longer hydrocarbon chain had higher efficiency.

Abbassian et al. [2.73], investigated the removal of phenolic contaminants from wastewater using Iso-kerosene. The highest distribution coefficient was ~2.3 achieved at 50 °C, pH of 6 and phenol concentration of 100 mg/L. A hydrophobic magnetic room temperature ionic liquid (MRTIL), $[3C_6PC_{14}][FeCl_4]$, was synthesized and explored for the solvent extraction of phenolic compounds from aqueous solutions by Deng et al. [2.74]. The experimental investigation showed that the ionic liquid exhibited significantly superior extraction efficiency than other traditional non-magnetic room temperature ionic liquids under identical experimental condition. Researchers used various extractant for the removal of phenol and phenolic compounds. The distribution coefficient reported or calculated from the experimental result are given in Table 2.2.

Another aspect that affects the extraction efficiency is the design of mass transfer contactors. Some of the conventional extractors are discussed in the following paragraphs. In these contactors, the flow hydrodynamics is dictated by terrestrial gravity.

Table 2.3. Various Extractant used for phenol extraction

Phenol Concentration	Extractant	Distribution Coefficient	References
5 mg/L	Tributyl Phosphate [TBP]	450	[2.75]
279.5 g/L	Cyanex 923	0.6 – 9.0	[2.76]
1500 – 3000 mg/L	Diisopropyl ether (DIPE)	36.5	[2.77]
1500 – 3000 mg/L	Methyl isobutyl ketone (MIBK)	100	[2.77]
2.0 g/L	DIO (70.1% n-octanol and 29.9% 2-octanone)	44.9	[2.78]
1.0–3.0 g/L	Toluene	1.5	[2.79]
0.5–10.0 g/L	Kerosene	0.22	[2.80]
2500-3000 mg/L	Aliquat 336	329.5	[2.81]

2.3.1 Conventional contactors

2.3.1.1 Spray Column

Spray tower features an empty shell with inlet and outlet connections at the top and bottom of the tower for introduction and exit of the heavy and light liquid phases [Figure 2.4 (a)]. Benefits of spray column include its uncomplicated design, and lack of internal elements such as plates or packing, which contributes to elevated throughputs per unit cross-sectional area. However, achieving more than one or two theoretical stages is practically challenging. A reason for suboptimal efficiency can be attributed to axial mixing in the continuous phase.

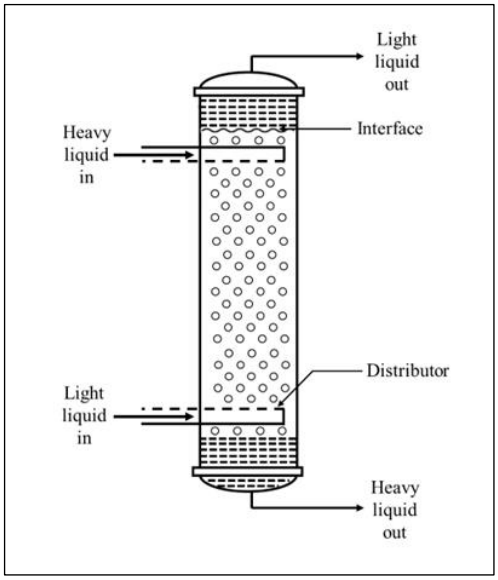

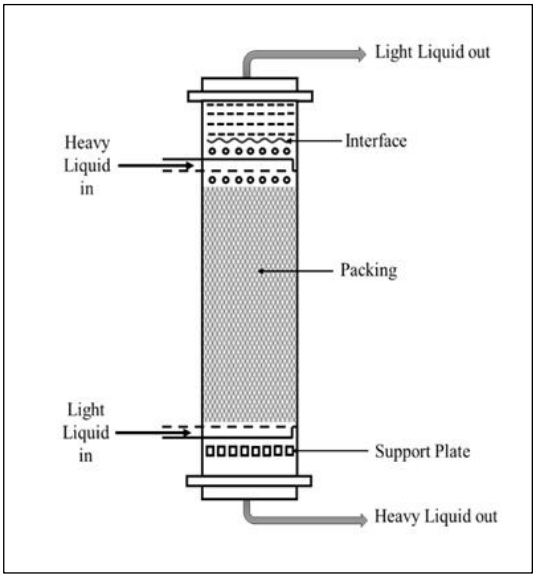

Figure 2.4 (a) **Figure 2.4 (b)**

Figure 2.4 (a) Spray Tower **(b)** Packed tower (for light liquid dispersed)

2.3.1.2 Packed Column

The packed towers commonly employed for gas-liquid system find application in liquid-liquid extraction as well. Figure 2.4 (b) shows a packed tower/column configured for dispersion of the light phase. The structure comprises of a cylindrical shell filled with packing material resting on a support plate. The presence of packing material results in substantial increase of interfacial area for phase interaction, leading to coalescence and reforming of drops. Consequently, packed towers exhibit significantly higher mass transfer rates compared to spray towers. The drawbacks of this equipment are liquid mal-distribution, and the tendency for solids to accumulate in the packing.

2.3.1.3 Perforated Plate/Sieve Tray Tower/Column

The perforated plate tower depicted in Figure 2.5 is designed for the dispersion of light liquid. These contactors operate as multistage, counter-current units where axial mixing of the continuous phase is limited to the space between trays. Re-dispersion occurs at each tray, enhancing mass transfer efficiency. It is particularly effective for systems with low interfacial tension. These contactors excel in both liquid handling capacity and extraction efficiency.

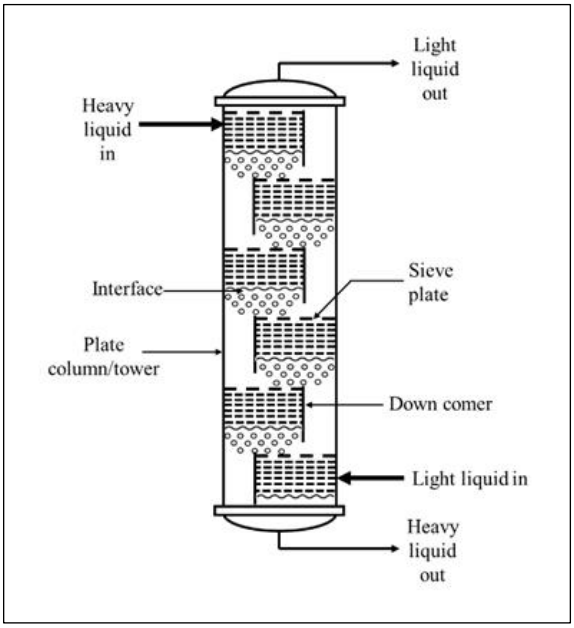

Figure 2.5: Perforated plate extraction column for continuous counter current flow

2.3.1.4 Mechanically Agitated Extraction Column

Many differential contactors utilize rotary agitation for phase dispersion. These extraction columns consist of a vertical structure housing a centrally positioned rotating shaft and internal impellers. The purpose of the rotating shaft is to agitate the fluids within the column. Mechanically agitated extraction columns include Scheibel extractor [Figure 2.6 (a)], Rotating disc contactor [Figure 2.6 (b)], Oldshue–Rushton extraction column [Figure 2.6 (c)], and Kuhni extractor [Figure 2.6 (d)].

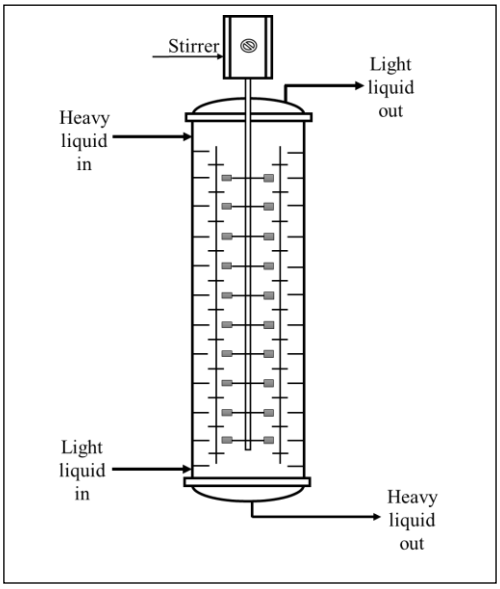

Figure 2.6 (a)

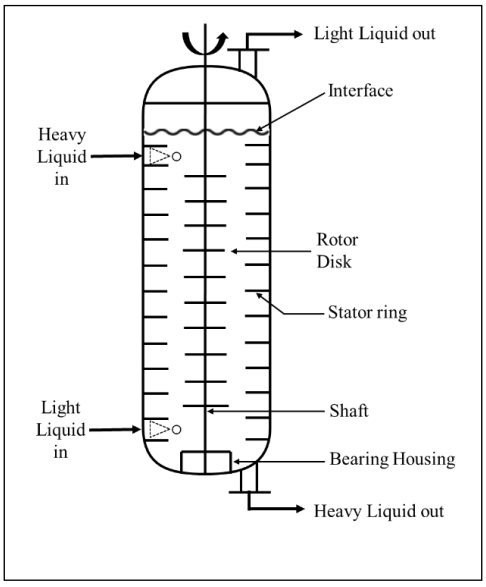

Figure 2.6 (b)

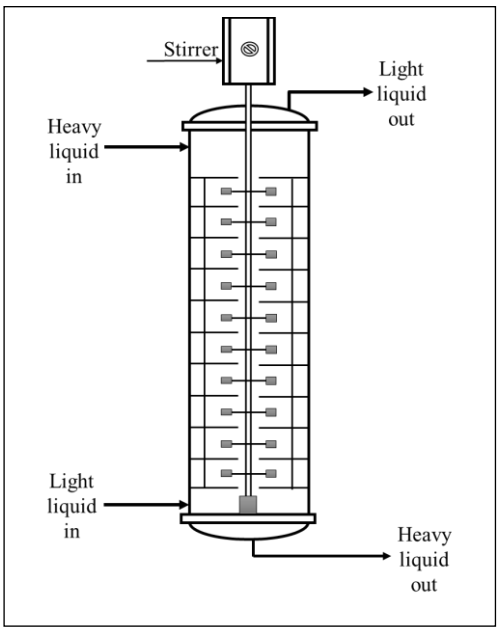

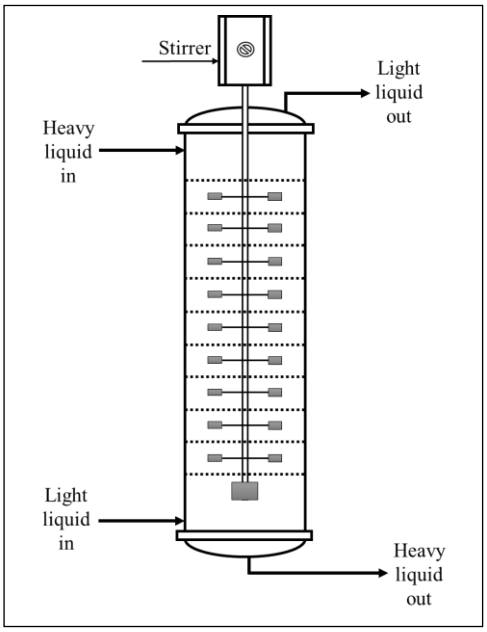

Figure 2.6 (c) **Figure 2.6 (d)**

Figure 2.6: Schematic diagram **(a)** Scheibel Extraction Column, **(b)** Rotating Disk Contactor (R.D.C.), **(c)** Oldshue–Rushton extraction Column, **(d)** Kuhni Extraction Column

Khorshidi and Esmsileli et al. [2.82] studied the system toluene/acetone/water in spray and packed column. They reported the value of sauter mean diameter and mass transfer coefficient in these extractors. At large values of Reynold's number, dispersed phase mass transfer coefficient, K_d is higher in packed bed in comparion to spray column. They also reported that K_d approached a maximum value and then decreased in both the extractors. The values of K_d was in the range of 10^{-5} m/s. Sovilj et al. [2.83] reviewed the hydrodynamics of spray and packed columns, compiling equations for slip velocity, Sauter mean diameter, and axial dispersion coefficient. Verma et al. [2.84] reported the effect of different types of packing on volumetric mass transfer coefficient based on continuous phase ($K_c a$) in packed column with different systems. The magnitude of $K_c a$ in packed column for all the packing studied was greater than spray column. Among the packings studied, 5/8" stainless pall ring was associated with the highest value of $K_c a$. Seibert et al. [2.85] studied two systems in spray and packed bed extractors namely, toluene/acetone/water and 1-

butanol/succinic acid/water. The overall volumetric mass transfer coefficient ($K_{oc}a$) was in the range of 10^{-3} s^{-1}. No. 15 IMPT packing gave better mass transfer characteristics in comparison to others studied.

NII et al. [2.86] reported the volumetric mass transfer coefficient for mixer settler by contacting heptane with an aqueous solution of I_2/KI. The magnitude varied between 0.08 s^{-1} to 4 s^{-1}. The overall mass transfer coefficient reported based on Sherwood number was higher when mass transfer was from dispersed to continuous phase. They proposed the following equation to correlate their experimental data.

$$Sh_{oc} = -40 + 23Re_r^{1/3} \tag{2.6}$$

where Re_r is based on droplet velocity in swarm. Torab-Mostaedi et al. [2.87] reported the volumetric mass transfer coefficient based on continuous phase for toluene/acetone/water system in a Hanson mixer settler extraction column. The coefficient reached a maximum value at agitator speed of 350 rpm at constant organic and aqueous flow rate and then decreased. The value of volumetric mass transfer coefficient based on continuous phase was reported to vary between $2.5 \times 10^{-3}\ s^{-1}$ and $7.5 \times 10^{-3}\ s^{-1}$. The continuous phase axial dispersion coefficient and volumetric mass transfer coefficient based on dispersed phase ($K_{od}a$) in Kuhni extraction column was studied by Dongaonkar et al. [2.88] for methyl isobutyl ketone/acetic acid/water system. The magnitude of mass transfer coefficient based on dispersed phase was in the range 0.7s^{-1} to 0.9 s^{-1}. Hemmati et al. reported $K_{od}a$ in Kui column for n-butyl acetate-acetone-water and toluene/acetone/water system. The values varied from $1.0 \times 10^{-3}\ s^{-1}$ to $3.5 \times 10^{-3}\ s^{-1}$ for the range of operating conditions studied.

Kumar and Hartland [2.89] proposed the following equations for calculating the mass transfer coefficients in rotating disk contactor.

$$\frac{Sh_c/_{1-x_d} - Sh_{c,rigid}}{Sh_{c,\infty} - Sh_c/_{1-x_d}} = 0.0526Re^{\left(\frac{1}{3}+0.0659Re^{0.25}\right)}Sc_c^{1/3}\left(\frac{V_s\mu_c}{\sigma}\right)^{1/3} \tag{2.7}$$

$$Sh_{c,rigid} = 2.43 + 0.775Re^{1/2}Sc^{1/3} + 0.0103ReSc_c^{1/3} \quad (2.8)$$

$$Sh_{c,\infty} = 50 + \frac{2}{\sqrt{\pi}} Pe_c^{1/2} \quad (2.9)$$

$$Sh_d = 17.7 + \frac{0.00319\left(ReSc_d^{1/3}\right)^{1.7}}{1+0.0143\left(ReSc_d^{1/3}\right)^{0.7}} \left(\frac{\rho_d}{\rho_c}\right)^{2/3} \frac{1}{1+k^{2/3}} \quad (2.10)$$

Hemmati et al. [2.90] reported that the magnitude of overall volumetric mass transfer coefficient based on dispersed phase ($K_{od}a$) varied between $7 \times 10^{-3}\ s^{-1}$ to $12 \times 10^{-3}\ s^{-1}$ for toluene-acetone-water system in perforated rotating disc contactor for rotational speed of 180 rpm and dispersed velocity varying between 5×10^{-4} m/s and 10×10^{-4} m/s. For n-butyl acetate-acetone-water, $K_{od}a$ was found in the range $8.5\times 10^{-3}\ s^{-1}$ and $11 \times 10^{-3}\ s^{-1}$. Martunus et al. [2.91] estimated the continuous-phase mass transfer coefficient in a rotating disk contactor by accounting for forward mixing. For the kerosene–acetic acid–water system, the coefficient ranged from 0.02 to 0.5 m/s as the agitator speed and the velocity ratio of dispersed to continuous phase varied between 1.1 and 5. Asadollahzadeh et al. [2.92] reported the extraction of Lanthanum and Cerium ions using the extractant D2EHPA diluted in kerosene in Scheibel column. They found that forward mixing model gave better fit to the experimental data as compared to backflow model and axial dispersion model. At continuous and dispersed phase flow rate of 30 L/h each and rotation speed of 155 rpm, the magnitude of $K_{od}a$ was 0.01224 s^{-1} for Lanthanium and 0.0256 s^{-1} for Cerium ions.

2.4 Centrifugal Extractors

The traditional extractors rely on gravitational force for counter-current flow of immiscible fluid phases. In centrifugal contactors, gravitational force is substituted with centrifugal force, achieved by rotating the extractor around a horizontal or vertical axis. Within this extractor, denser fluid moves radially outward. The advantages of centrifugal extractors include enhanced specific surface area, interphase velocity, low liquid holdup, rapid steady-state attainment, very high volumetric mass transfer coefficients, and reduced operational and maintenance costs. Examples of such

extractors include the Podbielniak type, the Alfa Laval centrifugal reactor, and the Luwesta centrifugal reactor.

2.4.1 Podbielniak extractor

The Podbielniak centrifugal extractor (Figure 2.7) comprises of a rotating cylindrical drum with multiple concentric shells. The denser liquid phase enters through the central shaft. If this phase is dispersed, the droplets are propelled radially outward to the drum's rim under centrifugal force. The less dense liquid phase is introduced at the rim, flowing radially inward. The internal shells facilitate consecutive coalescing and dispersion steps.

Todd and Davies reported the performance of a Podbiellniak extractor of i.d. 58 cm, rotor width 25 cm operating at over 3000 rpm. For extraction of n-butyl amine from kerosene using water, the number of stages varied between 3.6 to 6.7 for kerosene and water flow rate of 3.4 m^3/h and 1.7 m^3/h respectively.

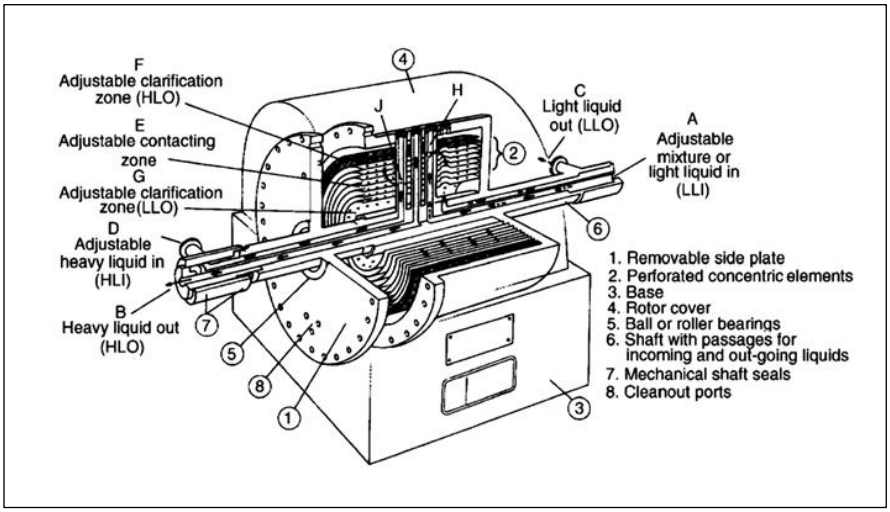

Figure 2.7: Schematic diagram of Podbielniak Extractor [2.118]

2.4.2 Rotating Spray Column extractor

The rotating spray column (Figure 2.8) is a cylindrical structure rotating about a horizontal or vertical axis. The denser phase enters near the rotational axis, while lighter phases is introduced at the opposite end. Centrifugal acceleration causes the outward movement of the denser phase,

displacing the lighter phase inward. The separation efficiency was 10-100 times superior to conventional spray columns.

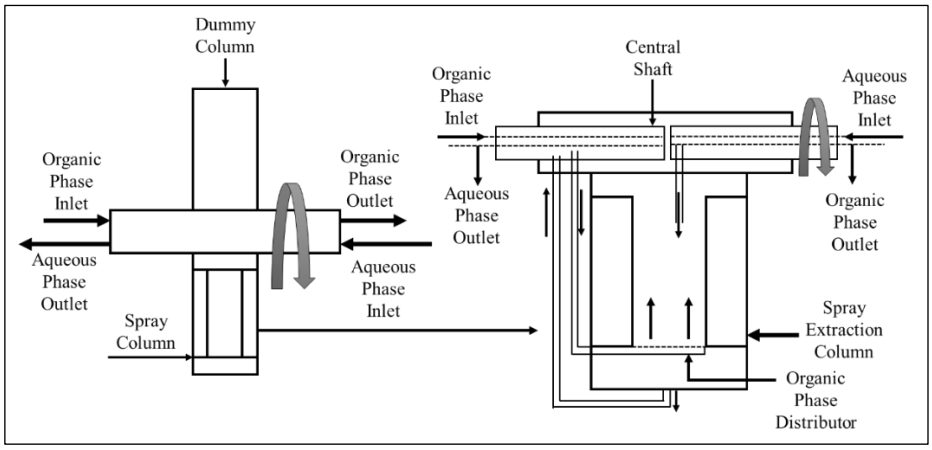

Figure 2.8: Schematic diagram of Rotating Spray Column

2.4.3 Other rotating contactors

In addition to rotating packed bed, various rotor designs have been developed, including waveform disk, helical, zigzag, spiral, multistage spraying, and split packing (Figure 2.9) configurations [2.121- 2.130]. Two of these designs are detailed in the following paragraphs.

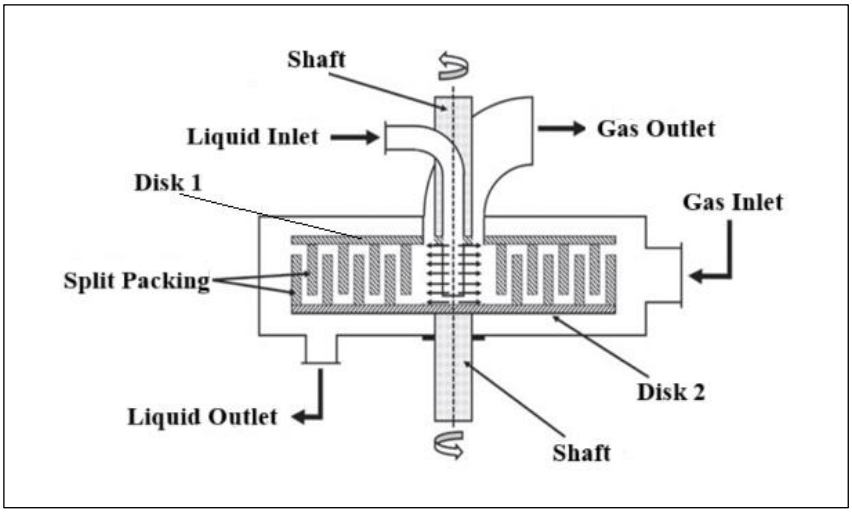

Figure 2.9: Schematic diagram of rotating packed bed with split packing

2.4.3.1 Rotating Zigzag Bed

The Rotating Zigzag Bed (RZB) illustrated in Figure 2.10 is an innovative contactor incorporating High-Gravity (HIGEE) technology. It features a rotor that couples a rotating disc with a stationary one. Concentric circular sheets are affixed to the rotational and stationary discs. These sheets include rotational baffles and stationary baffles, staggered alternately in a vertical direction. The perforated upper part of the rotational baffles is fixed to the lower disc, driven by a motor through a vertical shaft, while stationary baffles are fixed to the upper disc. For gas-liquid operation, the former phase is introduced into the casing and flows inward through the rotor due to pressure differences. The liquid, introduced at the center of the upper disc and flows outward facilitated by centrifugal force. A part of the liquid flows as droplets through the perforations. Wang et al. [2.129] noted that there are three gas-liquid mass transfer zones in the contactor- cross current contact between liquid droplets from the perforations and the gas; countercurrent contact when liquid falls along stationary baffles, and cross current contact when liquid travels from the edge of the rotating baffles onto the stationary baffles.

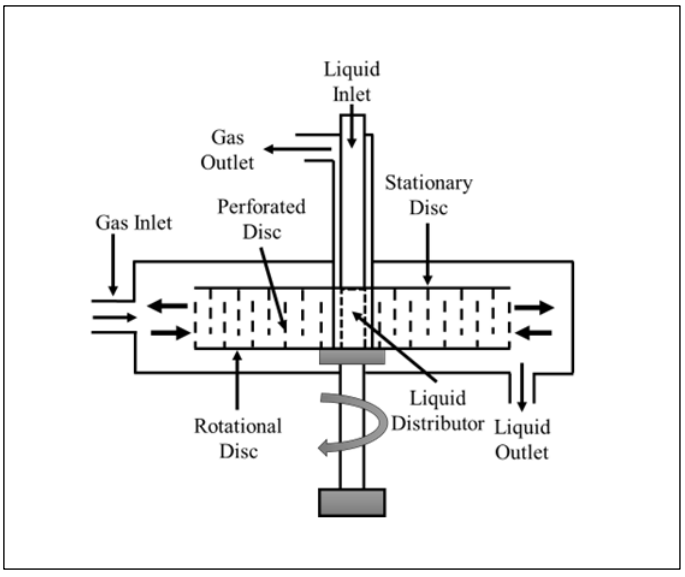

Figure 2.10: Schematic diagram of Rotating Zig-Zag Bed (RZB)

Yumin et al. [2.104] explored the effect of operating parameters on pressure drop, energy consumption in perforated and shutter-type baffle designs in rotating zigzag bed (RZB) using air–water system and examined. They found that high-velocity liquid jets through the baffle openings generate fine droplets, which help lower the unit's pressure drop when liquid is present by 16.2% with perforated baffles, and 30.1% with shutter baffles at 600 m^3/h gas flow and 1000 rpm.

Li et al. [2.126] studied liquid entrainment and flooding in a rotating zigzag bed (RZB). Entrainment occurs as both droplets and films patterns and observed that the film entrainment being dominant. The experimental finding noted that both droplet and film entrainment increase with gas flow rate and liquid flow. As increasing the rotational speed of RZB, the droplets and film entrainment initially decrease then increases with higher rotation speeds.

Li et al. [2.102] investigated the effective interfacial area and local liquid-side mass-transfer coefficient within the Rotating Zigzag Bed (RZB) through CO_2 absorption in NaOH solution. Results revealed an increase in effective interfacial area (from 125-345 m^2/m^3) and local liquid-side mass transfer coefficient (from 0.0025-0.003 m/s) as rotational speed varied from 800-1400 rpm.

Wang et al. [2.103] investigated gas–liquid mass transfer in rotating zigzag beds (RZBs) using ethanol - water distillation systems with multirotor configurations. Their studies demonstrated that RZBs significantly enhance mass transfer by increasing gas - liquid contact time. The number of theoretical plates increased with rotor speed, while efficiency initially declined at low reflux before stabilizing. For example, at 1100 rpm, the number of theoretical plates decreased from 15 to 10 as the reflux flow rate rose from 100 to 600 L/h.

2.4.3.2 Rotating Spiral Bed

The origin of the rotating spiral contacting concept is mainly credited to Podbielniak's early patents in the 1930s (Podbielniak 1935, 1936, 1937, 1938) [2.93 - 2.97]. A rotating spiral bed (RSB) is composed of a drive motor, a sealed unit, and a spiral channel element (Figure 2.11). The liquid flows as a layer on the channel wall. The flow resembles the falling film in a wetted-wall tower

[2.98 - 2.101]. Unlike gravity-driven liquid in wetted wall towers, RSB utilizes centrifugal force, stabilizing layer flow on the channel wall and enabling significantly larger specific throughput.

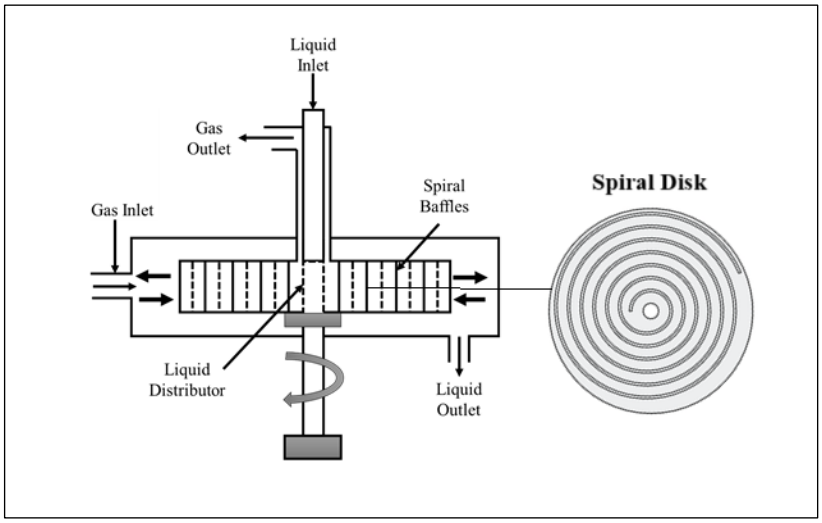

Figure 2.11: Schematic diagram of Rotating Spiral Bed (RSB)

Chen et al. [2.127] investigated CO_2 capture in a rotating spiral contactor (RSC) with a 2.5-revolution spiral channel (0.94 m total length). The contactor operated efficiently across a wide range of gas–liquid ratios, reaching 2700 at 1200 rpm, with film thickness remaining below 400 µm under tangential accelerations of 6.7–26.8 $m \cdot s^{-2}$ for a liquid viscosity of 14 $mPa \cdot s$. Film thickness was influenced by screw pitch, rotational speed, liquid flow rate, and viscosity, with higher liquid flow rates thickening the film but higher speeds counteracting this effect. Mass transfer studies showed that rotational speed had little effect on the overall gas-phase mass transfer coefficient (KG_{ae}) and capture efficiency (η), with only slight increases observed between 800 and 1000 rpm. In contrast, increasing the gas flow rate reduced KG_{ae} from 2.94 to 2.54 $kmol \cdot m^{-3} \cdot h^{-1} \cdot kPa^{-1}$ and η from 88% to 47% at 0.2 CO_2 lean loading, while lowering CO_2 loading from 0.32 to 0.2 increased η by ~30%. The maximum volumetric mass transfer coefficient reached 6.4 $kmol \cdot m^{-3} \cdot h^{-1} \cdot kPa^{-1}$, with capture efficiencies ranging from 38% to 98% at gas–liquid ratios of 200–1000.

However, limited research exists on liquid-liquid extraction in these rotating contactors. Modak et al. [2.105] investigated the extraction of methyl red dye using xylene in an RPB contactor, examining the impact of rotational speed and flow rates on percentage removal. The study achieved a notable maximum stage efficiency of approximately 0.98 and volumetric mass transfer coefficient between 0.015 and 0.205 s^{-1}. These values surpass those of conventional counter-current extractors namely, spray columns, packed beds, and mixer settlers by 25-40 times.

Karmakar et al. [2.106] carried out liquid-liquid extraction targeting hexavalent chromium removal from aqueous solution. They employed Aliquat-336 dissolved in kerosene as an extractant as the organic phase. Studies were carried out in Rotating Packed Bed (RPB), Rotating Zigzag Bed (RZB), and Rotating Spiral Bed (RSB). Notably, the RSB exhibited an impressive removal efficiency of approximately 99%, surpassing conventional extractors like mixer settlers and fixed beds by more than twenty-five times in terms of overall volumetric mass transfer coefficient. The performance of RSB was better than those of RPB and RZB.

2.4.4 Rotor-Stator Spinning Disk Contactor

The schematic of Rotor-Stator Spinning Disk Contactor rooted in HIGEE principles is depicted in Figure 2.12. This equipment comprises of disc rotating within a cylindrical casing, liquid injected near the center, flow outward over the disc surface driven by centrifugal force. This results in a highly sheared liquid film intensifying mass transfer rates and brief residence time.

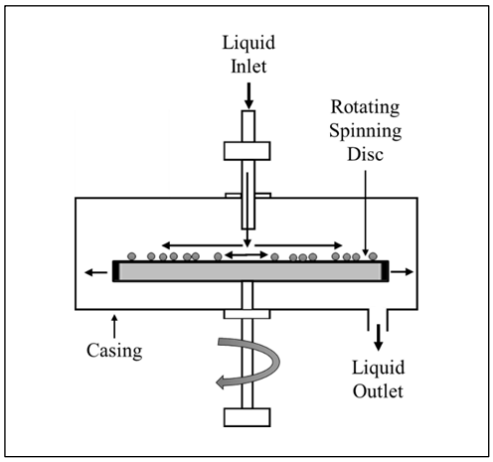

Figure 2.12: Schematic diagram of Rotor Stator Spinning Disk Contactor

With attributes like high heat and mass transfer coefficients, reduced residence time, plug flow, substantial surface area to volume ratio, and efficient mixing, this extractor finds application in liquid-liquid extraction and photocatalysis for pollutant removal. Wang et al. [2.107] explored phosphoric acid extraction in this contactor. The overall volumetric liquid phase mass transfer coefficient varied between 5.0×10^{-3} and 15.0×10^{-3} s^{-1}.

Table 2.3 provides the obtained volumetric mass transfer coefficients in various extractors.

Table 2.4. Overall volumetric mass transfer coefficient in different extractors

Extractor	Extractor Specification	Chemical System	Operating Parameters	Mass Transfer Coefficient	References
Spray Column	Internal Dia = 60 mm, Height = 1200 mm,	Toluene /Acetone /Water	Dispersed phase flow Rate Q_d = 60 mL/min - 80 mL/min, ---------- Continuous phase flow rate = 100 – 500 mL/min	4.1×10^{-5} $m.s^{-1}$ To 4.8×10^{-5} $m.s^{-1}$	[2.108]
Spray Column	Internal Dia = 10.24 cm, Height = 170 cm	Water/ Acetone/ Toluene	Aqueous Phase flow rate (Qa) = $20 \times 10^{-6} m^3 s^{-1}$ To $130 \times 10^{-6} m^3 s^{-1}$ ---------- Organic Phase flow rate (Qo) = $16 \times 10^{-6} m^3 s^{-1}$ To $130 \times 10^{-6} m^3 s^{-1}$	$0.0005\ s^{-1}$ To $0.008\ s^{-1}$	[2.109]
Packed Column	Internal Dia = 60 mm, Height = 1200 mm,	Toluene/ Acetone/ Water	Dispersed phase flow Rate Q_d = 60 mL/min - 80 mL/min, ---------- Continuous phase flow rate = 100 – 500 mL/min	4.8×10^{-5} $m.s^{-1}$ To 6.2×10^{-5} $m.s^{-1}$	[2.108]
Packed Column	Internal Dia = 10.24 cm, Height =	Water/ Acetone/ Toluene	Aqueous Phase flow rate (Qa) = $20 \times 10^{-6} m^3 s^{-1}$	$0.0005\ s^{-1}$ To $0.0055\ s^{-1}$	[2.109]

	170 cm		To $130 \times 10^{-6} m^3 s^{-1}$ ---------- Organic Phase flow rate (Qo) = $16 \times 10^{-6} m^3 s^{-1}$ To $130 \times 10^{-6} m^3 s^{-1}$		
Mixer Settler Column	Internal Dia = 100 mm, Height = 100 mm, Mixer Height = 59 mm, Settler Height = 38 mm	Heptane/ I_2-KI/ Water	Dispersed phase flow Rate Q_d = $4 \times 10^{-6} m^3 s^{-1}$	$0.08\ s^{-1}$ To $4.0\ s^{-1}$	[2.86]
Mixer Settler Column	Dia. of Mixing Chamber = 38 mm, Dia. of Settler Chamber = 50 mm, Length of Settler = 200 mm,	Toluene /Acetone /Water	Aqueous Phase flow rate (Qa) = $0.78 \times 10^{-6}\ m^3 s^{-1}$ ---------- Organic Phase flow rate (Qo) = $0.88\ m^3 s^{-1}$	$0.0015\ s^{-1}$ To $0.005\ s^{-1}$	[2.110]
Kuhni Extraction Column	Internal Dia = 117 mm, Height = 700 mm, Number of compartments = 10.	**(A)** Toluene /Acetone /Water ---------- **(B)** n butyl acetate/ Acetone /Water	**(A)** Rotational Speed = 120 – 270 rpm **(B)** Rotational Speed = 90 -240 rpm ---------- Aqueous Phase flow rate Q_c = 14 L/h – 32 L/h ---------- Organic Phase flow rate Q_d = 14 L/h – 32 L/h	**(A)** $1.60 \times 10^{-5}\ m.s^{-1}$ To $3.53 \times 10^{-5}\ m.s^{-1}$ ---------- **(B)** $1.32 \times 10^{-5}\ m.s^{-1}$ To $2.23 \times 10^{-5}\ m.s^{-1}$	[2.111]
Oldshue–Rushton Column	Internal Dia = 35 mm, Height = 2000 mm, Number of compartments = 99.	Ethanol/Carbon dioxide/ n butanol	Aqueous Phase flow rate (Qc) = 0.97 Kg/h – 2.15 Kg/h, ---------- Organic Phase flow rate (Qd) = 13.9 Kg/h – 14.1 Kg/h, ---------- Rotational Speed =	$0.009\ s^{-1}$ To $0.012\ s^{-1}$	[2.112]

			0 – 324 rpm		
Rotating Spray Column	Internal Dia = 25 mm, Column Length = 150 mm	Chromium/ Aliquat 336-Kerosene/Water	Aqueous Phase flow rate (Q_a) = 2.5 × 10^6 $m^3/_s$ To 6.8 × 10^6 $m^3/_s$ ---------- Organic Phase flow rate (Q_o) = 2.3 × 10^6 $m^3/_s$ To 3.9 × 10^6 $m^3/_s$ ---------- Rotational Speed = 750 – 1100 rpm	0.06 s^{-1} To 0.12 s^{-1}	[2.113]
Rotating Scheibel column	Internal Dia = 113 mm, Height = 1430 mm	Cerium and Lanthanum nitrate salts/D2EHPA – Kerosene /Water	Aqueous Phase flow rate (Qc) = 18 L/h – 42 L/h, ---------- Organic Phase flow rate (Qd) = 18 L/h – 42 L/h, ---------- Rotational Speed = 75 – 155 rpm	For Lanthanum 0.00246 s^{-1} To 0.02556 s^{-1} ---------- For Cerium 0.00103 s^{-1} To 0.01224 s^{-1}	[2.114]
Rotor-stator spinning disc extractor	Spiral grooved disc radius = 0.045 m,	TBP+kerosene/ Phosphoric acid /Water	Organic phase flow rate Q_O = 1.0 to 5.0 mL/min, ---------- Volume ratio of aqueous phase to organic phase = 1:1 ---------- Rotational Speed = 120 - 170 rpm	5.0 × 10^{-3} s^{-1} To 15.0 × 10^{-3} s^{-1}	[2.107]
Rotating Disc Contactor (RDC)	Internal Dia = 113 mm, Height = 1430 mm, Shaft with 36 discs	Zinc (II)/D2EHPA – Kerosene /Water	Aqueous Phase flow rate (Q_c) = 25 L/h – 40 L/h, ---------- Organic Phase flow rate (Q_d) = 25 L/h – 40 L/h, ---------- Rotational Speed = 195 – 555 rpm	2.5 × 10^{-3} s^{-1} To 15 × 10^{-3} s^{-1}	[2.115]

Rotating packed bed (RPB)	Rotor circular disks diameter = 160 mm, Axial distance between disk = 20 mm	Water/Methyl red/Xylene	Aqueous Phase flow rate (Q_a) = 4.16 × 10^6 m^3/s To 20.83 × 10^6 m^3/s ---------- Organic Phase flow rate (Q_o) = 0.83 × 10^6 m^3/s To 2.1 × 10^6 m^3/s ---------- Rotational Speed = 300 – 900 rpm	0.015 s^{-1} To 0.205 s^{-1}	[2.116]
Rotating Zig-Zag bed (RZB)	Spiral baffle Height = 17 mm, Width = 10 mm,	Chromium/ Aliquat 336-Kerosene/Water	Aqueous Phase flow rate (Q_a) = 6.67 × 10^6 m^3/s To 20.84 × 10^6 m^3/s ---------- Organic Phase flow rate (Q_o) = 0.83 × 10^6 m^3/s To 8.34 × 10^6 m^3/s ---------- Rotational Speed = 300 – 1100 rpm	0.057 s^{-1} To 0.28 s^{-1}	[2.117]
Rotating Spiral bed (RSB)	Spiral baffle Height = 20 mm, Width = 10 mm,	Chromium/ Aliquat 336-Kerosene/Water	Aqueous Phase flow rate (Q_a) = 6.67 × 10^6 m^3/s To 20.84 × 10^6 m^3/s ---------- Organic Phase flow rate (Q_o) = 0.83 × 10^6 m^3/s To 8.34 × 10^6 m^3/s ---------- Rotational Speed = 300 – 1100 rpm	0.076 s^{-1} To 0.36 s^{-1}	[2.117]

2.5 Summary

1. **Removal by adsorption (for fluoride removal)**
    i. There have many investigations on efficacy on many adsorbents for fluoride removal.
    ii. Industrial adsorption processes typically use fixed-bed adsorption columns. Liquid flows through the bed under gravity.
    iii. In recent years rotating packed bed adsorber has been investigated for removal of pollutants by adsorption. Results indicate that the adsorption rate can be increased by two to three times compared with fixed bed adsorber.
    iv. Investigators have noted that rotating packed bed is associated with efficient micro mixing, low holdup, low residence time and liquid mal-distribution.
2. **Precipitation and Coagulation (for Fluoride Removal)**
    i. The efficacy of different coagulations has been studied for removal of fluoride.
    ii. Removal of fluoride in industries is based on Nalgonda technique using lime and alum as chemical reagents because of its low-cost.
    iii. The industrial process adaptation of this technique is carried out in two separate continuous stirred tank vessels. However, there is no published data for evaluating the performance.
3. **Liquid-Liquid Extraction (for Phenol removal)**
    i. Conventional liquid-liquid extractors such as packed bed column, spray tower, Perforated plate column, rotating disc column, scheibel column among others has been widely studied.
    ii. Equipment based on high gravity has started to gain prominence only in recent years. The equipment investigated include rotating spray column, rotating packed bed, rotating zig-zag and rotating spiral contactor.

iii. Experimental investigation for removal of methylene blue, hexavalent chromium has shown that the size of conventional equipment can be reduced by nearly 25 times with high gravity equipment.

References:

2.1 J. Fawell, K. Bailey, J. Chilton, E. Dahi, L. Fewtrell and Y. Magara, Fluoride in Drinking-water, World Health Organization, *IWA Publishing*, London 2006.

2.2 A. Goyal, M. Verma, G. S. Toteja, K. Gauba, V. Mohanty, U. Mohanty, R. Kaur, Validation of ICMR index for identification of dental fluorosis in epidemiological studies, *Indian J. Med. Res.,* 144 (2016) 52-57.

2.3 F. Zhu, Z. Guo, X. Hu, Fluoride removal efficiencies and mechanism of schwertmannite from KMnO4/MnO2 –Fe (II) processes, *J. Hazard. Mater.,* 397 (2020) 122789.

2.4 J. Charles, C. Bradu, N. Morin-Crini, B. Sancey, P. Winterton, G. Torri, P.-M. Badot, G. Crini, Pollutant removal from industrial discharge water using individual and combined effects of adsorption and ion-exchange processes: Chemical abatement, *J. Saudi Chem. Soc.,* 20 (2016) 185–194.

2.5 M. N. Rashed, Adsorption technique for the removal of organic pollutants from water and wastewater, Organic Pollutants—Monitoring, Risk and Treatment. 2013.

2.6 A. K. Tolkou, N. Manousi, G. A. Zachariadis, I. A. Katsoyiannis, E. A. Deliyanni, Recently Developed Adsorbing Materials for Fluoride Removal from Water and Fluoride Analytical Determination Techniques:A Review, *Sustainability,* 13, 7061 (2021) 1 -26.

2.7 M. Talat, S. Mohan, V. Dixit, D. K. Singh, S. H. Hasan, O. N. Srivastava, Effective removal of fluoride from water by coconut husk activated carbon in fixed bed column: Experimental and breakthrough curves analysis, *Groundw. Sustain. Dev.,* 7 (2018) 48–55.

2.8 T. Pang, T. S. A. Chan, Y. A. C. Jande, J. Shen, Removal of fluoride from water using activated carbon fibres modified with zirconium by a drop-coating method, *Chemosphere,* 255 (2020) 126950.

2.9 R. T. Iwar, K. Ogedengbe, B. O. Ugwudike, Groundwater fluoride removal by novel activated carbon/aluminium oxide composite derived from raffia palm shells: Optimization of batch operations and field-scale point of use system evaluation, *Results Eng.,* 14 (2022) 100407.

2.10 S. S. A. Alkurdi, R. A. A. Juboori, J. Bundschuh, L. Bowtell, S. McKnight, Effect of pyrolysis conditions on bone char characterization and its ability for arsenic and fluoride removal, *Environ. Pollut.,* 262 (2020) 114221.

2.11 J. Saikia, S. Sarmah, T. H. Ahmed, P. J. Kalita, R. L. Goswamee, Removal of toxic fluoride ion from water using low-cost ceramic nodules prepared from some locally available raw materials of Assam, India, *J. Environ. Chem. Eng.,* 5 (2017) 2488–2497.

2.12 A. Elhalil, S. Qourzal, F.Z. Mahjoubi, R. Elmoubarki, M. Farnane, H. Tounsadi, M. Sadiq, M. Abdennouri, N. Barka, Defluoridation of groundwater by calcined Mg/Al layered double Hydroxide, *Emerg. Contam.,* 2 (2016) 42-48.

2.13 P. Shivaprasad, P. K. Singh, V. K. Saharan, S. George, Synthesis of nano alumina for defluoridation of drinking water, *Nano-Struct. & Nano-Obj.,* 13 (2018) 109–120.

2.14 P. Chinnakoti, R. K. Vankayala, A. L.A. Chunduri, L. Reddy Nagappagari, S. V. Muthukonda, V. Kamisetti, Trititanate Nanotubes as highly efficient adsorbent for fluoride removal from water: Adsorption performance and uptake mechanism, *J. Environ. Chem. Eng.,* 4 (2016) 4754–4768.

2.15 M. H. Dehghani, M. Farhang, M. Alimohammadi, M. Afsharnia, G. Mckay, Adsorptive removal of fluoride from water by activated carbon derived from $CaCl_2$-modified Crocus sativus leaves: Equilibrium adsorption isotherms, optimization, and influence of anions, *Chem. Eng. Commun.,* 205:7 (2018) 955-965.

2.16 S. Roy, S. Manna, S. Sengupta, A. Ganguli, S. Goswami, P. Das, Comparative assessment on defluoridation of waste water using chemical and bio-reduced graphene oxide: Batch, thermodynamic, kinetics and optimization using response surface methodology and artificial neural network, *Process Saf. Environ. Prot.,* 111 (2017) 221–231.

2.17 S. Raghav, D. Kumar, Adsorption Equilibrium, Kinetics, and Thermodynamic Studies of Fluoride Adsorbed by Tetrametallic Oxide Adsorbent, *J. Chem. Eng. Data,* 63(5) (2018) 1682–1697.

2.18 K. Singh, D. H. Lataye, K. L. Wasewar, Removal of Fluoride from Aqueous Solution by Using Low-Cost Sugarcane Bagasse: Kinetic Study and Equilibrium Isotherm Analyses, *J. Hazard. Toxic Radioact. Waste,* 20(3) (2016) (04015024) 1-13.

2.19 I. Abe, S. Iwasaki, T. Tokimoto, N. Kawasaki, T. Nakamura, S. Tanada, Adsorption of fluoride ions onto carbonaceous materials, *J. Colloid Interface Sci.,* 275 (2004) 35–39.

2.20 A. Chiavola, E. D'Amato, C. D. Marcantonio, Comparison of Adsorptive Removal of Fluoride fromWater by Different Adsorbents under Laboratory and Real Conditions, *Water,* 14 (2022) 1423.

2.21 A. Goswami, M. K. Purkait, Kinetic and Equilibrium Study for the Fluoride Adsorption using Pyrophyllite, *Sep. Sci. Technol.,* 46 (2011)1797–1807.

2.22 S. Waghmare, T. Arfin, S. Rayalu, D. Lataye, S. Dubey, S. Tiwari, Adsorption Behaviour of Modified Zeolite as Novel Adsorbents for Fluoride Removal from Drinking Water: Surface Phenomena, Kinetics and Thermodynamics Studies, *IJSETR,* 4 (12) (2015) 4114 – 4124.

2.23 L. Das, P. Das, A. Bhowal, C. Bhattacharjee, Enhanced biosorption of fluoride by extracted nanocellulose/polyvinyl alcohol composite in batch and fixed-bed system: ANN analysis and numerical modeling, *Environ. Sci. Pollut. Res.,* 28 (2021) 47107–47125.

2.24 M. Talat, S. Mohan, V. Dixit, D. K. Singh, S. H. Hasan, O. N. Srivastava, Effective removal of fluoride from water by coconut husk activated carbon in fixed bed column: Experimental and breakthrough curves analysis, *Groundw. Sustain. Dev.,* 7 (2018) 48–55.

2.25 D. E. Jayashree, P. S. Kumar, P. T. Ngueagni, D-V. Vo, K. W. Chew, Effective removal of excessive fluoride from aqueous environment using activated pods of Bauhinia variegata: Batch and dynamic analysis, *Environ. Pollut.,* 272 (2021) 115969.

2.26 A. Arya, M. Iqbal, V. Yadav, T. Agarwal, R. Gawali, S. K. Jana, D. Datta, Fluoride ion removal using amine modified polymeric resin: Batch and column studies, *Materials Today: Proceedings,* 57 (2022) 1626–1636.

2.27 B. Bera, S. S. Chowdhury, V. R. Sonawane, S. De, High capacity aluminium substituted hydroxyapatite incorporated granular wood charcoal (Al-HApC) for fluoride removal from aqueous medium: Batch and column study, *Chem. Eng. J.,* 466 (2023) 143264.

2.28 M. Sarkar, A. Banerjee, P. P. Pramanick, A. R. Sarkar, Design and operation of fixed bed laterite column for the removal of fluoride from water, *Chem. Eng. J.,* 131 (2007) 329–335.

2.29 S. Ghorai, K. K. Pant, Investigations on the column performance of fluoride adsorption by activated alumina in a fixed-bed, *Chem. Eng. J.,* 98 (2004) 165–173.

2.30 S. Roy, P. Das, S. Sengupta, S Manna, Calcium impregnated activated charcoal:Optimization and efficiency for the treatment of fluoride containing solution in batch and fixed bed reactor, *Process Saf. Environ. Prot.,* 109 (2017) 18 - 29.

2.31 E. Mulugeta, F. Zewge, A. Johnson, B. S. Chandravanshi, Aluminium hydro(oxide)–based (AO) adsorbent for defluoridation of drinking water: Optimisation, performance comparison, and field testing, *Water SA.,* 41(1) (2015) 121-128.

2.32 N. Chen, Z. Zhang, C. Feng, M. Li, R. Chen, N. Sugiura, Investigations on the batch and fixed-bed column performance of fluoride adsorption by Kanuma mud, *Desalination,* 268 (2011) 76–82.

2.33 B. Bishayee, B. Ruj, S. Nandi, R. P. Chatterjee, A. Mallick, P. Chakraborty, J. Nayak, S. Chakrabortty, Sorptive elimination of fluoride from contaminated groundwater in a fixed bed column: A kinetic model validation-based study, *J. Indian Chem. Soc.,* 99 (2022) 100302.

2.34 J. J. G. Sánchez, M. S. Ríos, V. M. Miranda, C. S. Morelos, Removal of fluoride ions from drinking water and fluoride solutions by aluminum modified iron oxides in a column system, *J. Colloid Interface Sci.,* 407 (2013) 410–415.

2.35 J. L. D. Rodriguez, V. A. E. Barrios, J. R. R. Mendez, Removal of fluoride from drinking water by a chitin-based biocomposite in fixed-bed columns, *J. Fluor. Chem.,* 140 (2012) 99–103.

2.36 Y. Ma, F. Shi, X. Zheng, J. Ma, C. Gao, Removal of fluoride from aqueous solution using granular acid-treated bentonite (GHB): Batch and column studies, *J. Hazard. Mater.,* 185 (2011) 1073–1080.

2.37 L. R. Brunson, D. A. Sabatini, Practical considerations, column studies and natural organic material competition for fluoride removal with bone char and aluminum amended materials in the Main Ethiopian Rift Valley, *Sci. Total Environ.,* 488–489 (2014) 580–587.

2.38 C. K. R. Mayorga, A. B. Petriciolet, F. J. S. Ruiz, J. M. Pérez, H. E. R. Ávila, I. A. A. Villarreal, D. I. M. Castillo, Breakthrough curvemodeling of liquid-phase adsorption of fluoride ions on aluminum-doped bone char using micro-columns: Effectiveness of data fitting approaches, *J. Mol. Liq.,* 208 (2015) 114–121.

2.39 S. Sinha, K. Pandey, D. Mohan, K. P. Singh, Removal of Fluoride from Aqueous Solutions by Eichhornia crassipes Biomass and Its Carbonized Form, *Ind. Eng. Chem. Res.,* 2003, 42, 6911-6918.

2.40 R. Mohan, R. K. Dutta, Continuous fixed-bed column assessment for defluoridation of water using HAp-coated-limestone, *J. Environ. Chem. Eng.,* 8 (2020) 103840.

2.41 A. Ghosh, S. Chakrabarti, K. Biswas, U. C. Ghosh, Column performances on fluoride removal by agglomerated Ce (IV)–Zr (IV) mixed oxide nanoparticles packed fixed-beds, *J. Environ. Chem. Eng.,* 3 (2015) 653–661.

2.42 L. Fang, K. N. Ghimire, M. Kuriyama, K. Inoue, K. Makino, Removal of fluoride using some lanthanum (III)-loaded adsorbents with different functional groups and polymer matrices, *J Chem. Technol. Biotechnol.,* 78 (2003) 1038–1047.

2.43 C. Ramshaw, R. H. Mallinson, Mass Transfer Process. U.S. Patent, 255, (1981) 4283.

2.44 S. Karmakar, A. Bhowal, P. Das, A comparative study of liquid-liquid extraction in different rotating bed contactors, *Chem. Eng. Process.: Process Intensif.,* 132 (2018) 187–193.

2.45 S. Munjal, M. P. Dudukovic, P. Ramachandran, Mass-Transfer in Rotating Packed Beds-II. Experimental Results and Comparison with Theory and Gravity Flow, *Chem. Eng. Sci.,* 44, (10) (1989) 2257-2268.

2.46 A. Das, A. Bhowal, S. Datta, Continuous Biosorption in Rotating Packed-Bed Contactor, *Ind. Eng. Chem. Res.,* 47 (2008) 4230–4235.

2.47 C. C. Lin, H. S. Liu, Adsorption in a Centrifugal Field: Basic Dye Adsorption by Activated Carbon, *Ind. Eng. Chem. Res.,* 39 (2000) 161-167.

2.48 A. Kundu, L. S. Hassan, G. Redzwan, D. Robinson, M. A. Hashim, B. SenGupta, Application of a rotating packed bed contactor for removal of Direct Red 23 by adsorption, *Desalin. Water Treat.,* (2015) 1–9.

2.49 C. F. Chang, S. C. Lee, Adsorption behavior of pesticide methomyl on activated carbon in a high gravity rotating packed bed reactor, *Water Res.,* 46 (2012) 2869 – 2880.

2.50 M. Panda, A. Bhowal, S. Datta, Removal of Hexavalent Chromium by Biosorption Process in Rotating Packed Bed, *Environ. Sci. Technol.,* 45 (2011) 8460–8466.

2.51 J. B. Modak, A. Bhowal, S. Datta, Experimental study and mathematical modeling of breakthrough curve in rotating packed bed, *Chem. Eng. Process.: Process Intensif.,* 99 (2016) 19–24.

2.52 W. Li, S. Wei, W. Jiao, G. Qia, Y. Liu, Modelling of adsorption in rotating packed bed using artificial neural networks (ANN), *Chem. Eng. Res. Des.,* 114 (2016) 89-95.

2.53 M. A. Hashim, A. Kundu, S. Mukherjee, Y. S. Ng, S. Mukhopadhyay, G. Redzwan, B. SenGupta, Arsenic removal by adsorption on activated carbon in a rotating packed bed, J. *Water Process Eng.,* 30 (2019) 100591.

2.54 E. J. Reardon, Y. Wang, A Limestone Reactor for Fluoride Removal from Wastewaters, *Environ. Sci. Technol.,* 34 (2000) 3247- 3253.

2.55 M. F. Chang, J. C. Liu, Precipitation Removal of Fluoride from Semiconductor Wastewater, *J. Environ. Eng.,* 133 (2007) 419-425.

2.56 S. Dubey, M. Agarwal, A. B. Gupta, Experimental investigation of Al-F species formation and transformation during coagulation for fluoride removal using alum and PACl, *J. Mol. Liq.,* 266 (2018) 349–360.

2.57 S. Aoudj, N. Drouiche, M. Hecini, T. Ouslimane, B. Palaouane, Coagulation as a Post-Treatment Method for the Defluoridation of Photovoltaic Cell Manufacturing Wastewater, *Procedia Eng.,* 33 (2012) 111 – 120.

2.58 S. G. Wang, Y. Ma, Y. J. Shi, W. X. Gong, Defluoridation performance and mechanism of nano-scale aluminum oxide hydroxide in aqueous solution, *J. Chem. Technol. Biotechnol.,* 84 (2009) 1043 –1050.

2.59 N. Ozairia, S. A. Mousavia, M. T. Samadi, A. Seidmohammadi, D. Nayeri, Removal of fluoride from water using coagulation–flocculation process: a comparative study, *Desalination Water Treat.,* 180 (2020) 265–270.

2.60 G. Zhang, Y. Gao, Y. Zhang, P. Gu, Removal of fluoride from drinking water by a membrane coagulation reactor (MCR), *Desalination,* 177 (2005) 143-155.

2.61 W. X. Gong, J. H. Qu, R. P. Liu, H. C. Lan, Effect of aluminum fluoride complexation on fluoride removal by coagulation, *Colloids and Surfaces A: Physicochem. Eng. Aspects,* 395 (2012) 88– 93.

2.62 P. Jarvis, E. Sharp, M. Pidou, R. Molinder, S. A. Parsons, B. Jefferson, Comparison of coagulation performance and floc properties using a novel zirconium coagulant against traditional ferric and alum coagulants, *Water Res.,* 46 (2012) 4179 – 4187.

2.63 S. Hussain, J. v. Leeuwen, C. W.K. Chow, R. Aryal, S. Beecham, J. Duan, M. Drikas, Comparison of the coagulation performance of tetravalent titanium and zirconium salts with alum, *Chem. Eng. J.,* 254 (2014) 635–646.

2.64 T. Priya, V. L. Mohanta, B. K. Mishra, Performance evaluation of zirconium oxychloride for reduction of hydrophobic fractions of natural organic matter, *Separation and Purification Technology,* 174 (2017) 104–108.

2.65 Y. Gan, X. Wang, L. Zhang, B. Wu, G. Zhang, S. Zhang, Coagulation removal of fluoride by zirconium tetrachloride: Performance evaluation and mechanism analysis, *Chemosphere*, 218 (2019) 860 – 868.

2.66 N. Zhang, Y. Yang, L. Fan, X. Zheng, J. Wang, C. Jiang, S. Xu, H. Xu, D. Wang, Coagulation effect of polyaluminum-titanium chloride coagulant and the effect of floc aging in fluoride removal: A mechanism analysis, *Sep. Purif. Technol.,* 325 (2023) 124674.

2.67 S. Ayoob, A. K. Gupta, V. T. Bhat, A Conceptual Overview on Sustainable Technologies for the Defluoridation of Drinking Water, *Crit. Rev. Environ. Sci. Technol.,* 38 (2008) 401–470.

2.68 P. Pillai, S. Dharaskar, S. Pandian, H. Panchal, Overview of fluoride removal from water using separation techniques, *Environ. Technol. Innov.,* 21 (2021) 101246.

2.69 F. Zewge, Combined Aluminium sulfate/hydroxide process for fluoride removal from drinking water, *Bull. Chem. Soc. Ethiop.,* 30(3) (2016) 391- 401.

2.70 K. G. Pavithra, P. S. Rajan, J. Arun, K. Brindhadevi, Q. H. Le, A. Pugazhendhi, A review on recent advancements in extraction, removal and recovery of phenols from phenolic wastewater: Challenges and future outlook, *Environ. Res.,* 237 (2023) 117005.

2.71 W. Wei, C.W. Cho, S. Kim, M.H. Song, J.K. Bediako, Y.S. Yan, Selective recovery of Au (III), Pt (IV), and Pd (II) from aqueous solutions by liquid-liquid extraction using ionic liquid Aliquat-336, *J. Mol. Liq.,* 216 (2016) 18-24.

2.72 H. Jiang, Y. Fang, Y. Fu, Q. X. Guo, Studies on the extraction of phenol in wastewater, *J. Hazard. Mater.,* B101 (2003) 179–190.

2.73 K. Abbassian, A. Kargari, T. Kaghazchi, Phenol Removal from Aqueous Solutions by a Novel Industrial Solvent, *Chem. Eng. Commun.,* 202 (2015) 408–413.

2.74 N. Deng, M. Li, L. Zhao, C. Lu, S. L. de Rooy, I. M. Warner, Highly efficient extraction of phenolic compounds by use of magnetic room temperature ionic liquids for environmental remediation, *J. Hazard. Mater.,* 192 (2011) 1350– 1357.

2.75 Y. I. Korenman, A. T. Alymova, I. V. Vatutina, Application of solvents mixtures based on tributylphosphate for selective extraction-sorption concentrating on phenol and guaiacol, *J. Radioanal. Nucl. Chem.,* 246 (3) (2000) 629–634.

2.76 R. Gutierrez, A. Urtiaga, I. Ortiz, Separation of phenol and formaldehyde from industrial wastes.Modelling of the phenol extraction equilibrium, *J. Chem. Technol. Biotechnol.,* 85 (2010) 1215–1222.

2.77 D. C. Greminger, G.P. Burns, S. Lynn, D.N. Hanson, C.J. King, Solvent extraction of phenols from water, *Ind. Eng. Chem. Process Des. Dev.,* 21 (1982) 51-54.

2.78 Q. Wang, Y. Shi, Y. Zhao, P. Ning, Design of solvent mixtures for removal of phenol from wastewater using a non-linear programming model with a multi-start method, *Emerg. Contam,* 8 (2022) 39-45.

2.79 B. Burghoff, E. L. V. Goetheer, A. B. de Haan, COSMO-RS-Based Extractant Screening for Phenol Extraction as Model System, *Ind. Eng. Chem. Res.,* 47 (2008) 4263–4269.

2.80 A. M. Urtiaga, M. I. Ortiz, E. Salazar, J. A. Irabien, Supported liquid membranes for the separation-concentration of phenol 2. Masstransfer evaluation according to fundamental equations., *Ind. Eng. Chem. Res.,* 31 (1992) 1745–1753.

2.81 N. N. Rao, J. R. Singh, R. Misra, T. Nandy, Liquid – liquid extraction of phenol from simulated sebacic acid Wastewater, *JSIR,* 68, (2009) 823-828.

2.82 A. Salimi-Khorshidi, H. Abolghasemi, A. Khakpay, Z. Kheirjooy, M. Esmaieli, Spray and packed liquid–liquid extraction columns: drop size and dispersed phase mass transfer, *Asia-Pac. J. Chem. Eng.,* 8(6) (2013) 940 – 949.

2.83 M. N. Sovilj, B. G. Nikolovski, M. Đ. Spasojević, Hydrodynamics in Spray and Packed Liquid-Liquid Extraction Columns: A Review, *Maced. J. Chem. Chem. Eng.,* 38 (2019) (2) 267–282.

2.84 R. P. Verma, M. M. Sharma, Mass Transfer in Packed Liquid-Liquid Extraction Columns, *Chem. Eng. Sci.,* 30 (1975) 279-292.

2.85 A. Frank Seibert, James R. Fair, Hydrodynamics and Mass Transfer in Spray and Packed Liquid-Liquid Extraction Columns, *Ind. Eng. Chem. Res.,* 27 (1988) 470-481.

2.86 S. Nii, J. Suzuki, K. Tani, K. Takahashi, Mass Transfer Coefficients in Mixer-Settler Extraction column, *J. Chem. Eng. Jpn.,* 30(6) (1997) 1083-1089.

2.87 M. Torab-Mostaedi, S. J. Safdari, M. A. Moosavian, M. Ghannadi Maragheh, Mass Transfer Coefficients in A Hanson Mixer-Settler Extraction Column, *Braz. J. Chem. Eng.,* 25 (3) (2008) 473 – 481.

2.88 K. R. Dongaonkar, H. R. Clive Pratt, G. W. Stevens, Mass Transfer and Axial Dispersion in a Kuhni Extraction Column, *AIChE Journal,* 37 (5) (1991) 694-704.

2.89 A. Kumar, S. Hartland, Mass Transfer in a Kuhni Extraction Column, *Ind. Eng. Chem. Res.,* 27 (7) (1988) 1198 – 1203.

2.90 A. Hemmati, M. Shirvani, M. Torab-Mostaedi, A. Ghaemi, Mass transfer coefficients in a perforated rotating disc contactor (PRDC), *Chem. Eng. Process.: Process Intensif.,* 100 (2016) 19–25.

2.91 Martunus, Z. Helwani, M.R. Othman, Forward mixing model in a rotating disc contactor for kerosene–acetic acid–water system, *Appl. Math. Model.,* 34 (2010) 2901–2909.

2.92 M. Asadollahzadeh, R. Torkaman, M. Torab-Mostaedi, M. Saremi, Assessment of mass transfer coefficients in extraction stages of La (III) and Ce (III) ions by using rotating Scheibel column with regular packing structure, *Sep. Purif. Technol.,* 274 (2021) 119118.

2.93 W. J. Podbielniak, 1935, Centrifugal Fractionation Method and Apparatus, U.S. Patent, 2003, 308.

2.94 W. J. Podbielniak, 1936, Method of Securing Counter-current Contact of Fluids by Centrifugal Action, U.S. Patent, 2044, 996.

2.95 W. J. Podbielniak, 1937, Method and Apparatus of Refining Hydrocarbon Oil, U.S. Patent, 2093, 645.

2.96 W. J. Podbielniak, 1938. Apparatus for Effecting Counter-current Contact Between Fluids, U.S. Patent, 2109, 375.

2.97 W. J. Podbielniak, 1942, Method of Securing Counter-current Contact between Fluids. U.S. Patent, 2286, 157.

2.98 J.M. MacInnes, J. Osorio, P.J. Jordan, G.H. Priestman, R.W.K. Allen, Experimental demonstration of rotating spiral microchannel distillation, *Chem. Eng. J.*, 159 (2010) 159-169.

2.99 J.M. MacInnes, M.J. Pitt, G.H. Priestman, R.W.K. Allen, Analysis of two-phase contacting in rotating spiral channel, *Chem. Eng. Sci.,* 69 (2012) 304-315.

2.100 J. M. MacInnes, M.K.S. Zamberi, Hydrodynamic characteristics of a rotating spiral fluid phase contactor, *Chem. Eng. Sci.,* 126 (2015) 427-439.

2.101 J. M. MacInnes, A.A. Ayash, Mass transfer characteristics of rotating spiral gas-liquid contacting, *Chem. Eng. Sci.,* 175 (2018) 320-334.

2.102 Y. Li, Y. Lu, X. Liu, G. Wang, Y. Ni, J. Ji, Mass transfer characteristics in a rotating zigzag bed as a HIGEE device, *Sep. Purif. Technol.,* 186 (2017) 156-165.

2.103 G.Q. Wang, Z.C. Xu, Y.L. Yu, J.B. Ji, Performance of a rotating zigzag bed—a new HIGEE, *Chem. Eng. Process.,* 47 (2008) 2131-2139.

2.104 L.I. Yumin, J.I. Jianbing, Y.U. Yunliang, X.U. Zhichao, L.I. Xiaohua, Hydrodynamic behavior in a rotating zigzag bed, *Chin. J. Chem. Eng.,* 18(1) (2010) 34-38.

2.105 J. B. Modak, A. Bhowal, S. Datta, Extraction of dye from aqueous solution in rotating packed bed, *J. Hazard. Mater.,* 304 (2016) 337–342.

2.106 S. Karmakar, A. Bhowal, P. Das, A comparative study of liquid-liquid extraction in different rotating bed contactors, *Chem. Eng. Process,* 132 (2018) 187–193.

2.107 Y. Wang, J. Li, Y. Jin, J. Luo, Y. Cao, M. Chen, Liquid-liquid extraction in a novel rotor-stator spinning disc extractor, *Sep. Purif. Technol.,* 207 (2018) 158 -165.

2.108 A. Salimi-Khorshidi, H. Abolghasemi, A. Khakpay, Z. Kheirjooy, M. Esmaieli, Spray and packed liquid–liquid extraction columns: drop size and dispersed phase mass transfer, *Asia-Pac. J. Chem. Eng.,* 8(6) (2013) 940–949.

2.109 A. F. Seibert, J.R. Fair, Hydrodynamics and mass transfer in spray and packed liquid-liquid extraction columns, *Ind. Eng. Chem. Res.,* 27 (1988) 470-481.

2.110 Abolghasemi, Hossein, Moosavian, M. Ali, Radpour, S. Reza, The effects of a surfactant concentration on the mass transfer in a mixer-settler extractor, *Iran. J. Chem. Eng.,* 25 (2006) 9-15.

2.111 A. Hemmati, M. Torab-Mostaedi, M. Asadollahzadeh, Mass transfer coefficients in a Kühni extraction column, *Chem. Eng. Res. Des.,* 93 (2015) 747 –754.

2.112 A. Laitinen, J. Kaunisto, Oldshue–Rushton Column in Supercritical Fluid Extraction, *Sep. Sci. Technol.,* 34(9) (1999) 1859–1872.

2.113 D. Bonam, G. Bhattacharyya, A. Bhowal, S. Datta, Liquid-liquid extraction in a rotating spray column: removal of Cr (VI) by aliquat 336, *Ind. Eng. Chem. Res.,* 48 (2009) 7687–7693.

2.114 M. Asadollahzadeh, R. Torkaman, M. Torab-Mostaedi, M. Saremi, Assessment of mass transfer coefficients in extraction stages of La (III) and Ce (III) ions by using rotating Scheibel column with regular packing structure, *Sep. Purif. Technol.,* 274 (2021) 119118.

2.115 M. Asadollahzadeh, R. Torkaman, M. Torab-Mostaedi, M. Saremi, Experimental investigation and mass transfer modelling in rotating disc contactor with asymmetric configuration for zinc recovery, *Sep. Purif. Technol.,* 273 (2021) 118961.

2.116 J. B. Modak, A. Bhowal, S. Datta, Extraction of dye from aqueous solution in rotating packed bed, *J. Hazard. Mater.,* 304 (2016) 337–342.

2.117 S. Karmakar, A. Bhowal, P. Das, A comparative study of liquid-liquid extraction in different rotating bed contactors, *Chem. Eng. Process.,* 132 (2018) 187–193.

2.118 W. J. Podbielniak, A. M. Gavin, H. R. Kaiser, Use of the centrifugal contactor for water washing of refined oils, *J. Am. Oil Chem. Soc.,* 36, (1959) 238.

2.119 J. R. Burns, C. Ramshaw, Process intensification: Visual study of liquid maldistribution in rotating packed beds, *Chem. Eng. Sci.,* 51 (8) (1996) 1347-1352.

2.120 K. Guo, F. Guo, Y. Feng, J. Chen, C. Zheng, N. C. Gardner, Synchronous visual and RTD study on liquid flow in rotating packed-bed contactor, *Chem. Eng. Sci.,* 55 (2000) 1699-1706.

2.121 J. Zhang, K. Guo, F. Guo, J. S. Zhu, C. Zheng, Experimental study about flow of liquid in rotating packed bed., *J. Chem. Eng. Chin. Univ.,* 14 (2000) 378 –381.

2.122 Z. Y. Yan, C. Lin, Q. Ruan, Dynamics of Droplets and Mass Transfer in a Rotating Packed Bed, *AIChE J.,* 60(7) (2014) 2705–2723.

2.123 Z. Mao, C. Yang, Micro-mixing in chemical reactors: A perspective, *Chin. J. Chem. Eng.,* 25 (2017) 381–390.

2.124 X. F. Duan, Z. Y. Yang, Y. B. Li, A. B. Banaga, L. Zhang, G. W. Chu, J. F. Chen, Liquid−Liquid Heterogeneous Mixing Characteristics in a Submerged Rotating Packed Bed, *Ind. Eng. Chem. Res.,* 63 (2024) 18134−18146.

2.125 H. J. Yang, G. W. Chu, J. W. Zhang, Z. G. Shen, J. F. Chen, Micromixing Efficiency in a Rotating Packed Bed: Experiments and Simulation, *Ind. Eng. Chem. Res.,* 44 (2005) 7730-7737.

2.126 Y. Li, Y. Lu, G. Wang, Y. Nie, H. Ying, J. Ji, X. Liu, Liquid Entrainment and Flooding in a Rotating Zigzag Bed, *Ind. Eng. Chem. Res.,* 54 (2015) 2554−2563.

2.127 T. Chen, M. Zheng, C. Zheng, Z. Yan, Z. Yan, C. Zhou, H. Zheng, CO_2 capture in a novel rotating spiral contactor with hydraulic seal: Hydromechanics, mass transfer and modeling, *Sep. Purif. Technol.,* 340 (2024) 126785.

2.128 G.-W. Chu, Y.-J. Song, W. -J. Zhang, Y. Luo, H.-K. Zou, Y. Xiang, J.-F. Chen, Micromixing Efficiency Enhancement in a Rotating Packed Bed Reactor with Surface-Modified Nickel Foam Packing, *Ind. Eng. Chem. Res.,* 54, (2015) 1697−1702.

2.129 G.Q. Wang, Z. C. Xu, J.B. Ji, Progress on HIGEE distillation-introduction to a new device and its industrial application, *Chem. Eng. Res. Des.,* 89 (2011) 1434-1442.

2.130 G.Q. Wang, Z.C. Xu, Y.L. Yu, J.B. Ji, Performance of a rotating zigzag bed—A new HIGEE, Chem. Eng. Process., 47 (2008) 2131–2139.

Chapter 03

AIMS & OBJECTIVES

A majority of nations globally rely on groundwater to sustain their populations and support agricultural irrigation. The presence of a variety of pollutants complicates the task of ensuring access to safe and uncontaminated water. The deleterious effects on water quality not only threaten ecosystems but also contribute to potential health risks for both humans and wildlife. The escalating demand for freshwater resources intensifies the urgency to address and mitigate the impact of pollutants on water resources.

The dual origin of fluoride in groundwater - geological and human-induced contribute to elevated fluoride levels in the environment. The anthropogenic sources, stemming from industrial processes, contribute to the introduction of fluoride into the environment beyond natural occurrences. Phenols have been marked as a significant pollutant due to their harmful nature and potential environmental build-up. The compound enters surface water through diverse industrial sources such as coal tar, gasoline, plastic, rubber proofing, disinfectant, pharmaceutical, and steel industries, along with domestic wastewater, agricultural run-off, and chemical spills. The acceptable fluoride limits in drinking water are regulated by authoritative bodies, including the World Health Organization (WHO), the Bureau of Indian Standards (BIS), and the Indian Council of Medical Research (ICMR). These organizations have set standardized permissible levels for fluoride concentration in drinking water at 1.5 mg/L, 1.0 mg/L, and 1.5 mg/L, respectively. As per the Bureau of Indian Standards (BIS) the permissible limit of phenol in the drinking water is 0.002 mg/L.

Defluoridation techniques such as Coagulation, Membrane separation, Electrodialysis, Electrocoagulation, Ion exchange resins, Direct contact membrane distillation, and adsorption have been studied on a laboratory scale to determine the efficacy of these methods to comply with

standardized permissible levels to ensure water quality management and public health protection. Techniques that have been investigated to address industrial wastewater containing elevated concentrations of phenolic compounds encompass liquid membrane extraction, liquid-liquid extraction, adsorption, Fenton's process, wet air oxidation, and ozonation. The diverse approaches offer a range of solutions for mitigating fluoride and phenol content in water.

Efficiency, cost-effectiveness and operational simplicity are pivotal factors in environmental remediation technology. The quest for optimal process costs involves endeavours to boost removal efficiency, curtail chemical requirements, and lower capital cost by reducing equipment volume. Adsorption along with precipitation and coagulation techniques have emerged as a reliable approach for defluoridation and is widely used in industrial application. The use of low-cost materials further improves the economic feasibility of the adsorption process. Removal of pollutant by liquid-liquid extraction offers the advantage of economics due to low costing of required chemicals as solvent phase can be reused after stripping, enhancement of control in the plant in continuous operation, safety and low environmental risk.

The first definition of Process intensification (PI) was given in 2000 by Stankiewicz and Moulijn [3.1]. It is about bringing significant benefits in terms of process and efficiency, higher quality of products, lower capital and operating expenses, less waste, and improved process safety. Strategies to implement process intensification mainly depend on the selection of a proper chemical transformation, a suitable catalyst, and a favourable reactor type. This study aims at assessing the potential of specialized equipment designed for operation under high gravity conditions for process intensification of three pollution mitigation methods targeting

- Fluoride (adsorption, and precipitation and coagulation)
- Phenols (liquid-liquid extraction)

3.1 Removal of Fluoride by adsorption

The rate of uptake of adsorbate by a spherical adsorbent particle can be described by solving the following equation

$$\frac{\partial q}{\partial t} = \frac{D_{eff}}{R^2}\frac{\partial}{\partial \theta}\left(\theta^2 \frac{\partial q}{\partial \theta}\right) \tag{3.1}$$

$$-\frac{D_{eff}}{R}\frac{\partial q}{\partial \theta} = k(C - C^*) \tag{3.2}$$

Where q is the concentration of adsorbate in the adsorbent particle at a non dimensionless radial distance θ; R, D_{eff} and k is the radius, effective intraparticle diffusion coefficient in the particle, and external phase mass transfer resistance.

The above equation suggests that utilizing powdered adsorbent particles would lower intraparticle diffusional resistance. The interfacial area for mass transfer per unit particle volume $\left(\frac{3}{R}\right)$ also increases with decreases of particle radius as also the external-phase mass transfer coefficient as given by the following relation [3.2].

$$Sh = 2 + 1.1Re^{0.6}Sc^{1/3} \tag{3.3}$$

Use of powdered adsorbents thus offers advantages of faster uptake rate resulting in faster approach to saturation and decrease of mass transfer zone, and more efficient adsorbent utilization contributing to minimizing solid waste generation upon disposal of the adsorbent bed.

Literature review indicates that the industrial practise of waste water treatment involving adsorption process is carried out in a fixed bed of adsorbent particles. Despite the numerous advantages of powdered adsorbent, large sized adsorbent particles are used. The reason is related to the pressure drop, and clogging of the bed due to presence of solids flowing along with the waste water. Estimate of the pressure drop calculated based on the following formulae

$$\frac{\Delta P}{h_{bed}} = \frac{f_m \rho_L u_o^2}{d_p} \tag{3.4}$$

$$f_m = \frac{1-\varepsilon_b}{\varepsilon_b}\left\{1.75 + 150\frac{1-\varepsilon_b}{Re}\right\} \quad (3.5)$$

show that the pressure drop is ~70,000 Pa/m when the particle size is 0.1 mm which reduces to ~750 Pa/m for particle size 1 mm and ~30 Pa/m for particle size 5 mm (superficial velocity = 0.002 m/s).

In recent years, investigators have studied the efficacy of Rotating packed bed adsorber wherein the adsorbent bed was rotated about its axis. Rotating Packed bed adsorber allows the use of smaller particles compared to fixed bed as the liquid flow through the bed is driven by centrifugal acceleration which can be hundreds of times higher than terrestrial gravity. The removal efficiency in this contactor is however constrained by the presence of liquid maldistribution that leads to ineffective utilization of adsorbent particles. Reduced bed depth as adsorbent particles thrown towards the outer radius of the bed under centrifugal acceleration also has a detrimental effect on removal. The consequent increased bed density also increases the chances of clogging due to reduced void space.

An alternative to overcome these issues is dispersing powdered adsorbent into the wastewater. All the adsorbent particles would always remain in contact with the liquid negating some of the consequences of liquid maldistribution in rotating packed bed adsorber. The other advantages with powdered adsorbent particles as mentioned earlier include lower intraparticle and external phase resistance, and high solid-liquid mass transfer area.

In this study, rotating contactors of three different rotor design was studied for slurry adsorption. The rotating zigzag contactor was modified by not having openings in the rotating baffles. This would force the liquid to ascend the entire baffle length and increase the residence time for mass transfer within the contactor. Furthermore, both the circular baffles were rotated rather than one of them being stationary as in rotating zigzag bed designed for gas-liquid operation. Another high gravity equipment in which experiments were carried out was a rotating spiral contactor. This was modified in this study to consist of two rotating spiral channels between the circular disks. The division of the liquid entering the contactor between the two channels lowers the thickness of the

liquid film over the adsorbent, thereby further reducing external phase resistance. The third rotating contactor used was a conventional rotating packed bed filled with glass beads.

The study employed commercially available powdered activated charcoal as an adsorbent. This adsorbent is commonly used in industrial practise as it has the advantage of have low density (2.31 g/cm^3), extensive external surface area (500 m^2/g), and high porosity.

The objectives of this investigation encompassed:

- Examining removal efficiency in the three rotating contactors—a rotating packed bed contactor, a rotating zigzag contactor, and a rotating spiral contactor with variation of operational parameters like rotational speed, slurry adsorbent quantity, flow rate etc.
- Determine the volumetric mass transfer coefficient in these contactors through a mathematical model.
- Compare the removal attained in rotating contactors with those in traditional contactors such as continuous stirred tank contactor and fixed bed to assess the enhancement of removal efficiency achievable through high-gravity operation.

3.2 Precipitation and Coagulation using Alum and Lime

The precipitation and coagulation technique developed by NEERI is the most promising treatment techniques to meet the regulatory guidelines for fluoride. As noted in Chapter 2, the industrial practise is to carry out the process in two stages in separate continuous stirred reactor. In the first reactor, lime is added to the industrial waste water containing fluoride. Lime induces fluoride to form insoluble calcium precipitates. The solution then flows to the second reactor when alum is added. Residual fluoride is adsorbed by the floc particles formed.

Researchers estimated that the value of segregation indices in continuous stirred tank reactors ranges from 0.3 to 0.7 [3.3]. This signifies poor micro mixing. The consequent lowering of the reaction rate of precipitation and floc formation requires installation of equipment of larger size to allow

sufficient residence time to attain the desired removal of fluoride. The low value of segregation index in RPB (< 0.01) would help to address the challenges associated with conventional reactors. However, there is no literature to examine the efficacy of use of high gravity contactors for removal of fluoride by precipitation and coagulation.

In this study, fluoride was dissolved in alum solution and contacted with lime solution in a single contactor. Thus, both precipitation and adsorption to the flocs formed occurred simultaneously. The main objectives of this study are

- To determine the efficiency of fluoride removal from wastewater using three distinct types of rotating contactors: a rotating packed bed contactor, a modified rotating zigzag contactor, and a modified rotating spiral contactor all operating under high gravity conditions. The study sought to investigate the impact of operational parameters such as rotational speed, flow rate, reactant concentration and other variables on the removal process.
- To evaluate the improvement achievable through high-gravity operation by comparing with the removal obtained in conventional contactors.

3.3 Liquid-Liquid Extraction of Phenol using Aliquat-336

Conventional equipment operating under terrestrial gravity for carrying out this process include mechanically stirred columns, packed columns, spray columns, Kuhni columns, centrifugal extractors and more. HIGEE (high gravity) stands out as a prominent process intensification technology for this removal technique. Literature survey indicates that there is significant increase in volumetric mass transfer coefficient that should decrease the equipment volume by ~20 times compared to conventional extractors like spray columns and packed beds. This highlights the potential of HIGEE technology in enhancing process efficiency while minimizing equipment size, offering a promising avenue for advancing liquid-liquid operations in various industrial applications.

In this investigation, the removal of carcinogenic phenol from synthetic waste water by liquid - liquid extraction was studied in rotating Higee contactors. The phenol removal was carried out by using Aliquat-336 as an extractant dissolved in kerosene.

The objectives of this study were

- To examine the influence of various operating parameters like rotational speed, flow rate, concentration among others on the removal efficiency of phenol in three rotating contactors, namely rotating packed bed, modified rotating zigzag, and modified rotating spiral contactors.
- Compare the removal efficiency attained in rotating contactors with that in conventional contacting systems to ascertain the enhancement potential of high-gravity operations.

Besides the specific advantages of high gravity equipment for each of the three applications mentioned above, some of the other advantages that would be applicable for all these processes include:

- **Fast response**: The residence time in this equipment is small as the liquid flows under centrifugal acceleration through the equipment. This consequent low liquid holdup facilitates faster approach towards steady state compared to conventional equipment. This allows quick process response for change in process conditions.
- **Compact equipment volume**: Due to efficient micro mixing and high mass transfer coefficients, rotating contactors require much smaller equipment volumes for the same separation.
- **Reduced capital cost:** The compact would reduce the material cost for fabricating the contactor and allow expensive materials to be used for construction. Furthermore, the cost of support structure is also reduced

- **Versatility in operation:** The centrifugal force driving the liquid through the contactor can be varied by changing rotational speed. This along with the ability to operate at any inclination providing additional degree of freedom in operation as compared to traditional contactors.

The concept of high gravity equipment is still in its nascent stage. So, optimal design of the equipment is not readily available as is the case for conventional contactors. The fabrication is much more complex. Additional energy input required to rotate the equipment would to be balanced with the advantages.

References:

3.1 A. Stankiewicz, J. A. Moulijn, Process intensification, *Ind. Eng. Chem. Res.*, 41 (2002) 1920–1924.

3.2 N. Wakao, S. Kaguei, T. Funazkri, Effect of Fluid Dispersion Coefficients on Particle-to-Fluid Heat Transfer Coefficients in Packed Beds, *Chem. Eng. Sci.*, 34 (1979) 325 – 336.

3.3 W. W. Lin, D. J. Lee, Micromixing effects in aerated stirred tank, *Chem. Eng. J.*, Vol. 52. Nos. 21(22) (1997) 3837-3842.

Chapter 04

EXPERIMENTAL SETUP

Continuous removal of fluoride and phenol was studied in two classes of equipment. One is the rotating contactors, and the other being conventional contactors. The rotating contactors investigated include the Rotating Packed Bed (RPB), Rotating Zigzag Contactor (RZC), and Rotating Spiral Contactor (RSC). Experiments in conventional contactors were performed out in the Fixed Bed (FB) and Stirred Tank Contactor (STC).

Figure 4.1 illustrates the schematic diagram of the experimental setup for the rotating contactor. The experimental setup included the necessary equipment for contacting different phases. The two reservoirs were used for storing liquid or slurry phase, pumps for conveying the phases into the contactor, and rotameters for measuring the flow rate of the phases. The rotor of the rotating contactors consisted of two stainless-steel circular disks, each with a diameter of 0.160 m, fixed coaxially and spaced apart axially by 0.02 m. A motor rotated these disks about a horizontal axis. The entire rotor assembly resided inside a stationary cylindrical casing of stainless-steel measuring 0.20 m in diameter and 0.05 m in axial length. The rotating contactors also included a stationery cylindrically shaped liquid distributor at the center of the rotor for distributing the liquid phase. The diameter of liquid distributor was 0.034 m featuring with 24 holes. Each hole is 1 mm in diameter and uniformly distributed over the surface. Digital tachometer (Lutron Electronic Pvt. Ltd. US) was employed to measure the rotational speed.

Figure 4.2(a), depict the photograph of the rotor of the rotating spiral contactor (RSC). Spiral channels were affixed to the two rotating disks. Each spiral baffle, mounted on the disks, measured 0.02 m in height with channels of 0.01m in width. These channels underwent approximately six revolutions and was of total length of ~1.9 m. The schematic diagram presented in Figure 4.2(b)

illustrates the arrangement of the rotating spiral disk when the spiral disks are fetched together and separated by the arrangement of spacers. On disk 1, the spiral baffles are indicated by solid line, whereas on disk 2, the spiral baffle is represented by a dotted line. When the two discs are brought together, the gap between the two spiral channels is reduced to approximately 0.005 m.

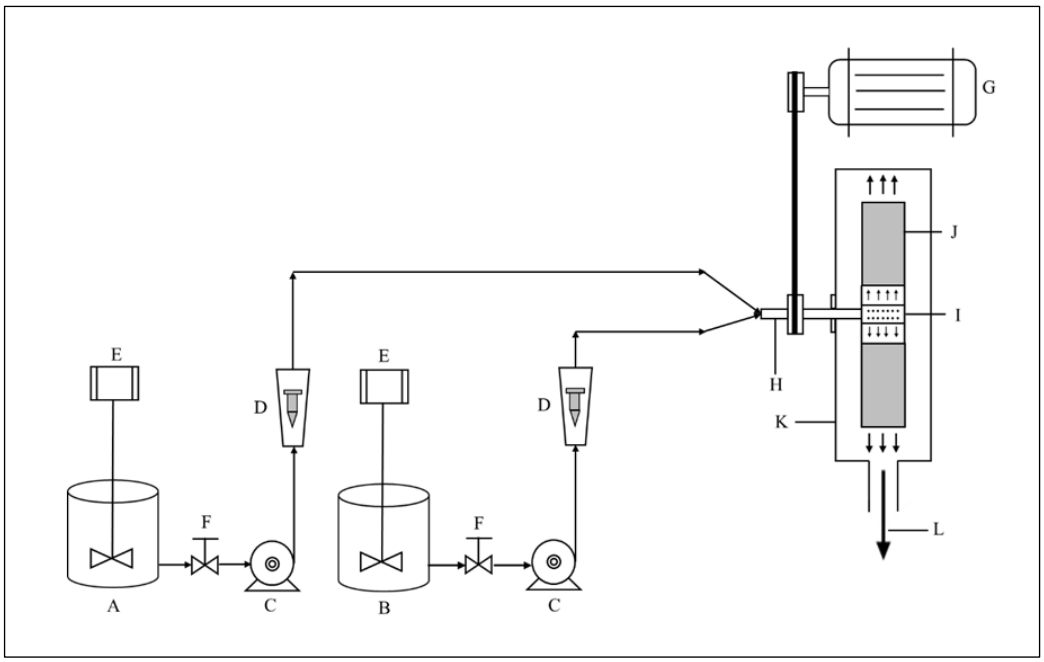

A: Aqueous phase tank, **B**: Organic phase/Lime slurry tank/Slurry tank, **C**: Pump, **D**: Rotameter, **E**: Mechanical stirrer, **F**: Valve, **G**: Electric driven motor, **H**: Rotating shaft, **I**: Liquid distributor, **J**: Rotating Contactor, **K**: Stationary casing, **L**: Sample Collection point

Figure 4.1: Schematic diagram of the experimental setup for continuous process in a rotating contactor

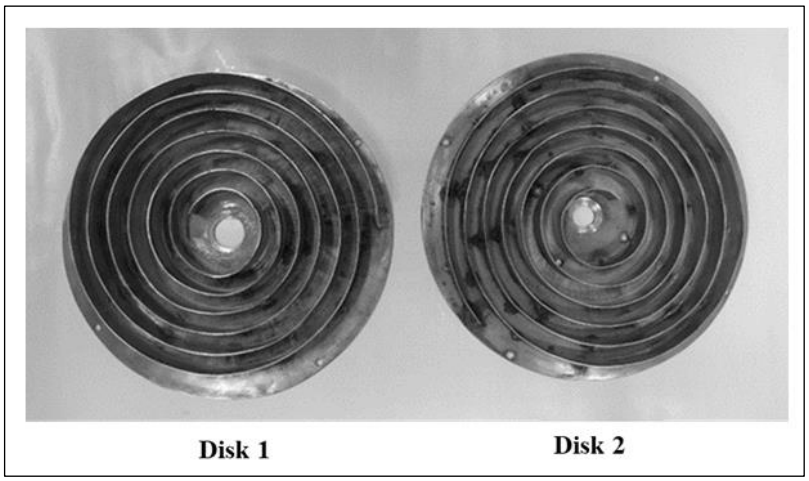

Figure 4.2 (a): Schematic representation of Rotating Spiral Contactor (RSC)

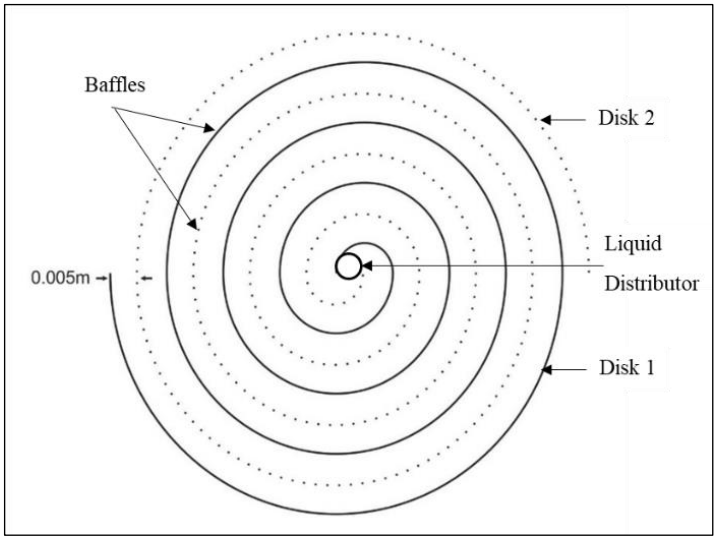

Figure 4.2 (b): Front view of Rotating Spiral Contactor (RSC)

Figure 4.3(a) is the photograph of the rotor in the rotating zig-zag contactor (RZC). Each disk features a sequence of circular concentric baffles of increasing radius. These baffles, measuring 0.017 m in height were spaced apart by a distance of 0.01 m. Disk 1 was fitted with seven circular baffles, while disk 2 had six circular baffles. On disk 2, the radial distances of the baffles from the center were 0.02 m, 0.03 m, 0.04 m, 0.05 m, 0.06 m, and 0.07 m respectively. Conversely, on disk 1, the baffles were positioned at radial distances of 0.015 m, 0.025 m, 0.035 m, 0.045 m, 0.055 m, 0.065 m, and 0.075 m from the center.

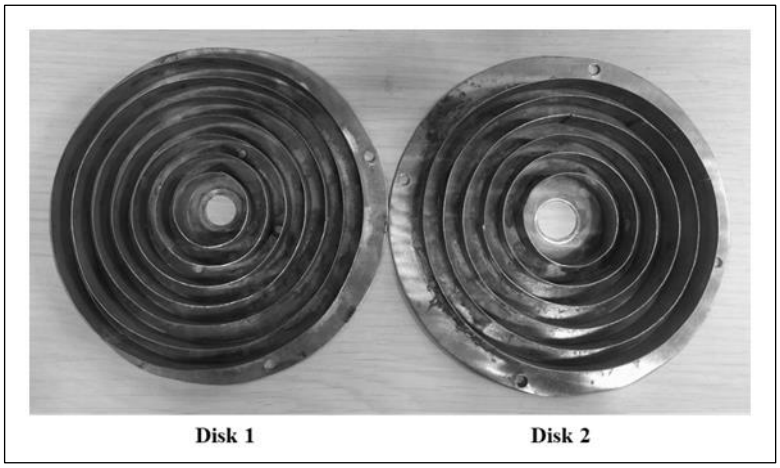

Figure 4.3 (a): Schematic representation of Rotating Zig-Zag Contactor (RZC)

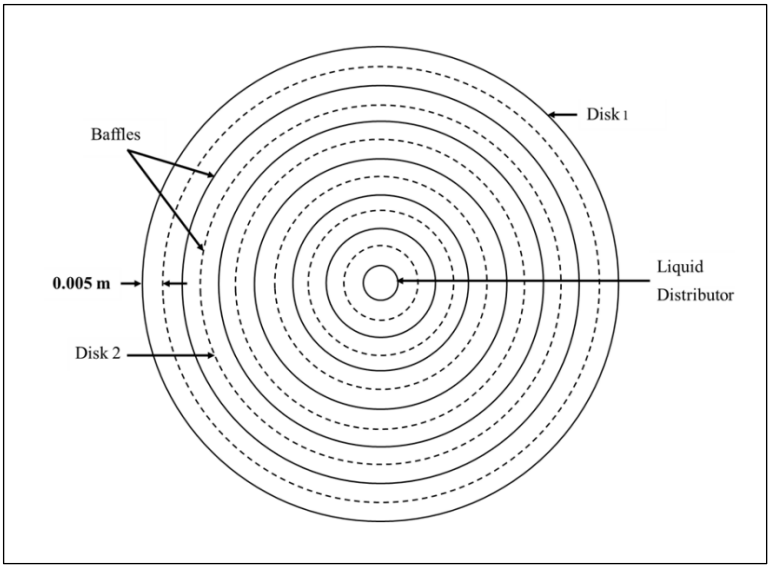

Figure 4.3 (b): Front view of Rotating Zig-Zag Contactor

The schematic diagram illustrates the arrangement of the baffles when the two disks were secured together is shown in Figure 4.3(b). Baffles on Disk 1 is denoted by solid lines and Disk 2 by dotted lines. To facilitate the flow of liquid from one baffle to the other at a larger radial distance, an axial clearance of approximately 0.003 m was maintained between the circular baffles and the disks.

Figure 4.4(a) illustrates the two disks of the rotating packed bed. One disk contains a circular baffle of 0.14 m diameter filled with packing material, whereas the other disk assisted in holding the packing in position. Glass beads, averaging around 3 mm in diameter, served as the packing material. Figure 4.4(b) showing the front view of the rotating packed bed filled with the packing material of glass beads.

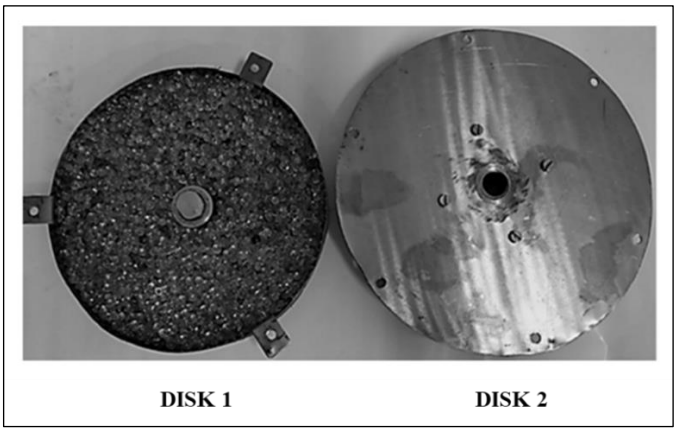

Figure 4.4 (a): Schematic diagram of Rotating Packed Bed (RPB)

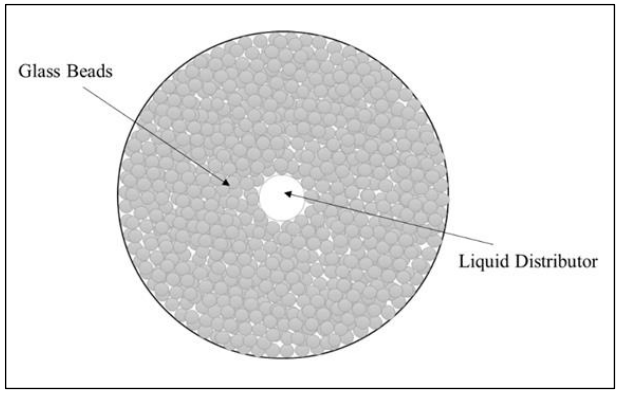

Figure 4.4 (b): Front view of Rotating Packed Bed (RPB)

In the rotating spiral contactor [4.1], the liquid sprayed onto the spiral walls through the liquid distributor moves towards the outer radius of the rotor along the spiral channels with gradual thinning of the liquid layer [4.1 – 4.3]. The flow is influenced by both centrifugal and Coriolis forces [4.1, 4.4].

Figure 4.5 shows the flow pattern of the liquid within the rotating zigzag contactor (RZC). The liquid discharged from the liquid distributor strikes the innermost periphery of the rotational baffles [4.5 - 4.6]. Propelled by centrifugal force, the liquid moves along the inner wall in the form of rivulets or films [4.7]. The liquid transitions into ligaments and/or droplets from the edge of the baffle to the adjacent rotating baffle.

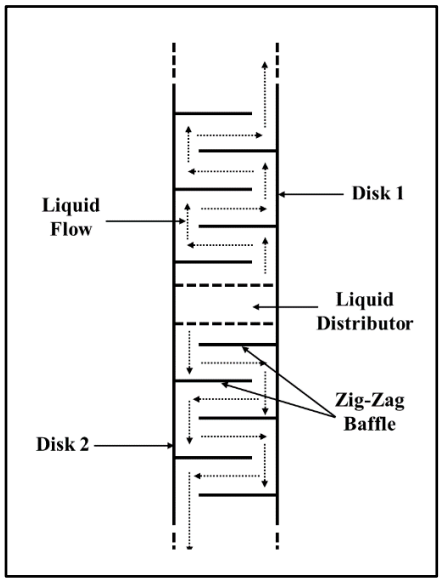

Figure 4.5: Liquid flow pattern of rotating zigzag contactor (RZC)

The experimental setup featuring fixed bed contactor is illustrated in Figure 4.6. The cylindrical column had dimensions of 0.05 m internal diameter and 0.55 m in height. The column was filled with glass beads which was used as the packing material to the suitable height. The liquid was distributed over the packing from the top of the column through a liquid distributor. A perforated plate positioned at the bottom of the fixed bed column supported the packed bed. The liquid solution cascaded downwards through the bed due to terrestrial gravity and was removed from an opening at the bottom.

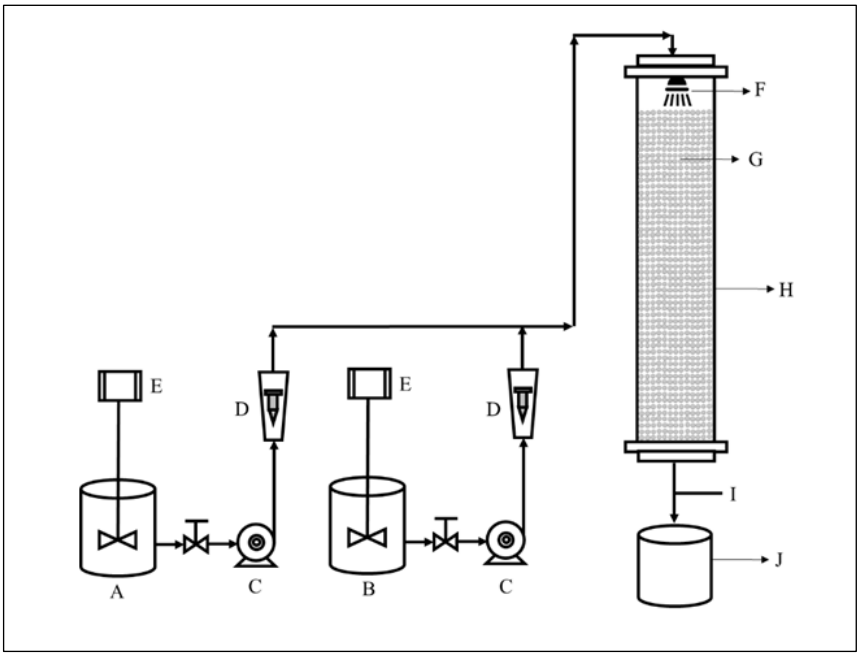

Figure 4.6: Schematic diagram of experimental setup for continuous process in fixed bed contactor

A: Aqueous phase tank, **B:** Organic phase/Lime slurry tank/Slurry tank, **C:** Pump, **D:** Rotameter, **E:** Mechanical stirrer, **F:** Liquid distributor, **G:** Glass bead packing, **H:** Fixed Bed Column, **I:** Sample Collection point, **J:** Treated Influent Collection Tank

Figure 4.7 provides a schematic diagram of the experimental setup involving Stirred Tank Contactor (STC). It was constructed from glass and was of diameter of 0.35 m and height of 0.1 m equipped with a mechanical stirrer and speed controller for varying agitator speed. The liquid was introduced

into the tank at its bottom. The outlet for the liquid was positioned at the top of the tank on the opposite diameter to facilitate the removal of treated liquid.

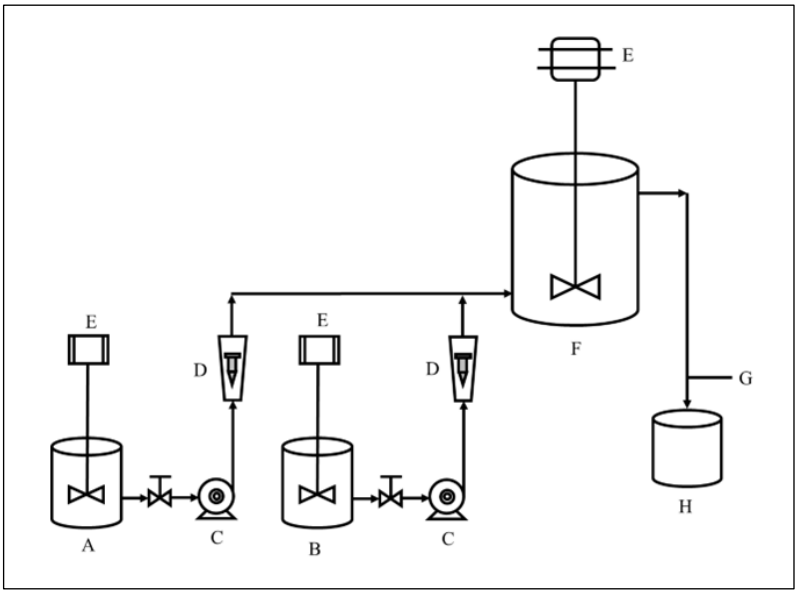

Figure 4.7: Schematic diagram of experimental setup for continuous process in STC.

A: Aqueous phase tank, **B**: Organic phase/Lime slurry tank/Slurry tank, **C**: Pump, **D**: Rotameter, **E**: Mechanical stirrer, **F**: CSTR, **G**: Sample Collection point, **H**: Treated Influent Collection Tank

References:

4.1 J. M. MacInnes, M. J. Pitt, G. H. Priestman, R. W. K. Allen, Analysis of two-phase contacting in rotating spiral channel, *Chem. Eng. Sci.*, 69 (2012) 304-315.

4.2 Y. Li, Y. Lu, X. Liu, G. Wang, Y. Ni, J. Ji, Mass transfer characteristics in a rotating zigzag bed as a HIGEE device, *Sep. Purif. Technol.*, 186 (2017) 156-165.

4.3 H. J. Yang, G. W. Chu, Y. Xiang, J.F. Chen, Characterization of micromixing efficiency in rotating packed beds by chemical methods, *Chem. Eng. J.*, 121 (2006) 147-152.

4.4 K. Yang, G. Chu, H. Chou, B. Sun, L. Shau, J.F. Chen, Determination of the effective interfacial area in rotating packed bed, *Chem. Eng. J.*, 168 (2011) 1377-1382.

4.5 K. Guo, F. Guo, Y. Feng, J. Chen, C. Zheng, N.C. Gardner, Synchronous visual and RTD study on liquid flow in rotating packed-bed contactor, *Chem. Eng. Sci.*, 55 (2000) 1699-1706.

4.6 J. M. MacInnes, M. K. S. Zamberi, Hydrodynamic characteristics of a rotating spiral fluid phase contactor, *Chem. Eng. Sci.*, 126 (2015) 427-439.

4.7 J. M. MacInnes, A. A. Ayash, Mass transfer characteristics of rotating spiral gas-liquid contacting, *Chem. Eng. Sci.*, 175 (2018) 320-334.

Chapter 05

CONTINUOUS REMOVAL OF FLUORIDE BY SLURRY ADSORPTION IN ROTATING CONTACTORS

5.1 Introduction

In the past decade and half, liquid flowing under centrifugal acceleration through a rotating packed bed adsorber (RPBA) had been widely investigated to improve the performance of fixed bed adsorber. There is need to look towards exploring better designs as mass transfer rate enhancement beyond three times could not be achieved due to inherent limitations of RPBA. Slurry adsorption wherein powdered adsorbent is dispersed into the feed solution has notable advantages as noted in Chapter 3. However, there are no reported studies on this process when the slurry under high gravity. This chapter focuses on assessing the efficiency of slurry adsorption process carried out in various types of mass transfer contactors for removal of fluoride ion from a synthetic solution using powder activated charcoal.

5.2 Materials and Method

5.2.1 Materials

Chemical reagents utilized for performing the experiments include Sodium Fluoride (NaF), Activated charcoal (particle size <100 μm), concentrated hydrochloric acid (HCl), TRIS (hydroxymethyl) aminomethane, and Disodium tartrate ($Na_2C_4H_4O_6 - 2H_2O$), These chemicals were procured from Merck Life Science Pvt Ltd. Mumbai. Sodium hydroxide was sourced from LOBA Chemie. The adsorbent employed has a pore volume of 0.52 cm^3/g and a specific surface area of 226.5 m^2/g.

5.2.2 Experimental Setup

The schematic diagram Figure 5.1 shows the experimental setup for continuous removal of fluoride by adsorption using activated charcoal slurry in rotating bed contactors. Fluoride solution of different concentrations was prepared by dissolving an appropriate amount of sodium fluoride in the double-distilled water. The pH was determined by a digital pH meter (Eutech).

The activated charcoal slurry and fluoride solution were kept in separate reservoirs provided with agitators for continuous stirring. The slurry and the feed were mixed just before entering the contactor. The rotors were rotated around the horizontal axis utilizing an electrically driven motor. The slurry (adsorbent particles dispersed in feed solution) entered the rotor through stationary distributor located at the eye of the rotor. The distributor dispersing the slurry inside the rotor.

Mass transfer of fluoride ions from the solution into the adsorbent particles dispersed in it occurs as the stream flows radially outward toward the outer edge of the rotor under the action of centrifugal force. After exiting the rotor, the slurry strikes the stationary wall of the casing and is discharged through an opening at the bottom. Experimental studies with rotating spiral, rotating zig-zag, rotating packed bed were carried out by replacing the rotating packed bed contactor in the setup shown in Figure 5.1 with any of these mass transfer contactors.

Samples were collected from the effluent stream and filtered to separate the adsorbent particles. The fluoride concentration in the solution was determined using a fluoride ion-selective electrode (Mettler Toledo perfect ion Seven Compact S220) by taking a 1:1 ratio of the sample and TISAB-IV. The adsorbent dosage, feed concentration, and feed flow rate reported in this study are the values obtained after mixing the feed and slurry stream from the reservoirs at the entrance of the rotor.

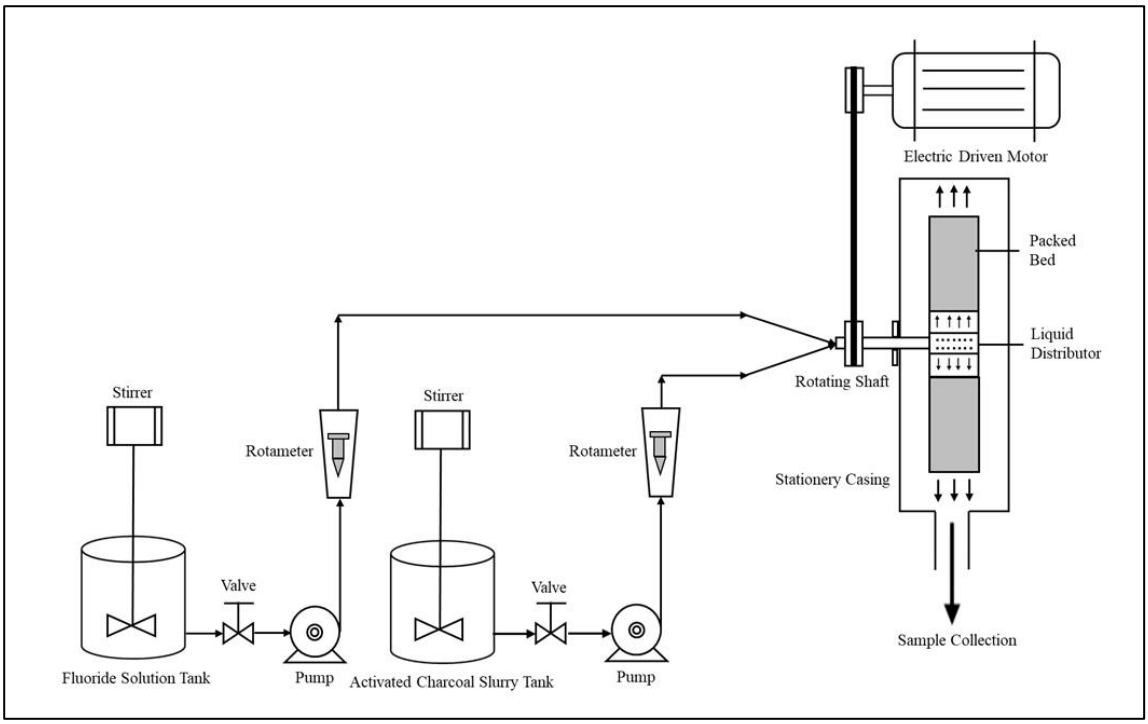

Figure 5.1: Schematic diagram of experimental setup for continuous removal of fluoride by adsorption in rotating contactor

5.2.3 Experimental Procedure

The equilibrium adsorption capacity of activated charcoal for fluoride was assessed by adding the adsorbent to a solution of sodium fluoride. The experiments were carried out in a temperature-controlled BOD shaker for 24 hours at 30°C. The initial pH of the solution was regulated using solutions of HCl and NaOH. The amount of fluoride adsorbed per unit mass of adsorbent at equilibrium, denoted as q_e, was determined from the experimental data by the following equation.

$$q_e = \frac{(C_o - C_e)}{\omega} \tag{5.1}$$

The percentage removal of fluoride denoted as η, was calculated by

$$\eta = \frac{(C_o - C_e)}{C_o} x100 \tag{5.2}$$

Where C_0 represents the initial fluoride concentration, C_e represents the residual concentration of fluoride in the solution at equilibrium, and ω represents the adsorbent dosage expressed as the mass of adsorbent per unit volume of solution.

Continuous experiments on fluoride adsorption were carried out in three rotating contactors, continuous stirred tank contactor (CSTR), and in a fixed bed contactor. Samples were obtained from the outlet stream of the contactor and filtered using Whatman No. 1 filter paper. The fluoride concentration within the solution was determined by employing a fluoride Ion-Selective Electrode (ISE), with a 1:1 proportion of the sample and TISAB-IV [5.1]. The pH was measured using an Eutech digital pH meter.

5.2.4 Mathematical modelling

The flow structure in the rotating contactors studied is complex and not fully understood. Investigators have made the simplified approach of assumed plug flow of the phases absence of mathematical model of the flow hydrodynamics.

In this system, the adsorbent flows along with the solution. The mass balance equation for fluoride ions over a differential element of volume, denoted as *dV*, and thickness, represented by *dr*, within the rotor at a radial distance *r* from the center can be expressed as:

$$Q_s dC_s = Ka(C_s - C_{s*})dV = Ka(C_s - C_{s*})2\pi r dr h \qquad (5.3)$$

Where Q_s is the solution flow rate, h is the distance between the disk, Ka is the overall volumetric mass transfer coefficient (assumed constant for a given operating condition), r is the radial distance from the centre of the contactor C_s is the fluoride concentration in the solution phase of the slurry, and C_{s*} is the concentration of fluoride in the solution at the solution-adsorbent interface in equilibrium with the average concentration of fluoride in the adsorbent particles, $\overline{q}_a$

$$\overline{q_a} = \frac{C_f - C_s}{\omega} \qquad (5.4)$$

Where, C_f is the feed concentration, and ω is the adsorbent concentration in slurry. Equation (5.5) obtained on rearranging eq. (5.3) represents the fluoride concentration in the solution phase at any radial distance

$$Q_s \frac{dC_s}{dr} = Ka(C_s - C_{s*})2\pi rh \tag{5.5}$$

If the Langmuir isotherm model

$$\frac{q_e}{q_{max}} = \frac{bC_e}{1+bC_e} \tag{5.6}$$

is used to represent the adsorption isotherm equilibrium data, the expression of C_{s*} obtained from equation (5.6) is given by

$$C_{s*} = \frac{\bar{q}_a/q_{max}}{b\left(1-\bar{q}_a/q_{max}\right)} \tag{5.7}$$

In the above equation, q_e is the fluoride concentration in the adsorbent in equilibrium with the solute concentration in the solution phase, C_e, q_{max} and b are the Langmuir isotherm model parameters. The volumetric mass transfer coefficient was estimated by solving eq. (5.5) in conjunction with eq. (5.4) and eq. (5.7) by ensuring that the value of C_s obtained at the outer radius of rotor matches the experimental data.

The fraction of maximum (equilibrium) loading of adsorbent particles, $\in$ at the outlet of the mass transfer contactors was calculated by dividing the adsorbate loading of the adsorbent obtained experimentally (q_{ex}) by the theoretical maximum loading, q^* for the given experimental condition i.e.

$$\epsilon = \frac{q_{ex}}{q^*} \tag{5.8}$$

where, the q_{ex} is given by

$$q_{ex} = \frac{C_f - C_{ex}}{\omega} \tag{5.9}$$

The term C_{ex} represents the concentration of fluoride obtained experimentally at the outlet of the contactor. The magnitude of q^* was calculated theoretically by solving the overall mass balance equation

$$C_f = C^* + \omega q^* = \frac{\frac{q^*}{q_{max}}}{b\left(1-\frac{q^*}{q_{max}}\right)} + \omega q^* \quad (5.10)$$

5.3 Result and Discussion

5.3.1 Characterization by Scanning Electron Microscope (SEM) Analysis and Brunauer–Emmett–Teller (BET) Analysis.

The activated charcoal was characterized through scanning electron microscopy (SEM) and Brunauer–Emmett–Teller (BET) surface area analysis. The SEM image depicted in Figure 5.2 (a) reveals the rough, uneven, and porous surface morphology of activated carbon. Figure 5.2 (b) showcases alterations in surface morphology post-adsorption, attributed to the filling of adsorbent pores by fluoride (F^-) molecules during sorption. This transformation underscores the interaction between the adsorbent and fluoride ions, elucidating the adsorption mechanism. The result of nitrogen adsorption/desorption isotherms illustrated in Figure 5.3 was utilized to determine the specific surface area of the activated carbon by employing the BET equation.

The activated carbon exhibited an average pore diameter of 2.74774 nm, with a BET-specific surface area measuring 226.5 m^2/g. The pore volume of the adsorbent was determined to be 0.52 cm^3/g. Analysis of the pore size distribution curves indicated that the activated carbon primarily contained micropores.

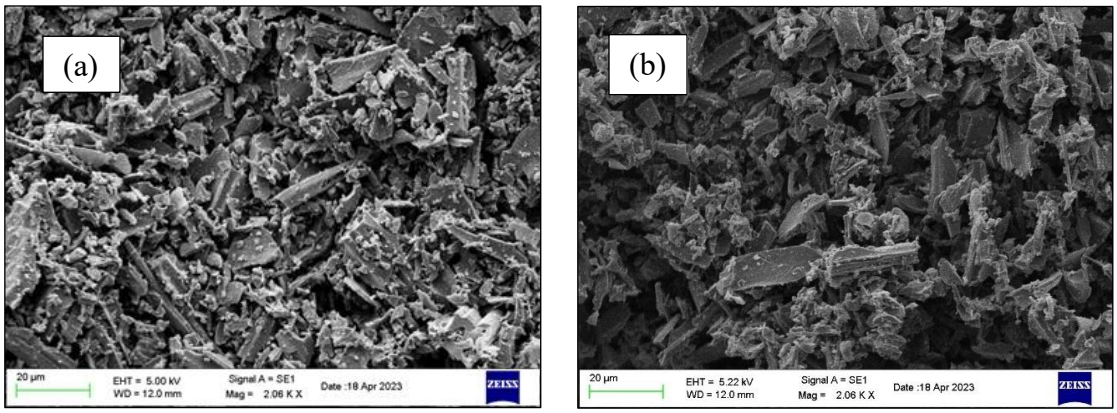

Figure 5.2: SEM images of Activated Charcoal (a) before adsorption, (b) after adsorption with F^-

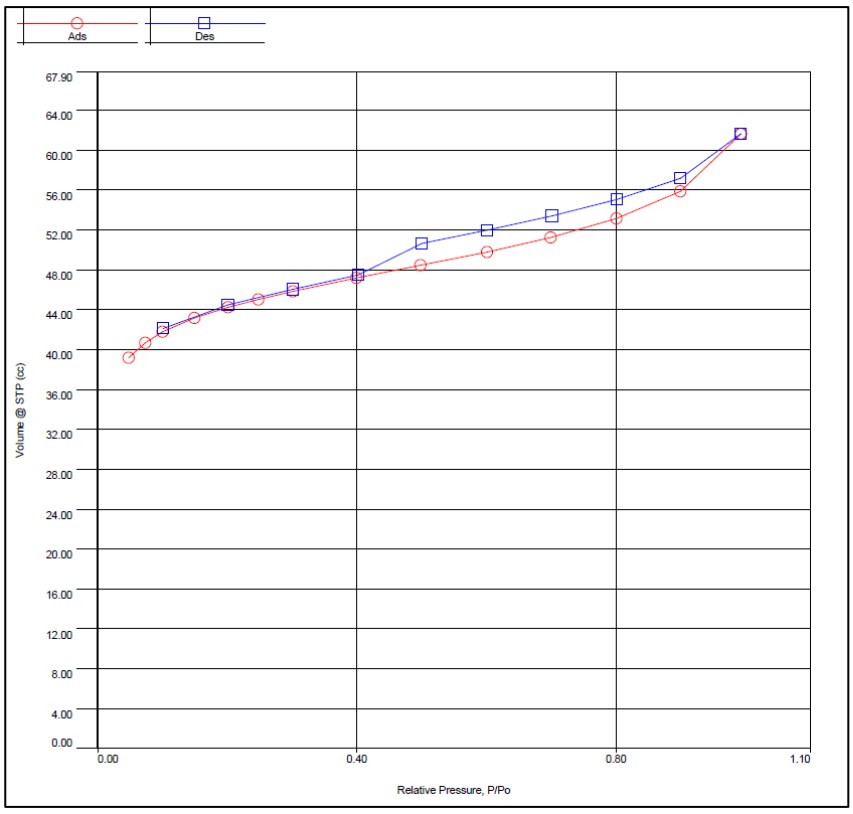

Figure 5.3: Nitrogen adsorption/desorption plot for the activated carbon.

5.3.2 Characterization by Fourier Transform Infrared Spectroscopy (FT-IR)

The Fourier Transform Infrared Spectroscopy (FT-IR) analysis, was conducted on the Perkin-Elmer, Spectrum Two FT-IR Spectrometer ranges from 400 to 4000 cm^{-1}. The characterization by FT-IR analysis was performed to reveal the nature of potential interactions between the fluoride and the

functional groups on the surface of the adsorbent. The Figure 5.4 depicted the FTIR analysis with the presence of fluoride and without fluoride. The dark solid line showing the FTIR peak after the adsorption (a) of fluoride ($F-$) on the surface of activated charcoal and light dotted lines shows FTIR peaks of adsorbent without fluoride noted as before adsorption (b). The efficiency of the adsorbent can be influence by porosity of adsorbent and the reactivity of the functional groups present on the surface of adsorbent [5.2].

The Figure 5.4 indicated the FTIR peaks at 3620.79 cm^{-1} correspond to $O-H$ stretching vibrations from hydroxyl group ($-OH$) respectively indicating the presence of free hydroxyl groups on the carbon surface which is plays the ion exchange mechanism with the fluoride ions by hydrogen bond [5.2 – 5.4]. The peaks identified at 2697.40 cm^{-1} and 2470.14 cm^{-1} identified to be $O-H$ stretching vibrations of carboxylic acid which can functioning for ionic interaction between fluoride ions and $-COOH$ group. The peak of 1738.71 cm^{-1} attributed to the $C=O$ stretching between the carbonyl compounds which can formed weak complexation with fluoride [5.2] [5.5].

The strong peak at 1552.39 cm^{-1} was correspond to $C=C$ stretching vibration with double bond in aromatic ring which can support the adsorption mechanism [5.2] [5.6]. Another strong peak associated to be 1007.38 cm^{-1} $C-O$ stretching between alcohol and ether which contribute for adsorption off fluoride by hydrogen bonding [5.4] [5.7]. The FTIR spectrum observed and reflecting the surface complex nature which is responsible for fluoride adsorption of activated charcoal. FTIR peaks observed to be significant shifting of band and changing the intensity due to adsorption of fluoride on the surface of active site of adsorbent.

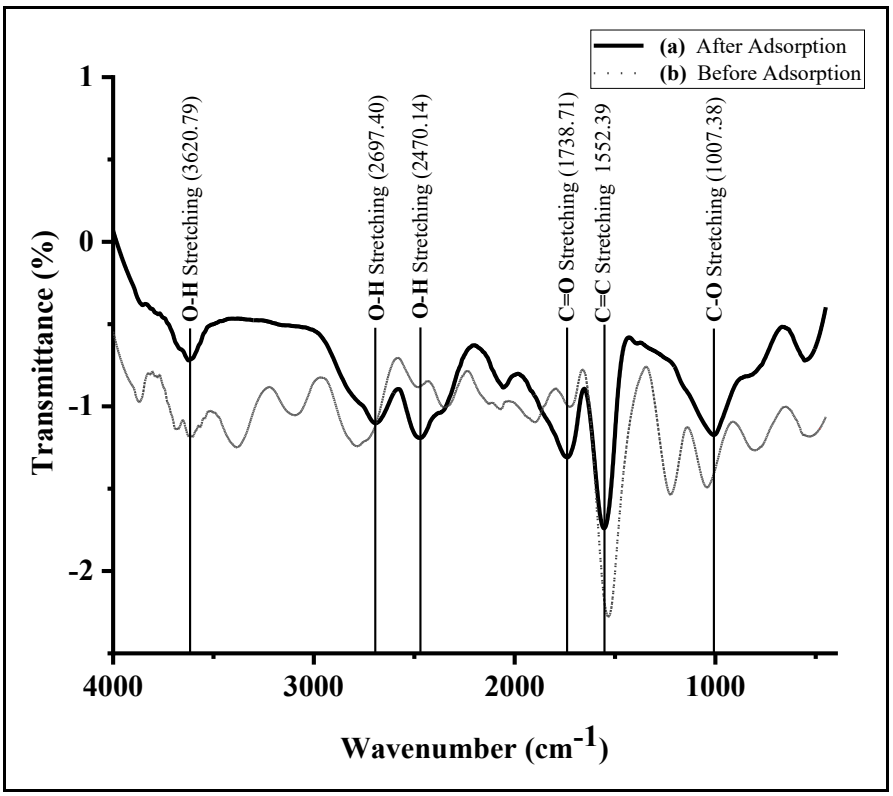

Figure 5.4: FTIR analysis of Adsorbent **a)** After adsorption **b)** Before adsorption

5.3.3 Equilibrium study

5.3.3.1 Effect of pH

The effect of pH on fluoride adsorption was investigated in equilibrium batch studies at a constant initial fluoride concentration of 10.0 mg/L and an adsorbent dose of 50.0 g/L. The initial pH in the solution was varied from 2.0 to 10.0 pH. The experimental observations depicted in Figure 5.5 show that the highest fluoride removal percentage is 80.1% at pH 2.0. The percentage removal of fluoride declined at higher values of solution pH.

The point of zero charge (pH_{pzc}) for the adsorbent shown in Figure 5.6 was determined from the change in pH after the adsorbent (dose = 50 g/L) was equilibrated at various starting pH levels for 24 hours. The magnitude of this parameter is ~6.15. The pH_{pzc} is the pH value of the solution at which the surface has no net charge. When the pH is below this value, the adsorbent surface becomes acquires positive charge due to protonation of functional sites. At pH levels higher than the pH_{pzc},

the surface acquires a negative charge as deprotonation occurs. In aqueous solution, fluoride ions carry a negative charge. Therefore, solution pH less than pH_{pzc} promotes fluoride adsorption by electrostatic attraction. In contrast, at pH values above the pH_{pzc}, the negatively charged surface repels fluoride ions reducing the adsorbent effectiveness.

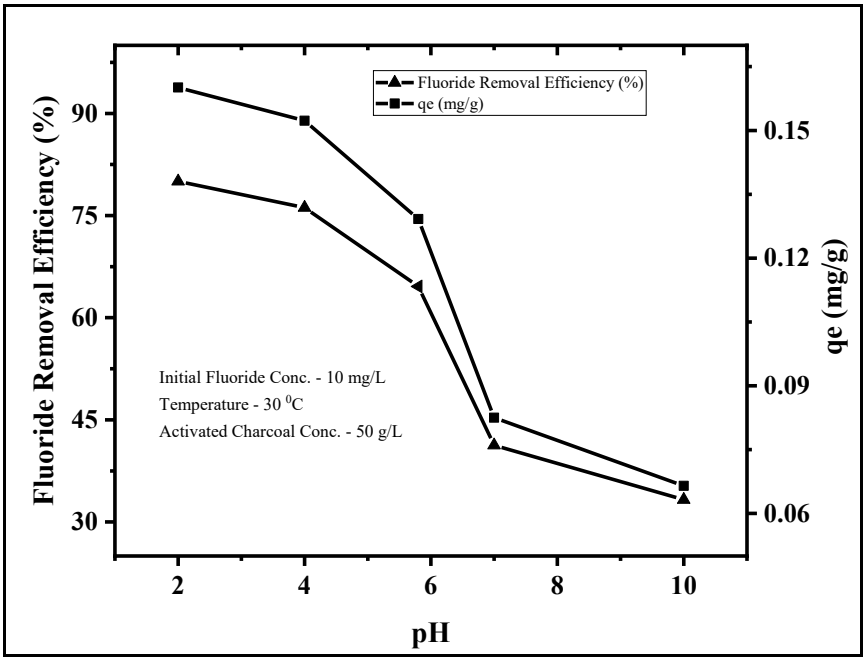

Figure 5.5: Effect of pH in equilibrium batch studies

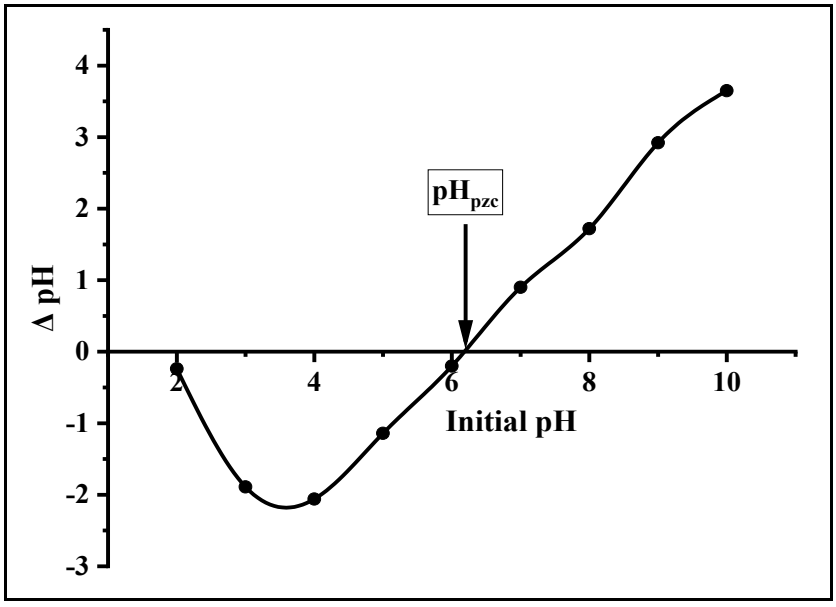

Figure 5.6: Determination of pH_{pzc} of Activated Charcoal

The equilibrium loading of the activated carbon versus concentration of residual fluoride in the solution at pH 2.0 is shown in Figure 5.7.

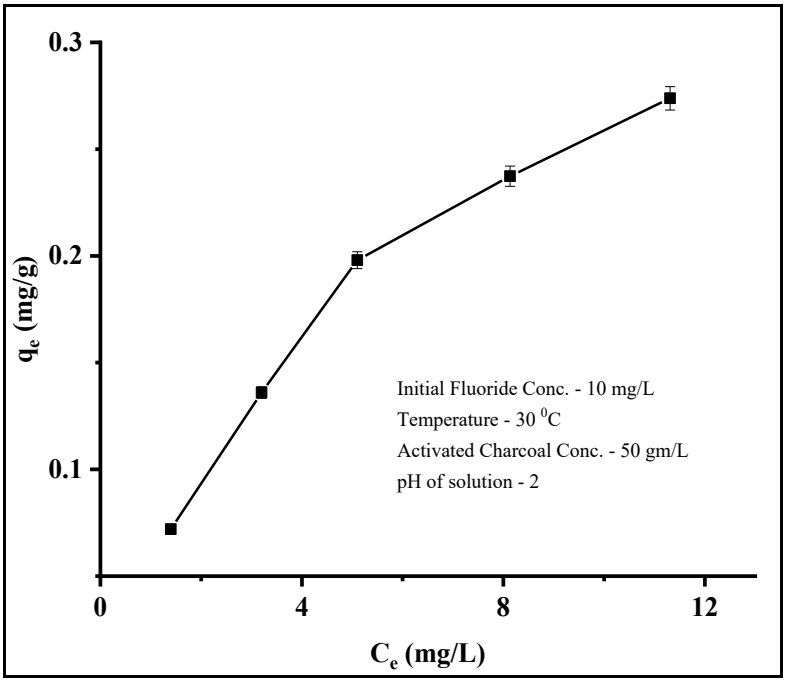

Figure 5.7: Plot q_e versus C_e at pH 2.0

The experimental data was fitted by three adsorption models,

Langmuir Isotherm: $$\frac{q_e}{q_{max}} = \frac{bC_e}{1 + bC_e} \quad (5.11)$$

Freundlich Isotherm: $$q_e = AC_e^{1/n} \quad (5.12)$$

Temkin Isotherm: $$q_e = \frac{RT}{B_T}\ln(A_T \times C_e) \quad (5.13)$$

The value of the parameters q_{max} and b of the Langmuir isotherm model obtained on fitting the experimental equilibrium adsorption data carried out at pH = 2.0 were 0.46 mg/g and 0.127 L/mg respectively and R^2 value is found to be at 0.9985. Corresponding values of R^2 for Freundlich and Temkin isotherm model are 0.9788 and 0.9925. Thus, Langmuir gives a better fit to the experimental data.

5.3.4 Continuous Experimental study in Rotating Contactors

Figure 5.8 depicts the influence of varying pH in the feed solution on the percentage removal in the Rotating Spiral Contactor (RSC), Rotating Zig-zag contactor (RZC), and Rotating Packed Bed (RPB). The experiments were carried out maintaining constant total flow rate of 1.0 L/min, feed fluoride concentration at 10.00 mg/L, and rotational speed of 1000 rpm. Percentage of adsorption exhibited a decline across the pH spectrum: 55.21% at pH 2.0, 33.17% at pH 5.5, and 11.88% at pH 10.0 in the case of RSC. A similar trend is observed in the case of RZC and RPB. In RZC, the fluoride removal efficiency at 2.0 pH is 50.43%, at 5.5 pH 29.35%, and 8.63% at 10.0 pH. In RPB, the fluoride removal efficiency at pH 2.0, 5.5 & 10 was 47.21%, 24.34%, and 6.30% respectively. This trend is consistent with the findings reported in equilibrium batch studies. The equilibrium uptake capacity of the adsorbent decreases at higher pH as seen in Fig. 5.5. This increases the magnitude of C_s^* and reduces the driving force for mass transfer resulting in decrease in percentage removal.

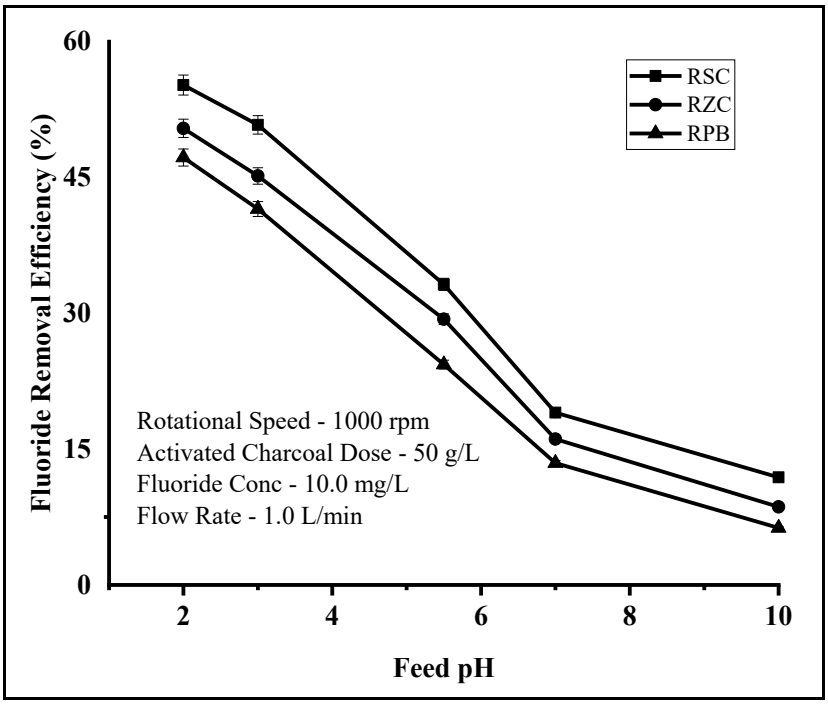

Figure 5.8: Effect of pH in Rotating Contactors

5.3.4.1 Effect of Rotational Speed

The effect of variation of rotational speed on fluoride removal in the rotating contactors is illustrated in Figure 5.9. The experiments were carried out at constant feed flow rate (1.0 L/min), dosage of activated charcoal (50.0 g/L), feed fluoride concentration (10.0 mg/L), and initial solution pH 2.0. There was a notable increase in the percentage removal of fluoride as the rotor speed was varied from 250 rpm to 1000 rpm. In RPB, η increased from 28.3% to 50.3%, while in RSC, it increased from 42.4% to 55.2% and from 37.2% to 52.9% in rotating zig-zag contactor. Highest removal of fluoride was obtained in rotating spiral contactor.

Increasing the rotational speed from 250 rpm to 1000 rpm amplifies the centrifugal acceleration, reaching values up to forty-five times the terrestrial gravity. In case of rotating packed bed, the liquid flows through the voids adhering to the glass beads [5.8]. Solute first diffuses through a liquid film to reach the adsorbent-solution interface before being adsorbed. Burns and Ramshaw [5.8] proposed the following equation for calculating film thickness, δ in rotating packed bed.

$$\delta = \left(\frac{3\mu Q_w}{\rho r N^2}\right)^{1/3} \tag{5.14}$$

$$\text{Where, } Q_w = \frac{Q}{2\pi r z a_w} \tag{5.15}$$

Where μ is the kinematic viscosity of liquid (m^2/s), Q_w is liquid flow per unit width of packing surface (m^2/s), ρ is density of liquid (kg/m^3), r is radial position within RPB (m), N is rotational speed (rad/s), Q_w is liquid flow per unit width of packing surface (m^2/s), Q is volumetric flow rate of liquid (m^2/s), z is the axial depth of packing (m), a_w is the wetted surface area per unit volume (m^{-1}). The equation indicates that the thickness decreases at higher rotational speed and hence over the adsorbent particles. The decrease in diffusional resistance in the liquid film result in higher uptake rate by the adsorbent and higher percentage removal is obtained.

In the case of the rotating spiral contactor (RSC), the slurry flows along the baffle wall as a liquid film [5.9]. Sinkunas et al. [5.10] established a correlation indicating that the thickness of the liquid

film on a vertical surface correlates with the Reynolds number and inversely with terrestrial gravity (centrifugal acceleration in rotating contactors). The augmented removal efficiency with rotational speed in this contactor can be attributed to the effect of decrease of liquid film thickness flowing over the baffles. In case of RZC, the liquid from the opening of the distributor flows over the immediate baffle as film/rivulets. It then flows in the gap between two successive baffles as ligament/drops and then impinges onto the baffle present at larger radial distance. Spreading of the ligament/drop on impact with the succeeding baffle and results in higher wetting of the baffle surface and possible creation of secondary droplets. The higher removal efficiency obtained in this contactor with increase in rotational speed is the contribution of thinner liquid film over the adsorbent due to spreading of liquid on the baffles surface, reduction of concentration gradient due to intensified mixing of the solution on impingement among others.

The removal is higher in the rotating spiral contactor and least in rotating packed bed. In a rotating spiral contactor, the slurry traverses a distance of approximately 1.9 m, which corresponds to the average length of the spiral, while in the rotating packed bed it transverse a distance of only 0.06 m, which represents the bed depth. The resultant higher holdup of slurry in the former due to prolonged residence time of the slurry in the former increases the amount of adsorbent in the contactor and also the interfacial area allowing more fluoride to be adsorbed. Furthermore, the surface area per unit volume of the three contactors are not significantly different (RPB: 225 m^2/m^3, RZC: 170 m^2/m^3, RSC: 200 m^2/m^3). Reported liquid mal-distribution in RPB prevents coverage of the available packing surface area with liquid resulting in higher film thickness as compared to RSC where the liquid flows as a film over the entire available packing surface.

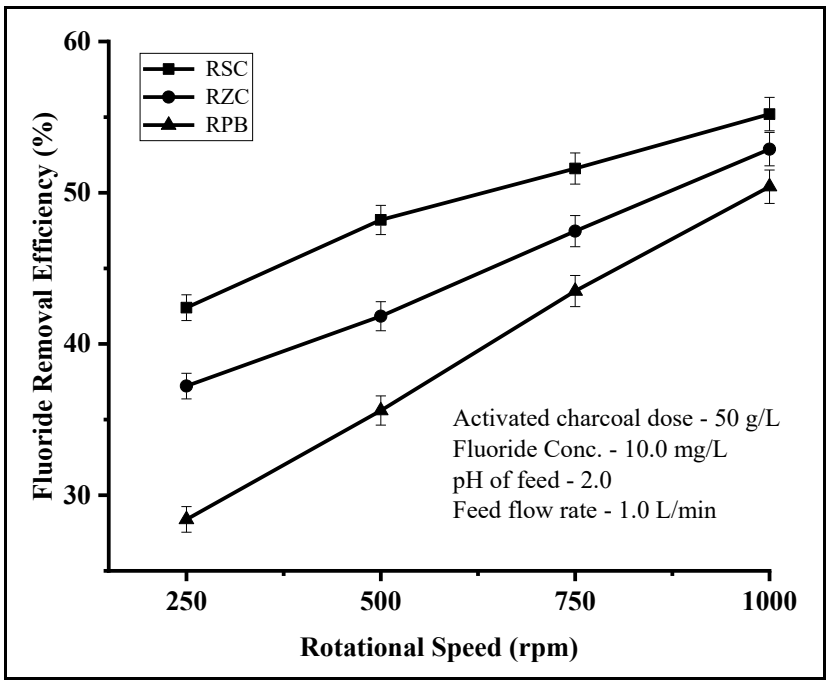

Figure 5.9: Effect of rotational speed on adsorption efficiency in rotating contactors

5.3.4.2 Effect of Total Liquid Flow Rate

The effect of liquid flowrate was investigated by varying the total flow rate from 0.5 L/min to 2.0 L/min keeping other operational parameters constant (feed fluoride concentration = 10 mg/L, pH = 2, slurry concentration = 5.0 wt%, rotational speed = 1000 rpm). The results were presented in Figure 5.10. The experimental observations suggested that the percentage of fluoride removal efficiency reduced from 57.9% to 46.2%, 55.00% to 43.7%, and 52.3% to 42.0%, respectively in the rotating spiral contactor (RSC), rotating zigzag contactor (RZC), and rotating packed bed contactor (RPB).

On the other hand, the amount of fluoride removed per minute increased with flowrate. For example, in RSC the value increased from 2.105 mg/g at flowrate of 0.5 L/min and 10.76 mg/g at 2.0 L/min.

More amount of adsorbent enters the contactor as the slurry flow rate is increased. This enhances the uptake capacity by the adsorbent as well as the interfacial area resulting in increased removal rate of fluoride.

In separate experiments, it was visually observed that more of the distributor openings becomes functional as the flowrate was increased. This should help in more uniform dispersion of slurry over the inner periphery of the contactor and subsequently over the entire contactor. On the other hand, an increase in flow rate reduces the residence time within the rotating packed bed contactor [5.11]. This along with increases the film thickness over the adsorbent at higher flowrate combine to contribute to the final observed trend.

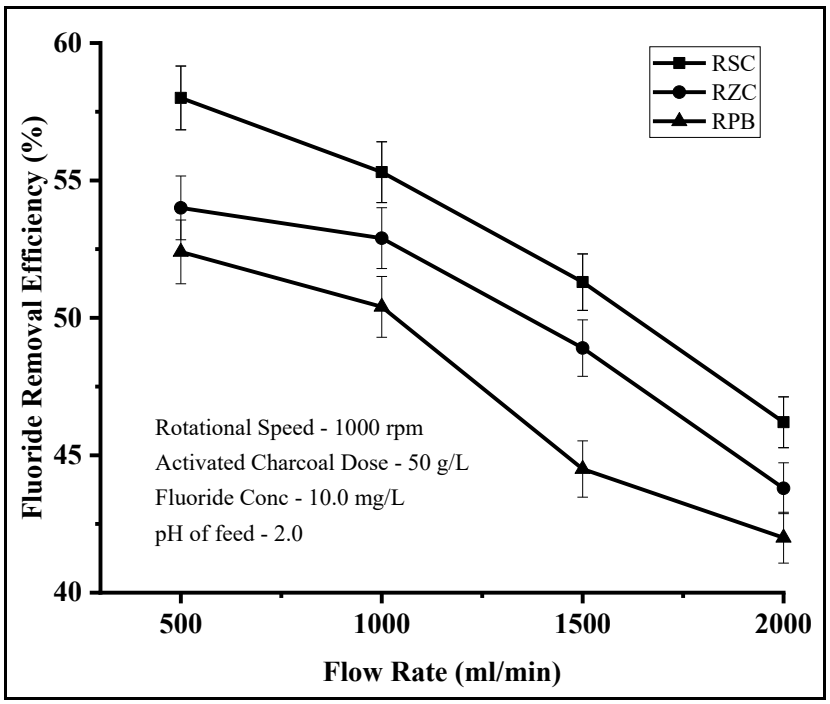

Figure 5.10: Influence of flow rate on adsorption efficiency in rotating contactors

5.3.4.3 Effect of Initial Fluoride Concentration

Continuous experiments were conducted at initial fluoride concentrations of 5, 10, 15, 20, and 25 mg/L and the experimental results are depicted in Figure 5.11. The variables are maintained constant were pH at 2.0, rotational speed at 1000 rpm, total feed flow rate at 1.0 L/min, and a slurry concentration at 5.0 w%. It is seen that as the feed concentration varied from 5 mg/L to 25 mg/L, the fluoride removal efficiency decreased from 65.9% to 24.0% in RSC, 61.2% to 21.1% in RZC and 57.1% to 19.0% in RPB. On the other hand, the amount of fluoride loading per unit mass of

adsorbent increased from 3.3 mg/g to 8.07 mg/g in RSC, 3.06 mg/g to 5.275 mg/g RZC and 2.85 mg/g to 4.75 mg/g in RPB for the same variation in feed concentration.

The equilibrium adsorption capacity of activated carbon at feed fluoride concentration 5 mg/L and 25 mg/L is 0.178 mg/g and 0.35 mg/g. The adsorption capacity thus increases by only two times whereas there is fivefold increase in fluoride ions entering the contactor. This contributes to the lower percentage removal at higher feed concentration. The increase in adsorbent loading was due to the increase in mass transfer driving force due to higher feed concentration.

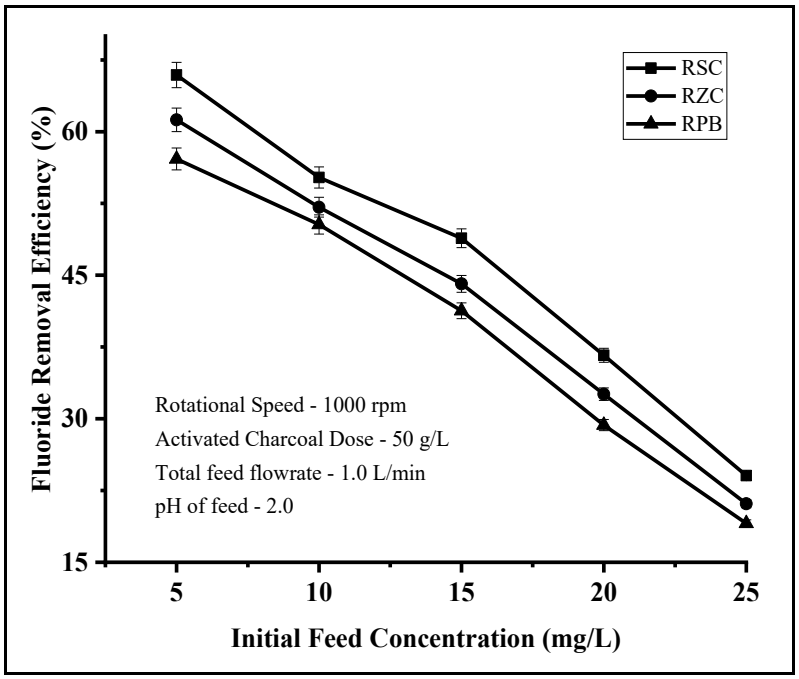

Figure 5.11: Influence of feed concentration on adsorption efficiency in Rotating Contactors

5.3.4.4 Effect of Slurry concentration

The study involved conducting experiments by varying slurry concentrations from 15.0 gm/L to 50.0 gm/L while maintaining constant feed pH of 2.0, fluoride concentration of 10 mg/L, along with a total flow rate of 1.0 L/min and a rotational speed of 1000 rpm. The results presented in Figure 5.12 show that the percentage removal of fluoride. With increase of slurry concentration from 10 g/L to 50 g/L, the percentage removal improved from 12.6% to 47.2% in RPB, 17.3% to 50.4% in RZC and 22.6% to 55.2% in RSC.

Calculation based on experimental data using eq. (5.4) suggest that with increase of adsorbent dosage, ω from 15.0 g/L to 50.0 g/L, the average adsorbate concentration in the solid phase, $\overline{q_a}$ decreased from 0.14 mg/g to 0.10 mg/g. Consequently, the term C_{s*}calculated using eq. (5.7) is also lower, resulting in increase in mass transfer driving force $C_s - C_{s*}$. This along with higher values of adsorbent surface area per unit volume, *a* due to increased ω brings about faster change in fluoride concentration in the contactor according to eq. (5.5) leading to lower outlet concentration.

Figure 5.13 also depicts the variation fractional approach, $\in$ calculated using eq. (5.8) with adsorbent dosage. Adsorbent exiting the contactor can be considered to be utilized to its maximum capacity if the adsorbate loading of the adsorbent, q_{ex} is equal to the theoretical maximum loading, q^* calculated using eq. (5.10) i.e. $\in = 1$ for the given experimental condition. Results show that the adsorbent particles approach the equilibrium value ($\in = 1$) more closely at higher adsorbent dosage. This is due to the increase in uptake rate as explained in the previous paragraph which allows adsorbent particles to approach $\in = 1$ faster at higher slurry concentration.

Figure 5.12 shows the variation of fractional utilization of adsorption capacity with feed concentration, C_f. The fractional utilization decreased from 92% to 44% as C_f increased from 5 mg/L to 25 mg/L. The uptake by the adsorbent particles was 0.07 mg/g and 0.12 mg/g at C_f = 5 mg/L and 25 mg/L respectively. Lower solute penetration into the adsorbent particles allow the mass transfer rates to be relatively higher and faster saturation of the adsorbent.

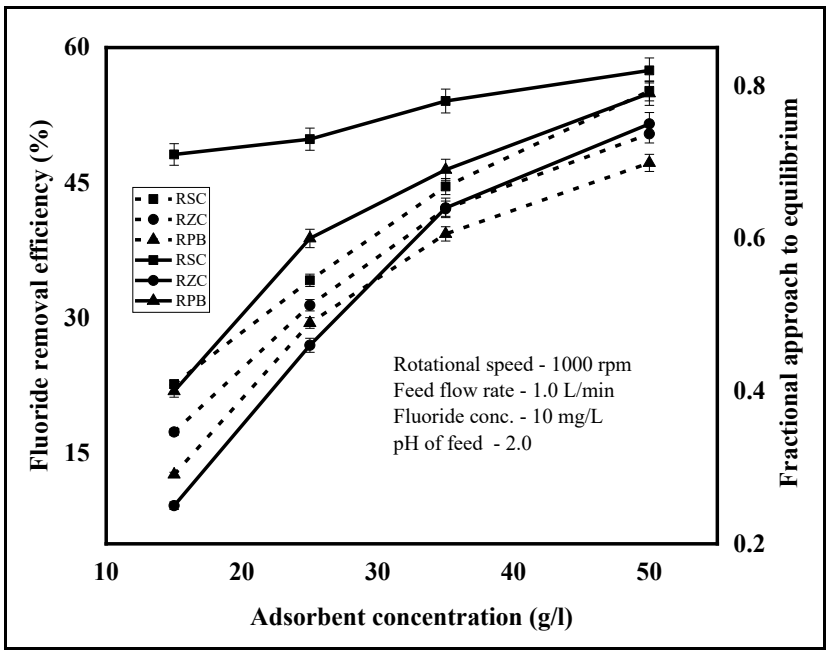

Figure 5.12: Effect of adsorbent dosage on fluoride removal efficiency and ∈ in rotating contactors

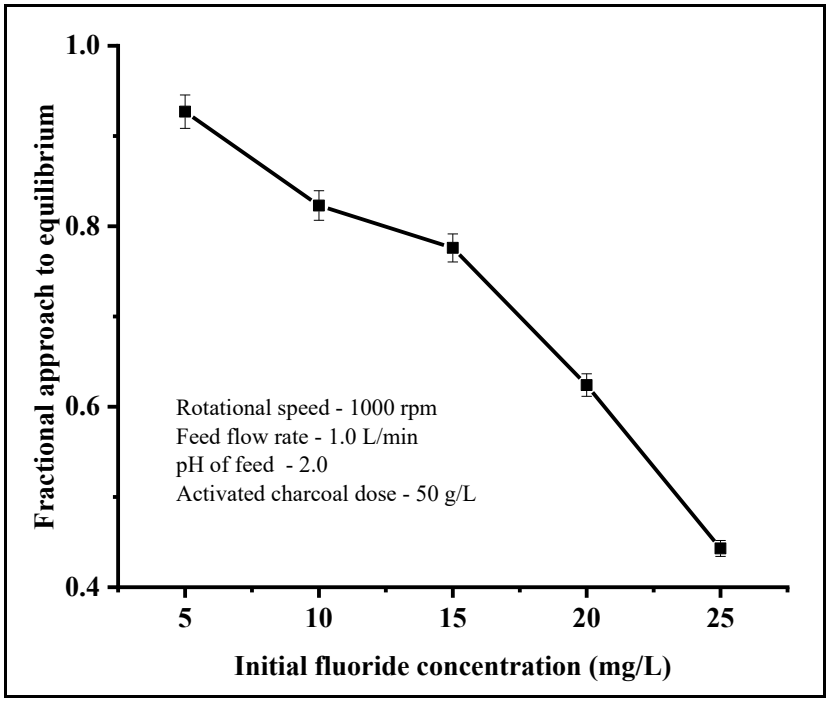

Figure 5.13: Fractional approach to equilibrium versus initial fluoride concentration

5.3.4.5 Overall volumetric Mass Transfer Coefficient

The variation of Ka with rotational speed and the flow rate in the rotating packed bed, rotating zig-zag contactor and rotating spiral contactor is given in Figure 5.14 and 5.15. It is seen that Ka varies from $2.8 \times 10^{-2} s^{-1}$ to $4.8 \times 10^{-2}\ s^{-1}$ in rotating spiral contactor, $2.3 \times 10^{-2}\, s^{-1}$ to $4.3 \times 10^{-2}\ s^{-1}$ in rotating zig-zag contactor, and from $1.6 \times 10^{-2}\, s^{-1}$ to $3.8 \times 10^{-2}\ s^{-1}$ in rotating packed bed on increasing the rotational speed from 250 rpm to 1000 rpm. The increase can be attributed to the decrease of diffusional resistance in the liquid film due to formation of thinner liquid films at higher rotational speed.

The overall volumetric mass transfer coefficient increases with the flow rate in the rotating contactors. The magnitude of Ka increased from $2.7 \times 10^{-2}\ s^{-1}$ to $6.6 \times 10^{-2}\ s^{-1}$ in the rotating spiral contactor, $2.2 \times 10^{-2}\, s^{-1}$ to $6.0 \times 10^{-2}\ s^{-1}$ in rotating zig-zag contactor, and from $2.0 \times 10^{-2}\ s^{-1}$ to $5.5 \times 10^{-2}\ s^{-1}$ in rotating packed bed as the flow rate increased from 0.5 L/min to 2.0 L/min. The increase is likely due to better liquid distribution in the contactors.

The volumetric mass transfer coefficient also increases with adsorbent dosage (Figure. 5.16). The magnitude of Ka takes into account both the mass transfer resistance in the solution phase and also the intraparticle resistance. Solute penetration into the adsorbent particles will be comparatively lower at adsorbent dosage of 50 gm/L compared to 15 gm/L as the average adsorbate concentration is lower in the particles at 50 gm/L. The magnitude of the intraparticle mass transfer coefficient can be considered to be inversely related to the penetration depth according to the film theory of mass transfer. Therefore, the higher value of Ka estimated at 50.0 gm/L adsorbent dosage compared to 15.0 g/L is due to lower intraparticle resistance, besides the increase of solid-liquid interfacial area in the contactor.

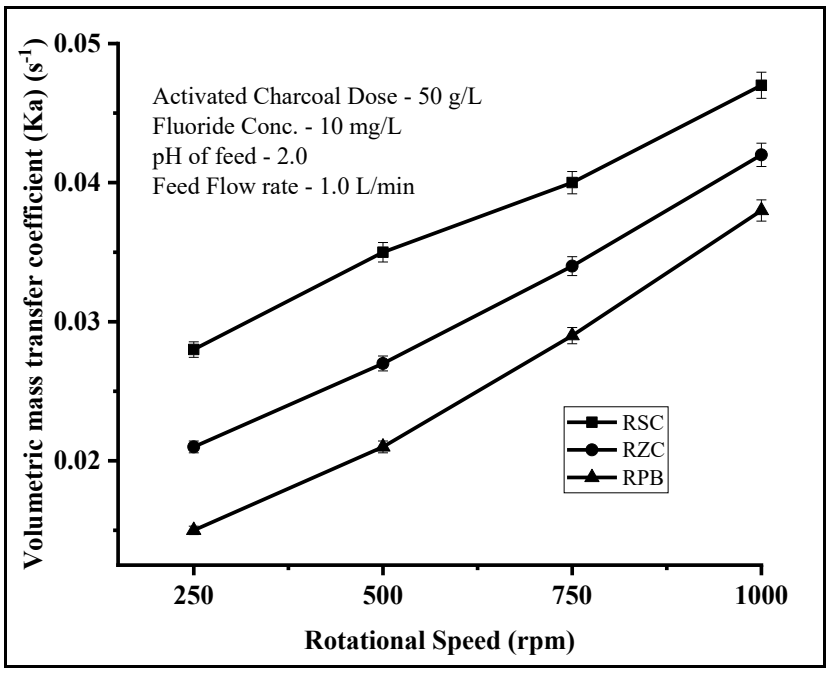

Figure 5.14: Variation of K_a with rotational speed in rotating contactors

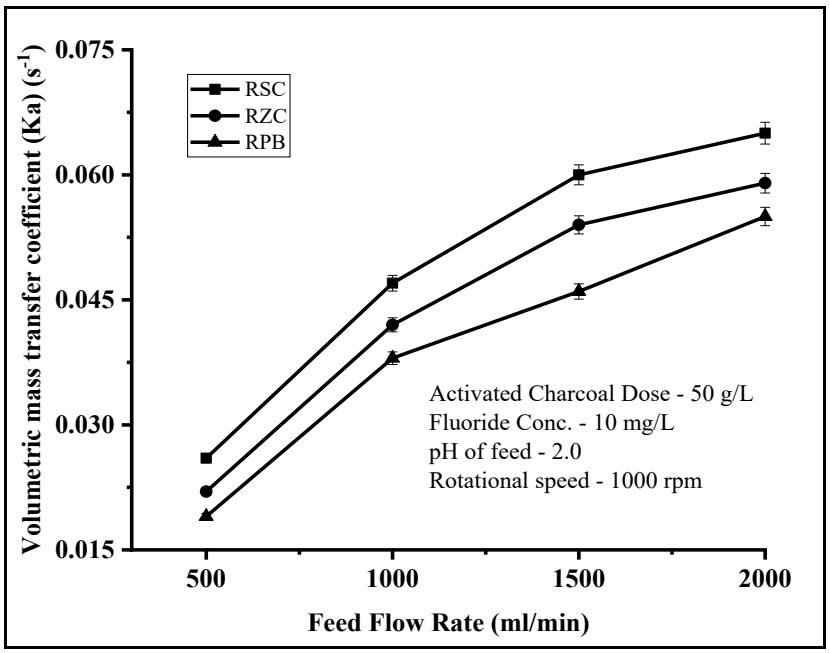

Figure 5.15: Variation of *Ka* with feed flow rate in rotating contactors

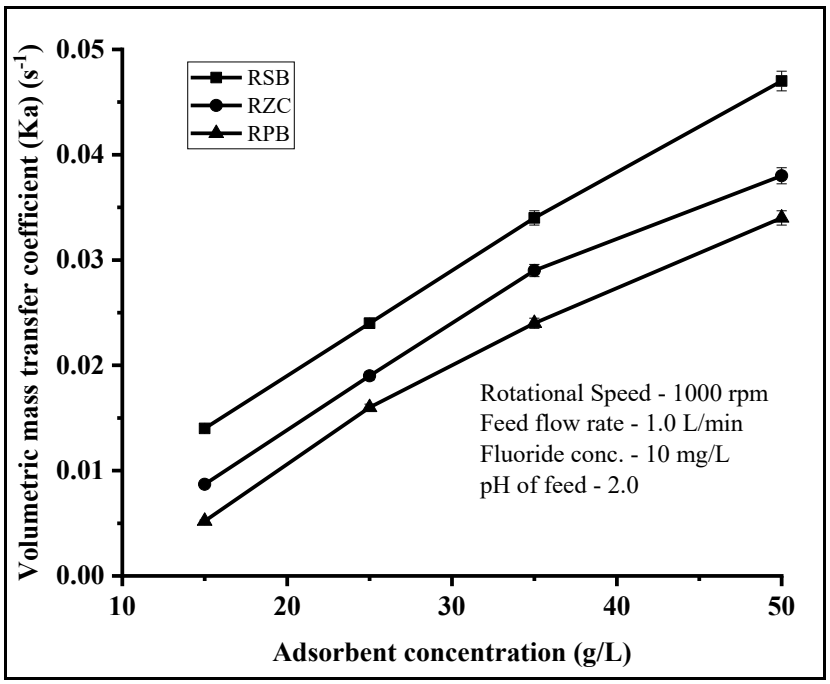

Figure 5.16: Variation of Ka with adsorbent dose in rotating contactors

5.3.4.6 Comparison of rotating contactors with fixed bed and agitated tank

Figure 5.17 compares the percentage removal of fluoride obtained in the agitated tank (agitator speed = 1000 rpm), fixed bed (height = 30 cm, diameter = 5.0 cm) rotating packed bed, rotating zig-zag contactor and rotating spiral contactor with the variation of feed concentration, all the contactors having the same volume. The results show that as the feed concentration was varied from 5.0 mg/L to 25.0 mg/L, the removal efficiency decreased from 66.0% to 23.7% in a rotating spiral contactor, 61.2% to 21.1% in rotating zig-zag contactor, 57.1% to 19.0% in rotating packed bed, 53.7% to 16.7% in a fixed bed, and from 51.7% to 12.3% in the continuous stirred tank.

In slurry adsorption, solute molecules diffuse through a liquid film before being adsorbed on the adsorbent. An estimation of film thickness can be obtained by dividing the flow rate by the surface area over which the liquid flows. The surface area per unit volume of the glass beads over which the slurry flows in the fixed bed with glass bead packing was approximately the same as in the rotating spiral contactor (210 cm^2/cm^3) but liquid maldistribution in fixed bed would reduce the surface area over which liquid flows. The film thickness over vertical surface can be obtained from

$$\delta = \left(\frac{3C\mu}{\rho^2 g}\right)^{1/3} \tag{5.16}$$

Where C is the mass flow rate per unit perimeter (kg/ms), μ is the viscosity (Pa·s), ρ is the density (kg/m^3) and g is terrestrial gravity (m/s^2). The influence of centrifugal acceleration fifty times the terrestrial gravity in rotating spiral contactor should lead to thinner liquid film in RSC as compared to that in the fixed bed. Due to this reason, lower diffusional mass transfer resistance results in higher values of η in RSC as compared to packed bed. Low values of solid-liquid mass transfer coefficient, short circuiting, dead zones and other non idealities result in even lower removal in continuous agitated contactor than in packed bed.

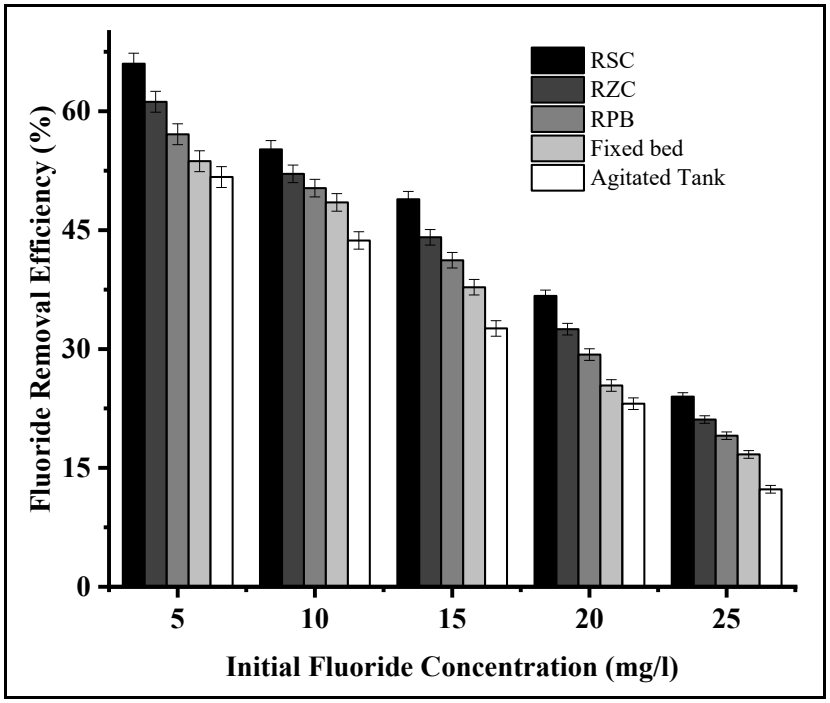

Figure 5.17: Comparison of performance of rotating contactors, fixed bed and continuous stirrer contactor with variation in feed concentration

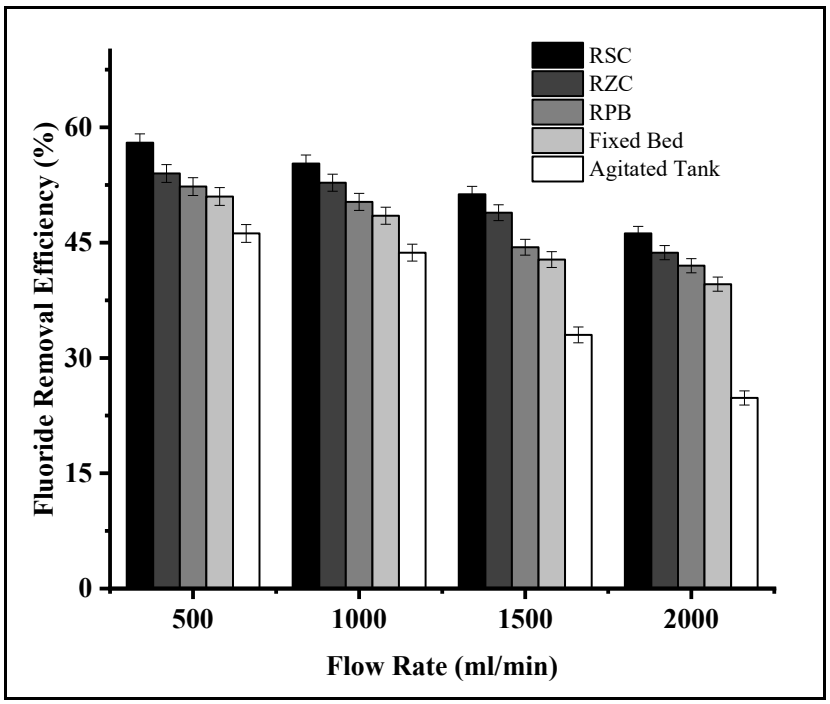

Figure 5.18: Comparison of performance of rotating contactors, fixed bed and continuous stirrer contactor with variation in feed flow rate

5.3.4.7 Comparison with rotating packed bed adsorber

Previous studies on adsorption under high gravity were carried out in rotating packed bed adsorber, the adsorbent particle is packed within the rotating bed and liquid was continuously circulated through this bed. Das et al. [5.12] reported that the time taken to reach 43% of the saturation value of the adsorbent bed required ~25 min of recirculation time for removal of Cu (II) using fish scale of Catla-Catla at the adsorbent packing density of 235 Kg/m^3 (95g adsorbent per liter solution), flow rate of 1.0 L/min and rotational speed of 1000 rpm. The time taken to reach ~43% saturation value of the adsorbent was ~15 min for removal of phenol by activated carbon [5.13]. at the feed concentration of 1000 mg/L, flow rate of 0.125 L/min and ~35g of adsorbent/L of solution. On the other hand, the same % saturation of the adsorbent was reached with slurry adsorption in rotating spiral contactor within a few seconds of residence time in the equipment. The slurry adsorber removes the solute at a much faster rate compared to rotating packed bed adsorber. The likely reason

is that liquid maldistribution has no effect on solid-liquid interfacial area as in slurry contactor as the adsorbent is present in the slurry itself.

5.4 Conclusion

The effectiveness of slurry contact adsorption in rotating contactors for the continuous removal of fluoride was studied. The major conclusions that could be reached are given below

1. In the rotating contactors, the percentage removal increased with rotational speed and slurry concentration. The percentage removal decreased with increase of feed flow rate though the amount of fluoride removed increased.
2. The percentage utilization of adsorbent capacity for fluoride in the contactors is higher at large adsorbate dosage and low feed concentration.
3. The rotating spiral contactor is the most efficient among the rotating contactors for removal of fluoride by this technique.
4. Use of high gravity makes the process more efficient compared to the conventional contactors, like continuous stirred tanks and fixed bed.
5. The mass transfer rates in slurry adsorption in rotating contactors is much faster than in rotating packed bed adsorber.

The reported values of the overall volumetric mass transfer coefficient in this study serve as a useful reference for designing this contactor. This approach can avoid the disadvantages of high pressure drop associated with fine adsorbents, high diffusion resistance with granular adsorbents.

Nomenclature

b Langmuir model parameter (L/mg)

C_e equilibrium concentration of fluoride in the solution in the batch experiment (mg/L)

C_{ex} experimental concentration of fluoride in solution at the contactor outlet (mg/L)

C_f feed concentration (mg/L)

C_0 initial fluoride concentration in the solution in the batch experiment (mg/L)

C_s fluoride concentration in the solution phase of the slurry at radial distance r from the center of the rotor (mg/L)

C^* minimum (equilibrium) concentration of fluoride at the contactor outlet (mg/L)

C_{s*} concentration of fluoride at the solution-adsorbent interface in equilibrium with the average concentration of fluoride in the adsorbent particle (mg/L)

Ka volumetric mass transfer coefficient (s^{-1})

q_e equilibrium concentration of fluoride in the solid phase (mg/g)

q_{ex} average fluoride concentration in the adsorbent at the contactor outlet obtained from experimental data (mg/g)

$\bar{q}_a$ average loading of adsorbent particles (mg/g)

q_{max} Langmuir model parameter representing maximum monolayer adsorption capacity (mg/g)

Q_s solution flow rate (L/min)

q^* theoretical equilibrium concentration of fluoride in the solid phase based on experimental conditions (mg/g)

Greek letters

$\in$ percentage approach to equilibrium

η percentage of fluoride removal

ω activated charcoal adsorbent dosage (g/L)

References:

5.1 S. Borjigin, Y. Ashimura, T. Yoshioka, T. Mizoguchi, Determination of fluoride using ion-selective electrodes in the presence of aluminum, *Anal. Sci.,* 25 (2009) 1437-1443.

5.2 S. Roy, P. Das, S. Sengupta, S. Manna, Calcium impregnated activated charcoal: Optimization and efficiency for the treatment of fluoride containing solution in batch and fixed bed reactor, *Process Saf. Environ. Prot.,* 109 (2017) 18 – 29.

5.3 G. Alagumuthu, V. Veeraputhiran, R. Venkataraman, Fluoride Sorption Using Cynodon dactylon-Based Activated Carbon, *Hem. ind.,* 65 (1) (2011) 23–35.

5.4 Y. Hanumantharao, M. Kishore, K. Ravindhranath, Characterization and Defluoridation Studies Using Activated Acacia Farnesiana Carbon as Adsorbent, *EJEAFChe,* 11(5) (2012) 442 - 458.

5.5 S. Bakhta, Z. Sadaoui, N. Bouazizi, B. Samir, O. Allalou, C. Devouge-Boyer, M. Mignot, J. Vieillard, Functional activated carbon: from synthesis to groundwater fluoride removal, *RSC Adv.,* 12 (2022) 2332 – 2348.

5.6 S. Ravulapalli, R. Kunta, Defluoridation studies using active carbon derived from the barks of Ficus racemosa plant, *J. Fluor. Chem.,* 193 (2017) 58 – 66.

5.7 Y. Ma, S. G. Wang, M. Fan, W. X. Gong, B. Y. Gao, Characteristics and defluoridation performance of granular activated carbons coated with manganese oxides, *J. Hazard. Mater.,* 168 (2009) 1140 – 1146.

5.8 J. R. Burns, C. Ramshaw, Process intensification: Visual study of liquid maldistribution in rotating packed beds, *Chem. Eng. Sci.,* 51 (8) (1996) 1347-1352.

5.9 J. M. MacInnes, J. Ortiz-Osorio1, P. J. Jordan, G. H. Priestman, R. W. K. Allen, Experimental demonstration of rotating spiral microchannel distillation, *Chem. Eng. J.,* 159 (2010) 159–169.

5.10 S. Sinkunas, J. Gylys, A. Kiela, Analysis of laminar liquid film flowing down a vertical surface, Fourth International Conference on CFD in the Oil and Gas, Metallurgical & Process Industries. 2005.

5.11 K. Guo, F. Guo, Y. Feng, J. Chen, C. Zheng, N. C. Gardner, Synchronous visual and RTD study on liquid flow in rotating packed-bed contactor, *Chem. Eng. Sci.,* 55 (2000) 1699-1706.

5.12 A. Das, A. Bhowal, S. Datta, Continuous biosorption in rotating packed-bed contactor, *Ind. Eng. Chem. Res.,* 47 (2008) 4230-4235.

5.13 W. Li, J. Yana, Z. Yan, Y. Song, W. Jiao, G. Qi, Y. Liu, Adsorption of phenol by activated carbon in rotating packed bed: Experiment and modeling, *Appl. Therm. Eng.,* 142 (2018) 760–766.

Chapter 06

REMOVAL OF FLUORIDE IN ROTATING CONTACTOR BY PRECIPITATION & COAGULATION

6.1 Introduction

The Nalgonda process is widely used industrially to remove fluoride from wastewater mainly due to the low cost of chemical reagents (alum and lime) required. The process is carried out in two separate continuous stirred tank reactors. Lime is added in the first reactor and alum in the second. In this study, the process has been carried out in a single reactor operating under high gravity. The objective was to determine the optimal conditions for continuous defluoridation in these reactors. The effectiveness of high gravity for this process has been studied by comparing the performance with conventional reactors.

6.2 Materials and Method

6.2.1 Materials

All chemicals utilized in the experiments were of analytical grade and were used without additional purification. Sodium Fluoride (NaF), TRIS (hydroxymethyl) aminomethane, and Disodium tartrate ($Na_2C_4H_4O_6 - 2H_2O$) were sourced from Merck Life Science Pvt. Ltd, Mumbai. Aluminum ammonium sulfate Dodecahydrate ($NH_4Al(SO_4)_2.12H_2O$), and calcium hydroxide $Ca(OH)_2$ was purchased from Loba Chemie Pvt. Ltd, Mumbai.

6.2.2 *Batch Studies*

A saturated calcium hydroxide solution was prepared by adding 7.0 g/L of this reagent in double-distilled water in a closed vessel and stirred for two hours under high agitation. The supernatant obtained after the separation of undissolved lime was used in further studies. Sodium fluoride was

dissolved in double-distilled water and specified amount of Aluminum ammonium sulfate dodecahydrate ($NH_4Al(SO_4)_2.12H_2O$) was added to the fluoride solution. The two prepared solutions were then mixed in a batch reactor equipped with an agitator. The supernatant after separation from the flocs was analyzed to determine the concentration of fluoride.

6.2.3 Continuous experimental studies

Continuous removal of fluoride was studied in rotating packed bed reactor (RPBR), rotating zig-zag bed reactor (RZR) and rotating spiral reactor (RSR), and in conventional ones - fixed bed (FB) and the continuous stirred tank reactor (CSTR).

The schematic diagram Figure 6.1 shows the experimental setup for continuous removal of fluoride by precipitation and coagulation using alum and lime in rotating bed contactors. Fluoride solution of different concentrations was prepared by dissolving an appropriate amount of sodium fluoride in the double-distilled water. The pH was determined by a digital pH meter (Eutech).

The experimental setup is shown in Figure 6.1. The saturated calcium hydroxide solution and solution comprising dissolved aluminum ions and fluoride were kept in separate reservoirs provided with agitators for continuous stirring. The two solutions were mixed just before entering the contactor and dispersed into the inner periphery of the rotor through the stationary distributor. The solution flows towards the outer radius of the reactor under the action of centrifugal force, splashed onto the casing wall and exited through an opening at the bottom of the casing. Continuous experiments were also carried out in fixed bed filled with glass beads, and in a CSTR equipped with an agitator rotating at 1000 rpm.

At specific intervals, samples were collected from the effluent and filtered through a Whatman 0.45-μm filter paper. The filtrate was analyzed to determine the residual fluoride concentration and solution pH using a Mettler Toledo Perfect Ion Seven Compact S220 fluoride ion selective electrode (ISE) and a digital pH meter (make: Eutech) respectively.

For analysis, the collected sample was mixed with TISAB-IV in a 1:1 ratio. The Ion Selective Electrode (ISE) method is widely used for the determination of fluoride concentration. However, the presence of aluminium interferes with the fluoride determination by ISE method due to fluoroaluminate complex formation. To overcome this problem related to the determination of fluoride due to complex formation, some suitable masking agents can be mixed with the total ionic strength adjustment buffer (TISAB). The tartrate (di-sodium tartrate) and tris (tris hydroxymethyl methylamine, hydrochloric acid) based TISAB-IV reduces the interference of aluminium majorly than other types of TISAB. The recovery rate of fluoride due to the addition of TISAB-IV is more than 95% even when the aluminium concentration in the solution reaches 500 mg/L. So TISAB-IV is used by the American Society for Testing and Materials (ASTM) [6.1].

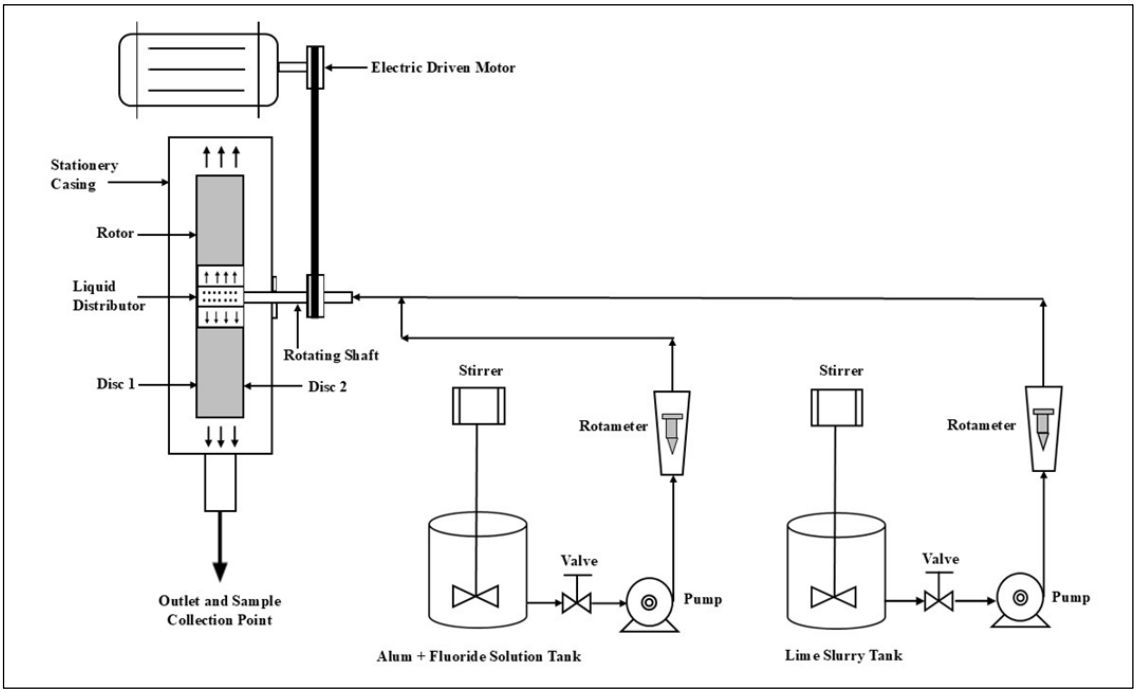

Figure 6.1: Schematic diagram of experimental setup for continuous removal of fluoride by precipitation and coagulation in rotating contactor

6.3 Result and Discussion

6.3.1 Characterization by Scanning Electron Microscope (SEM) Analysis

Scanning Electron Microscope (SEM) images of flocs obtained on contacting a solution containing alum with saturated calcium hydroxide solution is shown in Fig 6.2(a), whereas Fig 6.2(b) depicts the images of flocs obtained after adding saturated calcium hydroxide solution to a solution containing alum and fluoride. Prior to imaging, the flocs samples were dried. It is seen in Figure 4 that the flocs exhibited an amorphous structure with irregular surface morphology. These findings are consistent with the observations reported by Dubey et al [6.2].

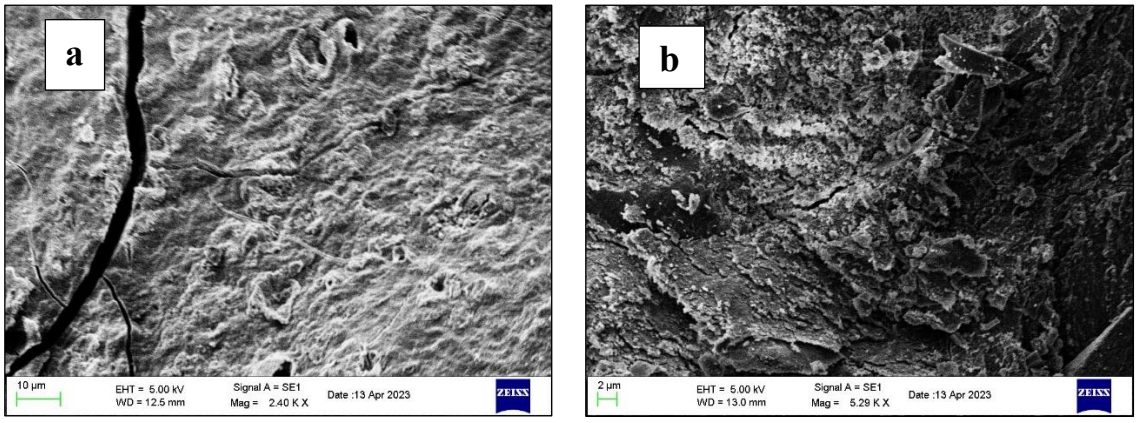

Figure 6.2: SEM images of reactant (Alum & saturated calcium hydroxide solution) **(a)** Without presence of fluoride, **(b)** With presence of fluoride.

6.3.2 Characterization by FTIR Analysis of Alum Lime Flocs after addition of fluoride

FTIR spectroscopy was used to explore the characteristics of flocs and amorphous oxides produced from alum and lime reactions. After the addition of fluoride, the flocs were studied using a Perkin-Elmer, Spectrum Two FT-IR Spectrometer, at atmospheric temperatures, between 400 and 4000 cm^{-1} shown in Figure 6.3.

Figure 6.3 shows the FTIR peak at 3456.63 cm^{-1} corresponds to the $O-H$ stretching vibration of hydroxyl groups in the $Al(OH)_3$ structure, which is key to forming the spectrum of aluminum hydroxide fluoride [6.3]. The 1645.96 cm^{-1} peak signifies the $O-H$ bending vibration, most often

associated with calcium's hydroxyl group. The prominent sharp and strong peak at 1115.73 cm^{-1} is attributed to $Al - O - H$ bending vibrations, which are closely linked to the formation of aluminum hydroxide fluoride [6.3]. A peak observed at 604.37 cm^{-1} corresponds to the $Al - F$ stretching vibration, which is essential for aluminum fluoride complex formation. The previous studies also denoted the same peak in their analysis [6.3 -6.5]. The formation of CaF_2 is attributed to the $Ca - F$ stretching vibration, typically appearing at the 523.11 cm^{-1} peak [6.6]. From this study, it was noted that the fluoride is chemisorbed onto the Aluminium hydroxide and calcium.

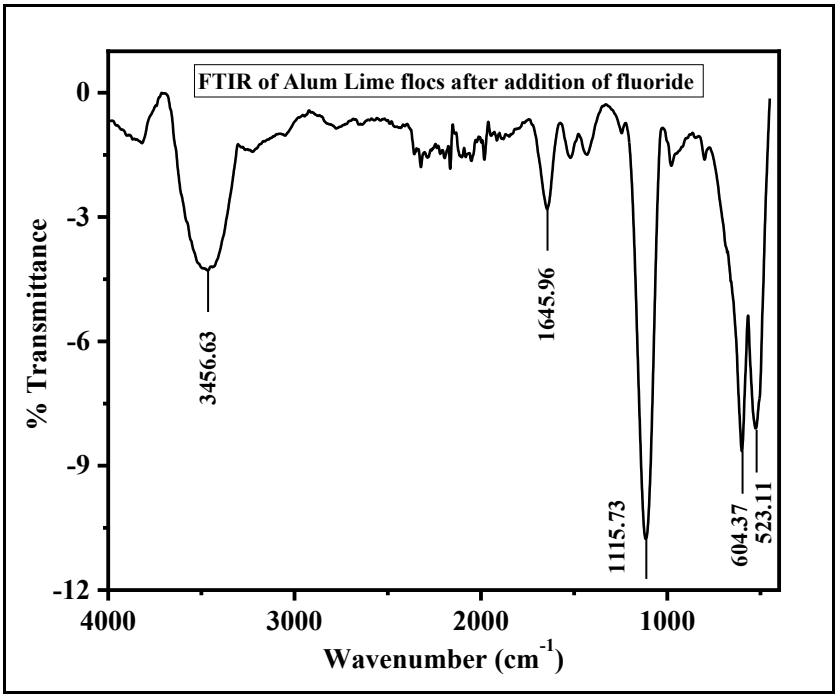

Figure 6.3: FTIR analysis of Alum Lime flocs with presence of fluoride

6.3.3 Characterization by XRD Analysis of Alum Lime Flocs with presence of fluoride

The X-ray diffraction (XRD) was recorded by an X'Pert Pro XRD diffractometer for flocs after the addition of fluoride, operating with anode material Cu with intended wavelength type Kα1 as radiation source. The XRD analysis is shown in Figure 6.4. The 2θ scanning was recorded from 5° to 90°. The spectrum of the XRD for the flocs shows shallow and broad diffraction peaks. The low intensity and broad peaks denoted that the flocs are amorphous and low crystalline [6.3, 6.7].

The medium peaks appeared at degrees 11.54, 32.13, 39.58, and 65.26 were those of hydrated Aluminum fluoride hydroxide [6.8 - 6.9]. Another very strong peak located at 18.84 and 20.74 degrees corresponds to Aluminum hydroxide fluoride and Aluminum hydroxide, respectively. The peaks that appeared at 47.75 and 55.48 degrees were identified to be those of calcium fluoride [6.10 – 6.11].

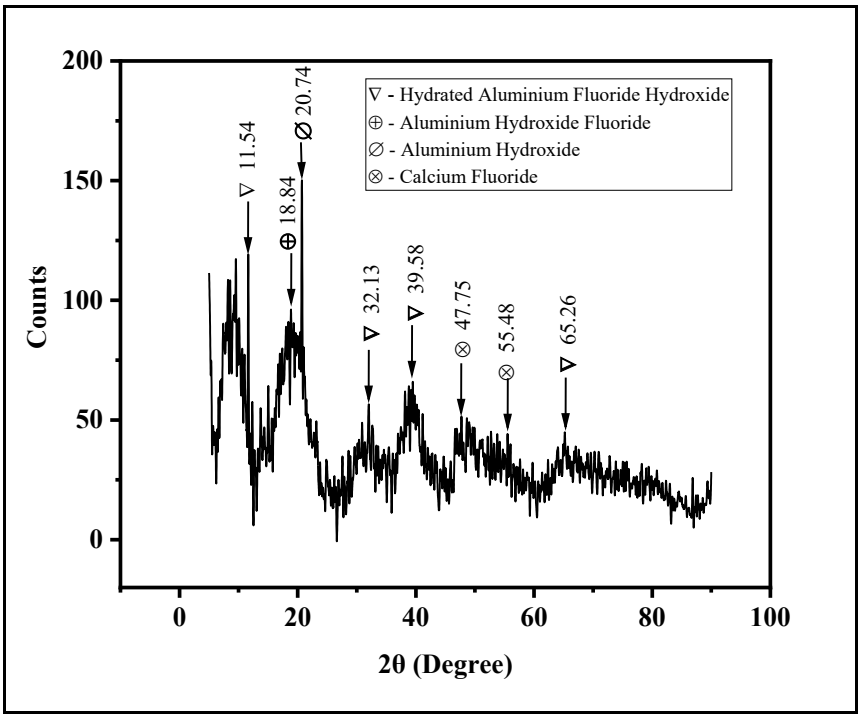

Figure 6.4: XRD analysis of Alum Lime flocs with presence of fluoride

6.3.4 Mechanism for fluoride removal

The chemistry behind fluoride removal by alum and lime is quite complex. Corbillon et al. [6.12] reported that complexes such as AlF_2^+, AlF^{2+} AlF_3, AlF_4^-, AlF_5^{2-} and AlF_6^{3-} are formed in the solution in the presence of Al^{3+}/F^- ions. Gong et al. [6.13] noted that at pH = 8.0, the fluoride existed as free fluoride anions in the solution, with the complex constituting 0.1% of the total fluoride concentration range of 5 - 80 mg/L. Fluoride ions in the form of complex was still negligible (below 0.5%) at pH 7.0 at total fluoride concentration below 40 mg/L. The fraction of fluoride in the form of the complex increased at lower pH and free F^- becomes negligible below pH 5.0.

Aluminum ions also exist in various hydrated and hydroxide forms [6.8]. As hydroxyl anions are added, $Al-F$ complexes are dissociated and the soluble species in the aqueous solution mainly consist of $Al-F$ complexes, $Al-OH$ complexes, Al^{3+} and free fluoride [6.2]. Ayoob et al. [6.14] noted that the likely mechanism for fluoride removal from the solution may be due to coprecipitation of fluoride and hydroxide ions with Aluminum ions to yield a precipitate with the general formula $Al_nF_m(OH)_{3n-m}$ given by eq. (6.1), and adsorption by (eq. 6.2). Gong et al. [6.13] proposed reaction of $Al-F$ complexes with OH^- such as given by eq. 6.3 to yield precipitates

$$nAl^{3+}(aq) + (3n-m)OH^-(aq) + mF^-(aq) \rightarrow Al_nF_m(OH)_{3n-m}(s) \quad (6.1)$$

$$Al_n(OH)_{3n}(s) + mF^-(aq) \rightarrow Al_nF_m(OH)_{3n-m}(s) + mOH^-(aq) \quad (6.2)$$

$$AlF_2^+ + OH^- \rightarrow AlF_2(OH)\,(s) \quad (6.3)$$

When calcium hydroxide solution was added, removal of fluoride also occurred due to precipitation reaction given by equation (6.4) if the solubility product is exceeded.

$$Ca(OH)_2 + 2F^- \rightarrow CaF_2 \downarrow + 2OH^- \quad (6.4)$$

Zuo et al. [6.15] noted that even if the concentration of the reacting species in the above reaction is below the solubility limit of calcium fluoride (CaF_2), Ca^{2+} has a positive influence on fluoride removal as it coprecipitates with $Al^{3+}$and Ca^{2+}

$$mAl^{3+} + nCa^{2+} + (3m+2n)H_2O = Al_mCa_n(OH)_{3m+2n}^+ \quad (6.5)$$

6.3.5 Batch experimental study

Alum dosage has been represented in terms of aluminum ion concentration (Al^{3+}), as the chemistry of this system is explained in the literature with reference to Al^{3+} concentration. The concentration of aluminum ions (Al^{3+}) and fluoride ions (F^-) reported in this study is the value obtained on mixing the two solutions/streams.

The percentage of fluoride obtained in kinetic studies carried out at agitator speed of 1000 rpm is shown in Figure 6.5. At an initial Al^{3+} concentration of 420 mg/L and F^{-} concentration of 50 mg/L, about 95% fluoride removal was achieved within the first 2 minutes. The removal gradually increased to 98.3% after 30 min and did not significantly change thereafter. This suggests that the reactions involved are fast and micro mixing is important for this system.

Figure 6.6 depicts the percentage removal obtained in the batch reactor after 1h at different concentrations of Aluminum ions along with the corresponding final pH. The percentage removal gradually increased with Al^{3+} concentration reaching a maximum value of 98.3% at Al^{3+} concentration of 420 mg/L (alum concentration of 7.0 g/L), and then decreased with further increase of Al^{3+} ion. The solution pH gradually decreased with an increase in Al^{3+} ion concentration and was ~7.0 at Al^{3+} concentration of 420 mg/L.

The concentration of calcium ions in saturated calcium hydroxide solution is ~0.01 mol/L, which is few orders of magnitude higher than the concentration required for fluoride precipitation as CaF_2. Thus, the reaction given by eq. (6.3) contributes to the removal of fluoride as also indicated in FTIR analysis of the precipitates. The speciation curve for Aluminum [6.16] suggests that the solubility of Al is minimum at around pH 7.0 and increases on either side of this value. Maximum amount of flocs would be formed around pH 7.0 facilitating the removal of fluoride. This was also partly substantiated by the amount of precipitate (0.83 g/L) collected being highest at this pH. The result is in agreement with earlier batch studies reporting maximum fluoride removal within the pH range of 6.0 - 8.0 [6.2].

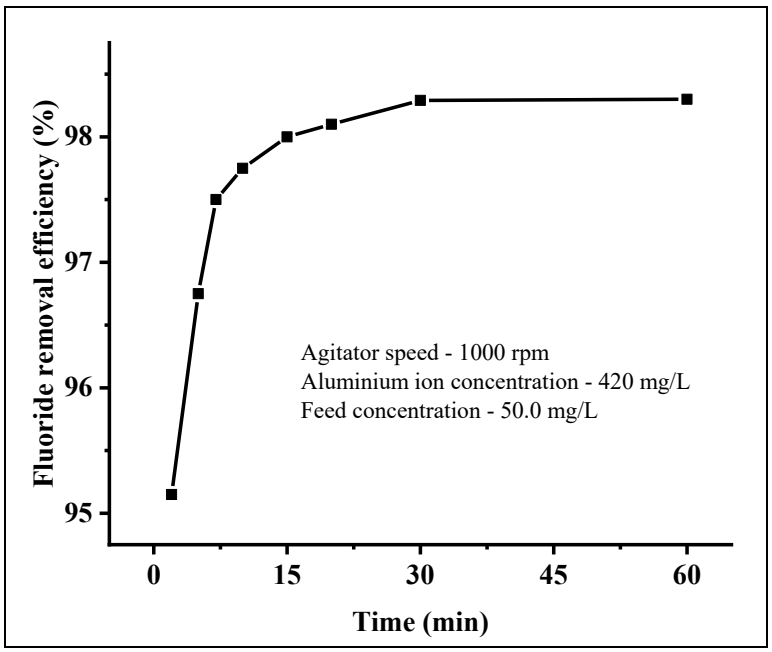

Figure 6.5: Variation of percentage removal of fluoride with time in batch reactor

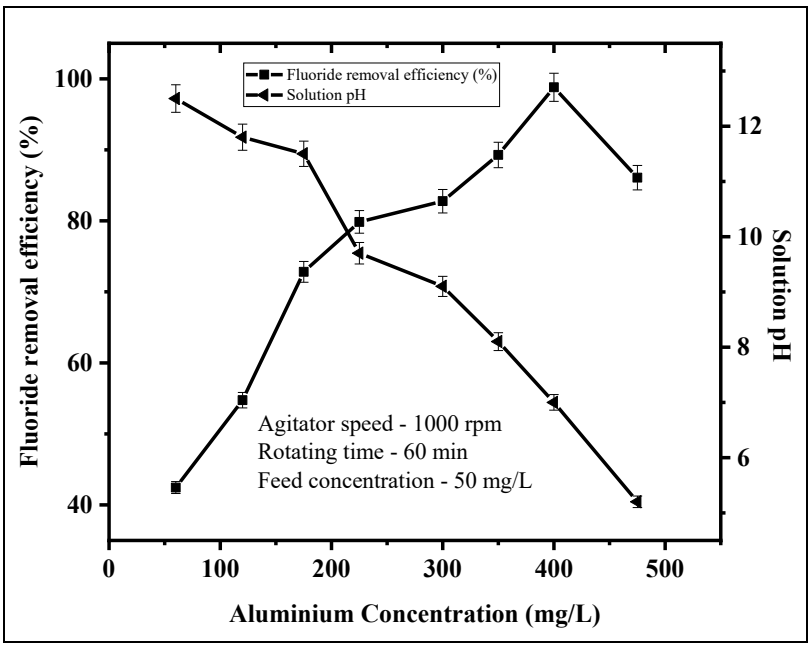

Figure 6.6: Solution pH and Fluoride removal efficiency with change in Aluminium concentration

6.3.6 Continuous experiments in Rotating contactors

Gong et. al. [6.13] reported that the removal of fluoride by coagulation (alkaline solution added to a solution containing Aluminum and fluoride ions) was much faster than when fluoride was added to a solution containing Al^{3+} and OH^{-} where flocs have already been formed. Therefore, lime water and alum solution were kept in separate reservoirs in this study to prevent the formation of flocs before entering the reactor. Fluoride was added to the alum solution rather than a saturated lime solution so that the removal occurs only in the reactor and not in the reservoir. In the continuous study, the pH of the solution in the reservoir containing Al^{3+} and F^{-} ions were in the range of 3.0. At this pH, fluoride is expected to exist mostly as a complex.

The reactions given by eq (6.1), (6.3) and (6.4), formation of $Al_n(OH)_{3n}$ flocs, and adsorption on the flocs proceeds simultaneously in the contactor as calcium hydroxide solution and alum-fluoride is mixed in it. Fluoride ions diffuse through a liquid film of the solution to reach the surface of the flocs before being adsorbed on it. Thus, removal of fluoride would be higher at operating conditions associated with efficient micro-mixing for faster chemical kinetics, larger holdup of solution in the reactor so that the greater amount flocs is present within the reactor to increase adsorption capacity as well as mass transfer surface area, and higher values of mass transfer coefficient in the solution film. Higher values imply lower the diffusional resistance thereby ensuring higher concentration of fluoride at the floc solution interface and enhancing the removal rate given by eq. (6.2).

6.3.6.1 Effect of Rotational Speed

The influence of rotational speed (ω) on the percentage removal of fluoride in the rotating reactor is illustrated in Figure 6.7. The flowrate mentioned in this study is the combined flowrate of both the solution entering into the reactor in 1:1 ratio. The experimental investigation was carried out by changing the rotational speed from 250 rpm to 1000 rpm, keeping other operating parameters constant. Increasing ω to 1000 rpm enhanced the centrifugal field to ~25 times that of terrestrial gravity. It is seen that, as the rotational speed was increased from 250 rpm to 1000 rpm, the

percentage removal of fluoride increased from 66.6% to 79.6% in the rotating packed bed reactor, 76.2% to 86.3% in rotating zig-zag bed reactor, and from 80.6% to 93.8% in the rotating spiral reactor.

Yang et al. [6.17] reported that micro mixing in RPBR increases with rotational speed thereby intensifying the reaction rate. Increased micro mixing also ensures the rapid formation of $Al_n(OH)_{3n}$ flocs within a short distance from the inlet of the reactor. Although there are no published studies on micromixing in rotating spiral reactor, the similarity of flow patterns (as a thin film) with spinning disk contactor (SDC) would suggest that this parameter would improve in RSR with increase in ω as is the trend in the latter equipment [6.18]. The increase of velocity of splashing of ligaments and drops onto the successive baffle walls with rotational speed should lead to higher micro-mixing. The mass transfer of fluoride onto flocs resembles the adsorption of fluoride onto powdered activated carbon reported in the previous chapter. It was noted that the overall volumetric mass transfer coefficient increases with rotational speed in these equipment. This along with efficient micro mixing contributes to higher percentage removal as rotational speed is increased.

The amount of flocs present in the contactor depends on the liquid holdup. In the rotating packed bed, the solution flows through the interstitial spaces of the glass beads while adhering to the surfaces of the packing [6.19]. In the rotating spiral reactor, the liquid flows along with the baffle wall as a film [6.20]. Though there are several theoretical relations and experimental studies for determining holdup, ε in RPB with wire mesh or metal foam packing, no such studies have been reported for glass bead packing. In absence of data on holdup in these reactors, the similarity of flow hydrodynamics under terrestrial gravity in conventional packed bed for RPBR, and falling film over a vertical wall for RSR suggest that an estimation of holdup can be obtained based on equations proposed for this equipment. The discussion has been limited to RPBR and RSR as there are no corresponding equipment based on which holdup can be estimated for RZR.

The holdup in RSR was obtained by estimating the thickness of liquid film, δ at different radial position, r along the length of baffle through the formulae given by eq. (6.6), by replacing the term terrestrial gravity g with $\omega^2 r$, followed by multiplying the average film thickness with the cross-sectional area of each spiral baffle.

$$\delta = \left(\frac{3\mathsf{C}\mu}{\rho^2 g}\right)^{1/3} \tag{6.6}$$

Where μ is the solution viscosity, C is the mass flow rate per unit perimeter, and ρ is the solution density. Eq. (6.7) proposed for estimation of holdup in fixed bed [6.21] was used for RPBR

$$\varepsilon = 16.13\left(\frac{\mu U^2 N}{\rho g^2}\right)^{1/4}(Nd^2)^{-1/3} \tag{6.7}$$

In the above equation, N is the number of beads per unit contactor volume, U is the superficial velocity and d is the diameter of glass beads.

The fractional holdup in RPBR and RSR at rotational speed of 1000 rpm and flowrate of 1 L/min is 0.017 (0.4 s) and 0.036 (0.87s). The values within bracket represent the corresponding residence time. The holdup and residence time was approximately 1.5 – 2 times higher in RSR compared to RPBR. Therefore, the amount of $Al_n(OH)_{3n}$ flocs on which adsorption occurs as well as the time for reaction and adsorption to occur would be more in RSR. These along with higher values of mass transfer coefficient contribute to the higher removal percentage observed in rotating spiral contactor.

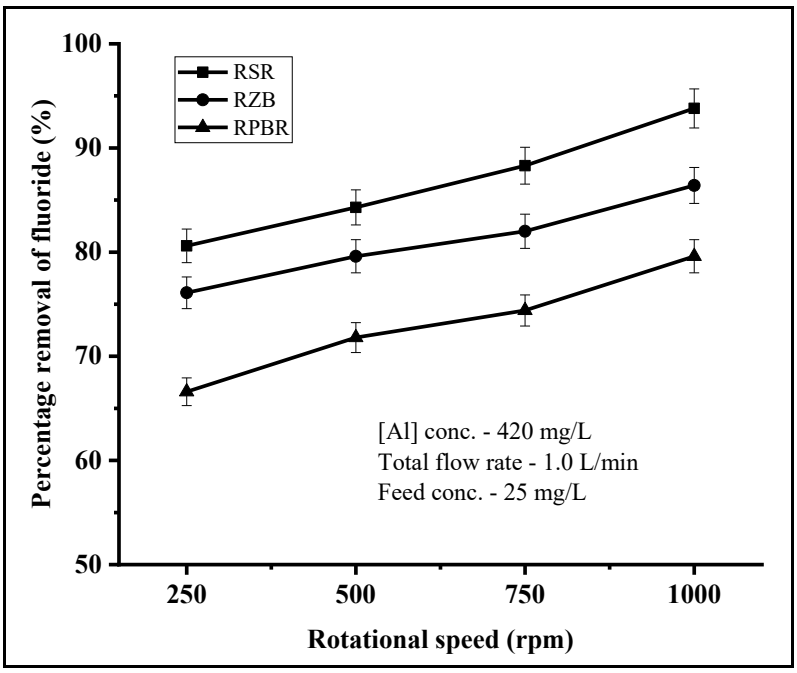

Figure 6.7: Effect of rotational speed on fluoride removal efficiency in rotating reactors

6.3.6.2 Effect of change in flow rate

These experiments were carried out at a rotor speed of 1000 rpm, Al^{3+} concentration of 420 mg/L, and initial fluoride concentration of 25 mg/L respectively. The results are depicted in Figure 6.8. The removal of fluoride concentration decreased from 94.4% to 73.0% in the rotating spiral reactor, 87.4% to 67.9% in the rotating zig-zag bed reactor, and 80.0% to 59.9% in the rotating packed bed reactor, as the flow rate increased from 0.5 L/min to 2.0 L/min.

At constant rotational speed of 1000 rpm, the holdup varied from 0.01 (0.48 s) to 0.028 (0.34 s) in RPBR, and from 0.025 (1.2 s) to 0.036 (0.43s) in RSR as the solution flow rate was increased from 0.5 L/min to 2.0 L/min. The corresponding residence time is given within bracket. The amount of flocs in the reactor increases with flow rate due to higher liquid holdup. Higher amount of $Al_n(OH)_{3n}$ flocs is also expected to be formed as the amount of chemical reagents entering the reactor increased with the flow rate. The volumetric mass transfer coefficient increases with flow rate as seen in the previous chapter for slurry adsorption. But micromixing efficiency [6.17, 6.18] and the residence time decreases at higher flow rate. The net effect of these was an increase in

removal rate of fluoride (obtained by multiplying the flow rate and the difference in inlet and outlet fluoride concentration) increased with flow rate. In RSR, the value was 12.61 mg/min at a total flow rate of 0.5 L/min and 39.01 mg/min at 2.0 L/min. However, the increase was not sufficient to remove the increased amount of fluoride that entered the reactor per unit time and the percentage removal decreased.

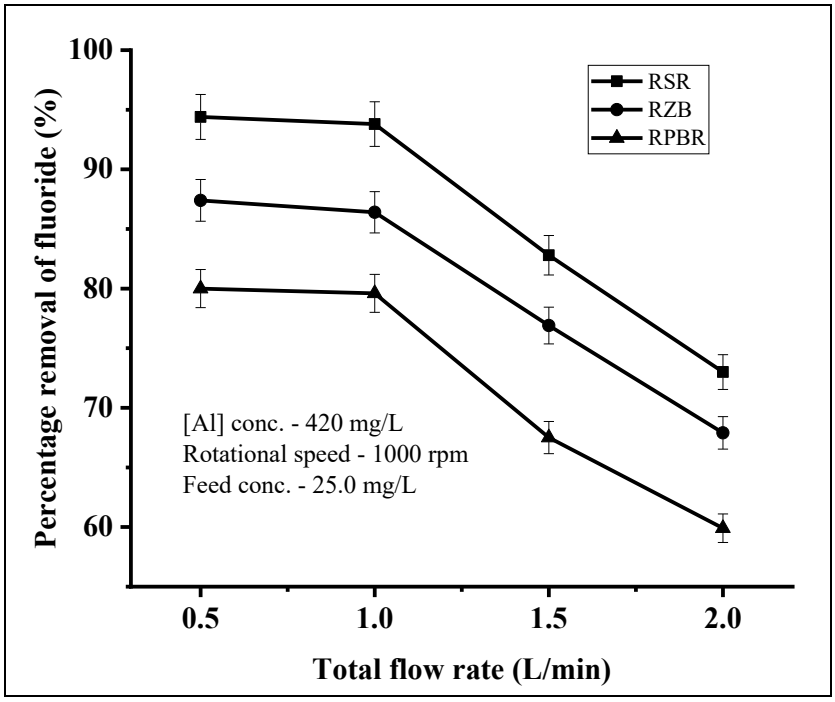

Figure 6.8: Effect of change in flow rate on fluoride removal efficiency in rotating contactors

6.3.6.3 Effect of feed concentration

The effect of feed concentration on fluoride removal is depicted in Figure 6.9 and was studied at constant 1000 rpm rotational speed, 0.5 L/min flow rate of each of Aluminum ion-fluoride and saturated lime solution, and Al^{3+} concentration of 420 mg/L respectively. The percentage removal of fluoride decreased from 97.6% to 80.6% in the rotating spiral contactor, 91.7% to 72.7% in the rotating zig-zag contactor, and 86.0% to 64.3% in the rotating packed bed as the feed concentration increased from 5.0 mg/L to 50.0 mg/L. The rate of fluoride removal however increased in the contactors with an increase in feed concentration. In the rotating spiral contactor, the rate increased from 5.87 mg/min to 40.96 mg/min.

Aluminum hydroxide starts precipitating at pH > 4 [6.16]. Gong et al. [6.13] noted that the presence of fluoride ions makes Al^{3+} ions more soluble. The solubility is higher at pH = 6.0 compared to pH = 7.0. Higher solubility reduces the amount of flocs formed onto which F^- is adsorbed. The fraction of F^- ions existing as a complex with Al^{3+} is dominant at the solution pH and fluoride concentration [6.13] in the solution flowing into the reactor. The dissociation kinetics of the *Al-F* complex may have a role in slower release of free F^- ions for removal by chemical reaction and adsorption. The possible increase of the rate of chemical reaction as well as mass transfer driving force for adsorption due to higher concentration of fluoride ion in feed is clearly not sufficient to remove the higher amount of fluoride entering the reactor resulting in decrease of percent removal.

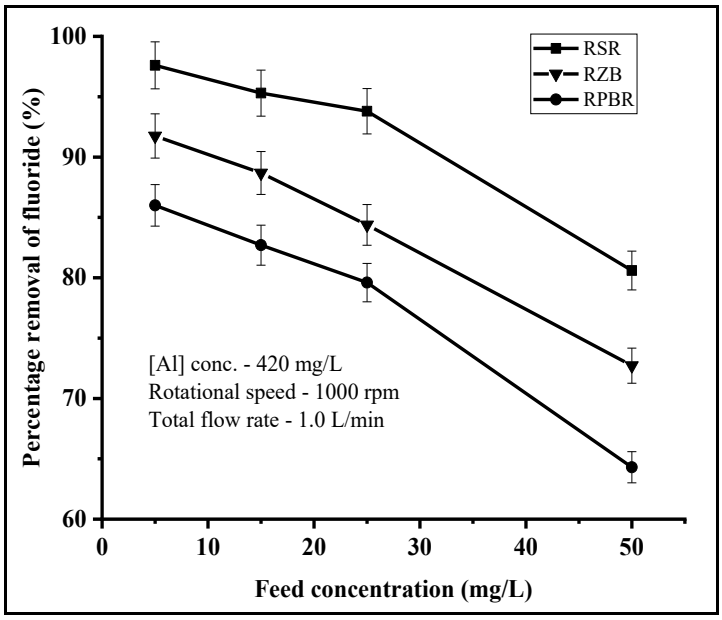

Figure 6.9: Effect of change in feed concentration on fluoride removal efficiency in rotating contactors

6.3.6.4 Effect of Aluminum Concentration

The variation of *Al* concentration was investigated at a constant rotational speed of 1000 rpm, initial fluoride concentration at 25 mg/L, and flow rate of aluminum fluoride solution and saturated lime slurry at 0.5 L/min respectively, and the result is illustrated in Figure 6.10. It is observed that on increasing the concentration of *Al*, the fluoride removal efficiency also increases up to 420 mg/L

and then decreases in all the contactors. The percentage of fluoride removal increased from 36.1% to 93.7% in the rotating spiral reactor. In rotating zig-zag bed reactor and rotating packed bed reactor, it increased from 31.0% to 86.3%, and 28.2% to 79.5% respectively. On further increase from 420 mg/L to 475 mg/L, the efficiency in removal of fluoride decreased from 93.7% to 88.9% in rotating spiral reactor, 86.3% to 81.3% in rotating zig-zag bed reactor, and 79.5% to 76.7% in the rotating packed bed reactor.

Increasing the concentration of Al^{3+}, decreases the solution pH. The pH of the outlet stream was ~11 at an Al^{3+} concentration of 175 mg/L (alum dosage = 3.0 g/L), which decreased to ~7.0 at an Al^{3+} concentration 420 mg/L and ~5.0 at 475 mg/L (alum dosage = 8.0 g/L). The amount of solubility of Aluminum hydroxide flocs into which fluoride is adsorbed approaches a maximum value at pH = 7.0 and decreases on either side of this value [6.23]. Thus, fluoride removal by eq. (2) is highest at $[A^{3+}]$ = 420 mg/L.

Results of batch studies of one hour duration show that at an initial fluoride concentration of 25 mg/L, fluoride removal at Al^{3+} ion concentration of 175 mg/L, 300 mg/L, and 420 mg/L was approximately 75%, 87%, and 100% respectively. In RSR, wherein the removal was maximum, the percentage removal was approximately 36% (11.5), 56% (9.0), and 94% (7.0) respectively. The values given within bracket gives the approximate value of pH of the effluent stream. The deviation from the maximum removal attainable is 52%, 36%, and 6% respectively, and decreased as pH value of 7.0 is approached. There was no significant difference in the solution pH and the concentration of precipitates obtained in batch studies and in the solution exiting RSR. Adsorption onto flocs plays a leading role in fluoride removal with this technique. At pH 8 and above, electrostatic repulsion of fluoride ions with the negatively charged surface and the competition for active sites with the hydroxyl ions has been proposed by researchers [6.24 – 6.25] to explain the lower removal at higher pH. The increasing deviation as hydroxyl ion concentration increases at higher pH can be justified if the above stated mechanism negatively affects the adsorption kinetics. The residence time of a

second or less associated with this equipment [6.22] is not sufficient for the removal given by eq. (2) to proceed to a great extent.

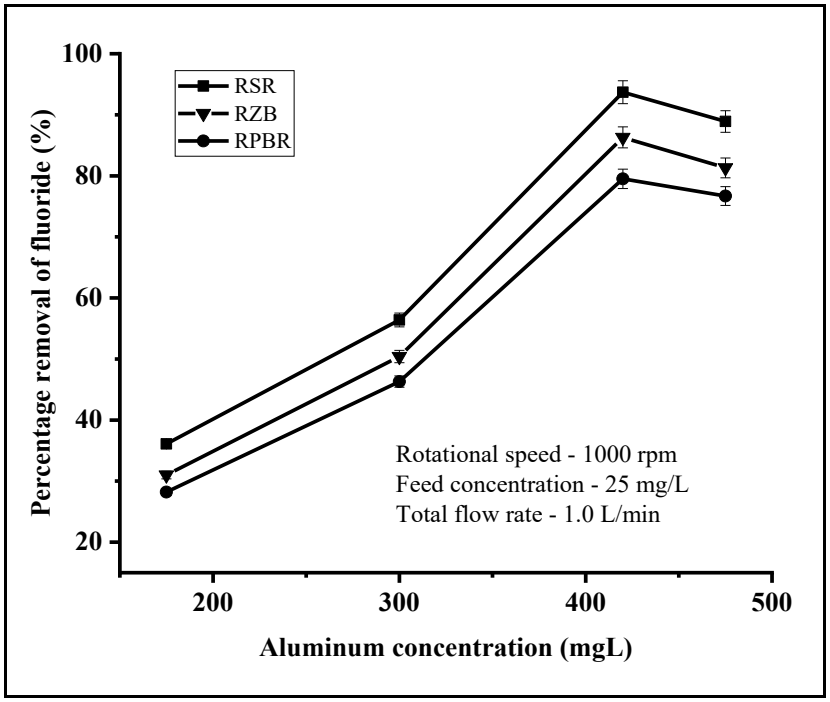

Figure 6.10: Effect of change in reactant concentration on fluoride removal efficiency in rotating contactors

6.3.6.5 Comparison between the rotating contactors and conventional reactor

The comparison of rotating contactors (RSR, RZBR, and RPBR) and conventional reactors (Fixed bed and CSTR) was carried out at varying feed concentrations and is shown in Figure 6.11. The other parameters such as aluminum concentration at 420 mg/L, and flow rate of reactant aluminum ion solution and saturated lime solution at 0.5 L/min each were kept constant. The experimental investigation showed that the removal of fluoride was highest in the rotating spiral reactor (RSR) and the least in the continuous stirrer tank reactor (CSTR).

The overall volumetric mass transfer coefficient in packed bed was obtained from the experimental data of the equipment in chapter 5 using eq. (6.7)

$$K_{oc}a = \frac{Q_s}{V}\int \frac{dC_s}{(C_s - C_{s*})} \qquad (6.8)$$

Assuming complete mixing, $K_{oc}a$ was obtained in CSTR from the equation

$$K_{oc}a = \frac{Q_s(C_f - C_{ex})}{(C_s - C_{s*})} \tag{6.9}$$

The magnitude of $K_{oc}a$ in packed bed and CSTR at flow rate of 1.0 L/min was determined to be ~ 0.01 1/s and ~8x10^{-3} 1/s (flow rate = 1 L/min). The residence time is higher in fixed bed and CSTR due to larger fractional holdup. But the lower values of mass transfer coefficient, poor micro-mixing (which could delay formation rate of flocs), coupled with the presence of liquid mal-distribution in fixed bed and non-idealities in CSTR [6.26-6.27] result in lower percentage removal in the conventional contactors.

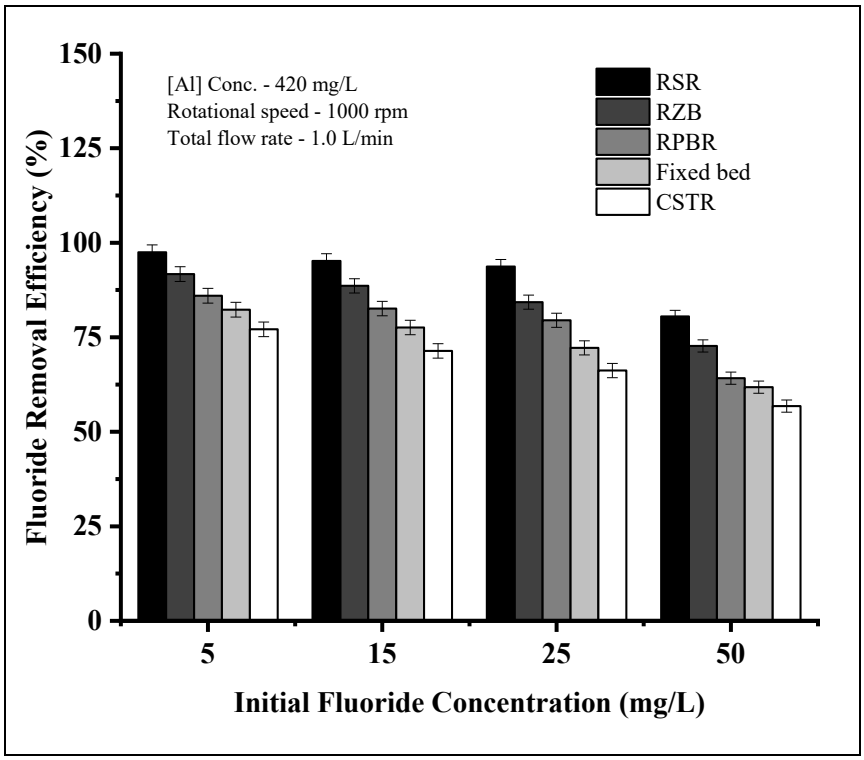

Figure 6.11: Comparison of performance of RSR, RZBR, RPBR, fixed bed, and CSTR with variation in feed concentration

6.4 Conclusions

This research focused on continuous removal of fluoride through precipitation and coagulation in rotating contactors of different designs, and conventional ones. The influence of operational parameters like rotation speed, flow rate, feed concentration, and alum concentration on removal efficiency in rotating contactors was evaluated through experimental studies. The following conclusions could be drawn.

1. The optimal pH for which maximum removal of fluoride is obtained in both batch and continuous studies is around pH 7.0 for the range of operating conditions varied.
2. In high gravity reactors, the percentage removal of fluoride increased with rotational speed. Increase in flow rate reduced the percentage removal but increased the rate of removal of fluoride.
3. The performance of rotating spiral reactor was superior to rotating packed bed reactor with percentage removal closely approaches the maximum value at optimal pH within a small sized reactor in the latter.
4. The deviation from maximum removal obtained in batch studies for the same value of alum dosage and feed concentration increased at pH greater than the optimal value.
5. The experimental findings demonstrated that the high gravity reactors significantly outperformed the conventional reactors, suggesting that this equipment has significant potential in reducing reactor volume for industrial applications of this process.
6. The fundamental mechanism of the removal process remaining same with the different coagulants containing aluminium ions, the results can be used for other system.

References:

6.1 S. Borjigin, Y. Ashimura, T. Yoshioka, T. Mizoguchi, Determination of fluoride using ion-selective electrodes in the presence of aluminum, *Anal. Sci.*, 25 (2009) 1437-1443.

6.2 S. Dubey, M. Agarwal, A. B. Gupta, Experimental investigation of Al-F species formation and transformation during coagulation for fluoride removal using alum and PACl., *J. Mol. Liq.*, 266 (2018) 349-360.

6.3 S. Vasudevan, B. S. Kannan, J. Lakshmi, S. Mohanraj, G. Sozhan, Effects of alternating and direct current in electrocoagulation process on the removal of fluoride from water, *J Chem. Technol. Biotechnol.,* 86 (2011) 428-436.

6.4 M. Karthikeyan, K. P. Elango, Removal of fluoride from water using aluminium containing compounds, *J. Environ. Sci.,* 21 (2009) 1513-1518.

6.5 W. Kleist, C. Haeßner, O. Storcheva, K. Kohler, A simple aqueous phase synthesis of high surface area aluminum fluoride and its bulk and surface structure, *Inorganica Chim. Acta.,* 359 (2006) 4851-4854.

6.6 A. Khoudro, T. Zarouri, M. Alhasno, Studying the Infrared Spectroscopy and Structural Properties of Compounds Fluoride that Blotched by in, *JMSN.,* 11(1) (2023) 1-14.

6.7 D. Ghosh, C. R. Medhi, M. K. Purkait, Treatment of fluoride containing drinking water by electrocoagulation using monopolar and bipolar electrode connections, *Chemosphere,* 73 (2008) 1393-1400.

6.8 M. M. Emamjomeh, M. Sivakumar, A. S. Varyani, Analysis and the understanding of fluoride removal mechanisms by an electrocoagulation/flotation (ECF) process, *Desalination,* 275 (2011) 102-106.

6.9 S. Aoudj, N. Drouiche, M. Hecini, T. Ouslimane, B. Palaouane, Coagulation as a Post-Treatment Method for the Defluoridation of Photovoltaic Cell Manufacturing Wastewater, *Procedia Eng.*, 33 (2012) 111-120.

6.10 M. Chaudhary, A. Maiti, Defluoridation by highly efficient calcium hydroxide nanorods from synthetic and industrial wastewater, *Colloids Surf. A,* 561 (2019) 79-88.

6.11 M. M. Khunur, A. Risdianto, S. Mutrofin, Y. P. Prananto, Synthesis of Fluorite (CaF_2) Crystal from Gypsum Waste of Phosphoric Acid Factory in Silica Gel, *Bull. Chem. React. Eng. Catal.,* 7 (1) (2012) 71-77.

6.12 M. S. Corbillon, M. A. Olazabal, J. M. Madariaga, Potentiometric Study of Aluminium-Fluoride Complexation Equilibria and Definition of the Thermodynamic Model. *J. Solution Chem.*, 37 (2008) 567-579.

6.13 W. X. Gong, J. H. Qua, R. P. Liu, H. C. Lan, Effect of aluminum fluoride complexation on fluoride removal by coagulation. *Colloids Surf. A: Physicochem. Eng. Asp.* 395 (2012) 88-93.

6.14 S. Ayoob, A. K. Gupta, Venugopal T. Bhat, A Conceptual Overview on Sustainable Technologies for the Defluoridation of Drinking Water, *Crit. Rev. Environ. Sci. Technol.,* 38 (2008) 401-470.

6.15 Q. Zuo, X. Chen, W. Li, G. Chen, Combined electrocoagulation and electroflotation for removal of fluoride from drinking water, *J. Hazard. Mater.,* 159 (2008) 452-457.

6.16 W. Wang, H. Yang, X. Wang, J. Jiang, W. Zhu, Factors effecting aluminum speciation in drinking water by laboratory research. *J. Environ. Sci.,* 22(1) (2010) 47-55.

6.17 H. J. Yang, G. W. Chu, Y. Xiang, J. F. Chen, Characterization of micromixing efficiency in rotating packed beds by chemical methods. *Chem. Eng. J.,* 121 (2006) 147-152.

6.18 L. B. Yao, W. Wu, X. S. Wu, G. W. Chu, Y. Luo, B. C. Sun, Intensification of micromixing efficiency in a spinning disk reactor: Experimental investigation. *Chem. Eng. Process.: Process Intensif.* 166 (2021) 108500.

6.19 J. R. Burns, C. Ramshaw, Process intensification: Visual study of liquid maldistribution in rotating packed beds. *Chem. Eng. Sci.,* 51(8) (1996) 1347-1352.

6.20 T. Chen, M. Zheng, C. Zheng, Z. Yan; Z. Yan, C. Zhou, H. Zheng, CO_2 capture in a novel rotating spiral contactor with hydraulic seal: Hydromechanics, mass transfer and modelling. *Sep. Purif. Technol.* 340 (2024) 126785.

6.21 D. M. Mohunta, G. S. Laddha, Prediction of liquid phase hold-up in random packed beds, *Chem. Eng. Sci.,* 20 (1965) 1069-1072.

6.22 J. M. MacInnes, J. Ortiz-Osorio, P. J. Jordan, G. H. Priestman, R. W. K. Allen, Experimental demonstration of rotating spiral microchannel distillation. *Chem. Eng. J.,* 159 (2010) 159-169.

6.23 H. J. Yang, G. W. Chu, J. W. Zhang, Z. G. Shen, J. F. Chen, Micromixing efficiency in a rotating packed bed: experiments and simulation. *Ind Eng Chem Res.* 44(20) (2005) 7730-7737.

6.24 B. Shimelis, F. Zewge, B. S. Chandravanshi, Removal of excess fluoride from water by aluminum hydroxide. *Bull. Chem. Soc. Ethiop.,* 20(1) (2006) 17-34.

6.25 S. Jain, R. V. Jayaram, Removal of Fluoride from Contaminated Drinking Water using Unmodified and Aluminium Hydroxide Impregnated Blue Lime Stone Waste, *Sep. Sci. Technol.,* 44 (2009) 1436–1451.

6.26 N. Cherkasov, S. J. Adams, E. G. A. Bainbridge, J. A. M. Thornton, Continuous stirred tank reactors in fine chemical synthesis for efficient mixing, solids-handling, and rapid scale-up, *React. Chem. Eng.,* 8 (2023) 266-277.

6.27 A. Zahir, P. Kumar, A. Saptoro, M. Shah, A. N. T. Tiong, S. Hameed, Parametric Study of Experimental and CFD Simulation Based Hydrodynamics and Mass Transfer of Rotating Packed Bed: A Review, *Arch. Comput. Methods Eng.,* 30 (2023) 4001-4031.

Chapter 07

LIQUID-LIQUID EXTRACTION OF PHENOL IN ROTATING CONTACTORS

7.1 Introduction

Continuous removal of phenol from aqueous solutions was carried out by liquid-liquid extraction using Aliquat-336 as the extractant and kerosene serving as the diluent. The mass transfer studies were conducted in three rotating contactors: Rotating packed bed (RPB), Rotating zig-zag contactor (RZC), and rotating spiral contactor (RSC) and in conventional contactors, including fixed bed and stirred tank reactor. The primary objective of this investigation was to study the influence of process parameters on percentage extraction in the rotating mass transfer contactors and determine whether the use of centrifugal force improves the percentage extraction over that of conventional contactors.

7.2 Materials and Method

7.2.1 Materials

The chemical reagents used in this study included phenol crystalline, sourced from Sisco Research Laboratories (SRL), Mumbai, India. Aliquat-336 (Methyl trialkyl ammonium chloride) and 1-decanol, also procured from Merck Germany. Additional reagents included ammonium chloride (NH_4Cl), ammonium hydroxide (NH_4OH), 4-aminoantipyrine ($C_{11}H_{13}N_3O$), and potassium ferricyanide ($K_3Fe(CN)_6$) were acquired from Merck Life Science Pvt. Ltd., Mumbai, India. Double distilled water was used in the experiments.

7.2.2 Experimental Procedure

7.2.2.1 Equilibrium studies

Phenol solution was prepared by dissolving premeasured amount of phenol crystalline in double-distilled water to make an aqueous phase solution with the desired concentration. The solvent phase solution was prepared by mixing the Aliquat-336, and 2 % vol of 1-decanol in kerosene. The latter reagent was added to prevent formation of solid phase of the complex that is formed in organic phase following extraction of phenol. Equilibrium extraction experiments were conducted by contacting 100 mL of phenol solution with 100 mL solvent phase. This mixture was agitated in a temperature-controlled shaker for 24 hours.

7.2.2.2 Experimental Setup

The experimental set for carrying out continuous mass transfer experiments is illustrated in Figure 7.1. These studies involved a series of systematic investigations of the effect of different experimental parameters on liquid-liquid extraction. The phenol solution and the solvent phase were kept in two separate containers. Both phases were pumped into the rotating contactor simultaneously. The aqueous and solvent phases were mixed just prior to entering the contactor and dispersed within the rotor by a liquid distributor. The effluent stream splashed onto the rotor's casing wall from the outer edge of the rotor and exited the apparatus through an opening at its base.

Samples from the exiting stream were collected from the outlet of the casing. The extracting and raffinate phases were separated using a separating funnel. The aqueous raffinate phase underwent further centrifugation to remove any fine suspended solvent phase droplets and the phenol concentration was ascertained. Samples were collected 10 min after the start of experiment in rotating contactors after which there was no further variation in phenol concentration. Experimental studies with rotating spiral, rotating zig-zag, rotating packed bed were carried out by replacing the rotating packed bed contactor in the setup shown in Figure 7.1 with any of these mass transfer contactors.

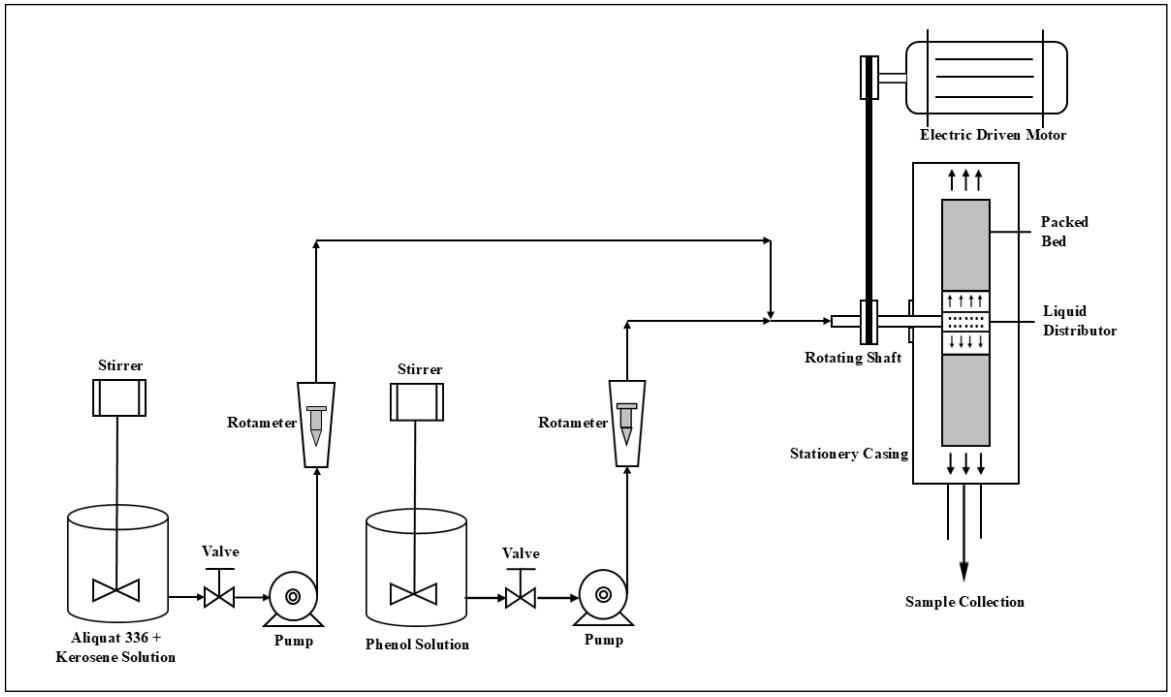

Figure 7.1: Schematic diagram of the experimental setup for phenol extraction in a rotating reactor

7.2.3 Determination of Phenol concentration

The concentration of phenol was determined using a Thermo-Scientific ultraviolet/visible light spectrophotometer (UV spectrophotometer). This method relies on the spectrophotometric analysis of a magenta chromogen with a peak wavelength of approximately 510 nm. The phenol was quantified using the 4-amino antipyrine (4AAP) method at 510 nm [7.1].

To prepare the buffer solution, 16.9 g of ammonium chloride (NH_4CL) was dissolved in 143 mL of concentrated ammonium hydroxide (NH_4OH) and diluted to 250 mL with distilled water. This buffer was used to adjust the pH of a 100 mL phenol aliquot solution to ~10.0. Amino antipyrine solution was prepared by dissolving 2.0 g of 4-amino antipyrine in distilled water and diluting it to 100 mL. Potassium ferricyanide solution was arranged by dissolving 8.0 g of potassium ferricyanide ($K_3Fe(CN)_6$) in distilled water and diluting it to 100 mL.

The phenol aliquot was diluted to 100 mL, and 2 mL of the buffer solution was added to adjust the sample pH to 10 ± 0.2. Following this, 2.0 mL of amino antipyrine solution and 2.0 mL of potassium

ferricyanide solution were added and mixed thoroughly. After 15 minutes, the absorbance was recorded at 510 nm.

7.2.4 Mathematical modeling

The solute mass balance over a differential volume, $dV(= 2\pi rdrh)$ at a steady state assuming the plug flow of the phases is given by,

$$Q_a dC_a = -K_{oc}a\{(C_a - C_a^*)\}dV \tag{7.1}$$

Where Q_a is aqueous phase flow rate, C_a is the aqueous phase concentration of phenol at a radial distance *r* from the centre of the rotor, $K_{oc}a$ is the overall volumetric mass transfer coefficient, C_a^* is the aqueous phase concentration of phenol in equilibrium with solvent phase concentration, C_o, and h is the axial distance between rotating disks.

The above equation was transformed into the following.

$$Q_a dC_a = -K_{oc}a\left\{\left(C_a - \frac{C_O}{D}\right)\right\}2\pi rdrh \tag{7.2}$$

The parameter *D* is the distribution ratio defined as $\frac{C_O}{C_a}$ at equilibrium.

The mass balance of phenol between the inner periphery of rotating equipment r_i and at a radial distance r within the rotor is given by,

$$Q_a C_a^i = Q_a C_a + Q_o C_o \tag{7.3}$$

$$C_o = \frac{Q_a}{Q_o}\left[C_a^i - C_a\right] \tag{7.4}$$

Where C_a^i is the inlet concentration of phenol in the aqueous phase and Q_O is the flow rate of the solvent phase. Eq. (7.5) relating the variation of phenol concentration in the aqueous phase with radial position in the rotor was obtained by replacing Eq (7.4) in Eq (7.2)

$$Q_a \frac{dC_a}{dr} = -K_{oc}a\left\{\left(1 + \frac{1}{C_D}\frac{Q_a}{Q_o}\right)C_a - \frac{Q_a C_a^i}{C_D Q_o}\right\}2\pi rh \tag{7.5}$$

The volumetric mass transfer coefficient was obtained from eq. (7.5) for a given experimental run by ensuring that the experimental determined concentration of phenol in the exiting stream matches with that calculated from the above equation.

7.3 Result and Discussion

7.3.1 Equilibrium Study

Equilibrium studies were performed by varying the phenol concentration from 50 mg/L to 400 mg/L and the Aliquat-336 extractant concentration dissolved in kerosene from 0.25 % (v/v) to 1.50 % (v/v) in a 250 ml conical flask under agitation in a temperature-controlled shaker for 24 hrs. The percentage extraction (% *E*) of phenol is expressed as the following equation:

$$\% E = \frac{[Phenol]_{aq,initial} - [Phenol]_{aq,final}}{[Phenol]_{aq,initial}} x\ 100 \qquad (7.6)$$

The percentage extraction obtained with kerosene only was around 20% at a feed concentration of 200 mg/L. The value drastically increased to over 60% on adding 0.25 % (v/v) extractant to kerosene.

Phenol ($ArOH$)is a weak acid. It dissociates according to the following reaction:

$$ArOH \leftrightarrow H^+ + ArO^- \qquad (7.7)$$

The dissociation constant, K_d of phenol expressed as

$$K_d = \frac{[H^+][ArO^-]}{[ArOH]} \qquad (7.8)$$

is 1.3×10^{-10} at 25°C. The fraction of phenol existing in dissociated form in the aqueous solution was obtained by solving the following equations.

Mole balance $$[T_{ArOH}] = [ArOH] + [ArO^-] \qquad (7.9)$$

Electroneutrality: $$[H^+] = [OH^-] + [ArO^-] \qquad (7.10)$$

Where $[T_{ArOH}]$, $[ArOH]$, $[ArO^-]$,$[H^+]$ and $[OH^-]$ are the molar concentration of total phenol in both dissociated and undissociated form, undissociated phenol, phenolate ion, hydronium, and hydroxyl ion respectively.

At a phenol concentration of 25 mg/L, the dissociation of phenol is around 6.5%, which reduces to 2.5% when the phenol concentration increases to 200 mg/L. When kerosene is the solvent, only the undissociated phenol is soluble in kerosene as it is a solvent. The drastic improvement in percentage extraction on the addition of Aliquat-336 to kerosene cannot be explained only by the ion exchange mechanism of phenolate ion (ArO^-) with Cl^- ion of Aliquat-336 at the aqueous-solvent interface as given below

$$AQCl(org) + X^-(aq) \leftrightarrow AQX(org) + Cl^-(aq) \qquad (7.11)$$

due to the low concentration of the phenolate ions in the aqueous solution. Likely, the following complexation reaction of phenol with Aliquat-336 ($AQCl$) contributes significantly to the extraction of phenol into the solvent phase.

$$AQCl(org) + ArOH(aq) \leftrightarrow AQCl - ArOH(org) \qquad (7.12)$$

The above equation has also been used to explain the extraction of phenol by TPB [7.2]. Thus, extraction of phenol into the solvent phase is not only due to its solubility in kerosene but also due to the reactions given by Equations 7.10 and 7.11.

Figure 7.2 shows the percentage extraction of phenol at different feed concentrations and Aliquat-336 concentration in the solvent phase. The corresponding plot of the equilibrium loading of the solvent phase versus residual concentration of phenol in aqueous solution is shown in Figure 7.3.

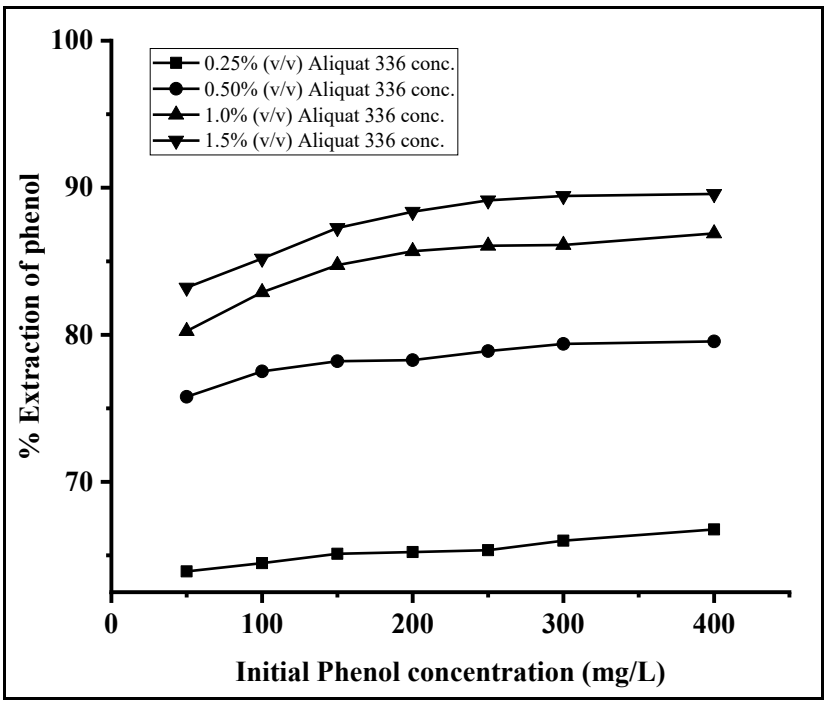

Figure 7.2: Percentage extraction of phenol with variation of feed concentration

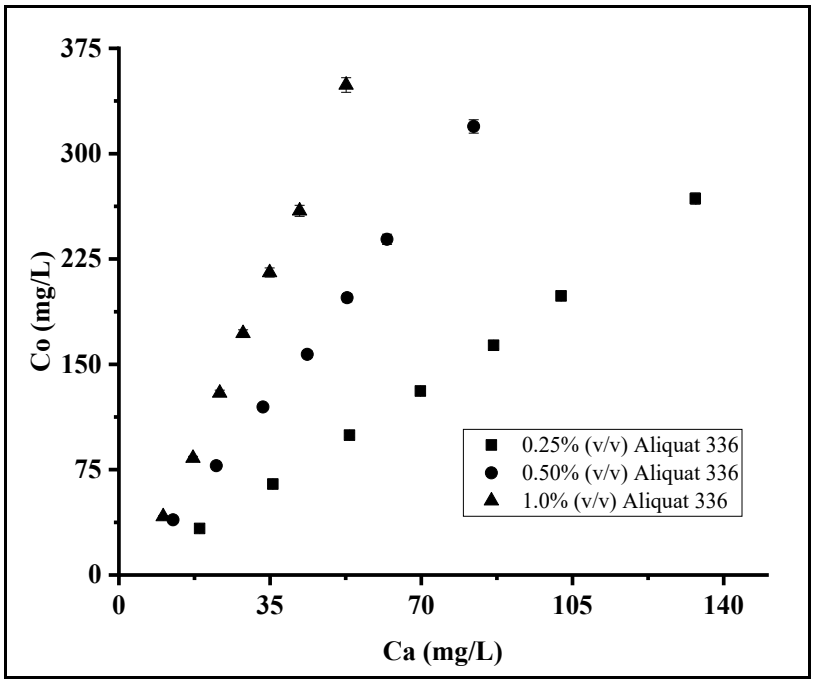

Figure 7.3: Equilibrium distribution of phenol between aqueous and solvent phase

The distribution ratio is given by the following formulae $D = \frac{C_O}{C_a}$. The distribution ratio was related to the aqueous phase concentration of phenol by the following equation,

$$D = aC_a \quad (7.13)$$

The value of R^2 for different Aliquat-336 concentrations is given in Table 7.1 below.

Table 7.1. Equilibrium R^2 and distribution ratio at different Aliquat-336 concentration

Aliquat-336 Concentration % (v/v)	Distribution Ratio (D)	R^2
0.25%	1.9	0.9983
0.50%	3.7	0.9987
1.0%	6.0	0.9984
1.5%	7.0	0.9957

7.3.2 Continuous Experimental Study in Rotating contactors

The experimental results of continuous liquid-liquid extraction studies have been presented in terms of percentage extraction and the overall volumetric mass transfer coefficient $(K_{oc}a)$ based on the aqueous phase.

7.3.2.1 Effect of Rotational Speed

The influence of rotational speed (ω) on percentage extraction in continuous removal of phenol, in the three rotating contactors and overall volumetric mass transfer coefficient are depicted in Figure 7.4 and Figure 7.5 respectively. For this study, the parameters kept constant were feed concentration (=100 mg/L), Aliquat-336 concentration (= 0.50 % v/v), aqueous and solvent phase flow rate (= 0.5 L/min each). The variation change in the magnitude of % *E* with change in the rotational speed is shown in Figure 7.4. The percentage extraction increased from 69.77% to 78.77% in the rotating spiral contactor, from 64.47% to 74.44% in the rotating zig-zag contactor, and from 62.45% to 72.36% in the rotating packed bed on increasing the ω from 300 rpm to 1100 rpm.

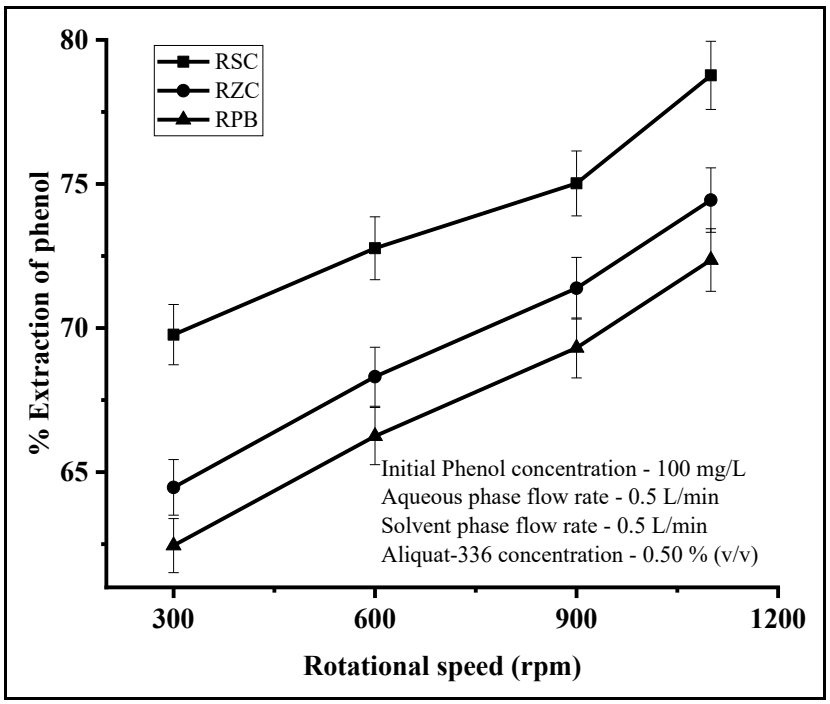

Figure 7.4: Effect of rotational speed on % extraction in rotating contactors

Figure 7.4 shows the volumetric mass transfer coefficient calculated from the experimental data. The magnitude of $K_{oc}a$ at 1100 rpm for the three contactors was determined to be 0.096 s^{-1} for RSC, 0.049 s^{-1} for RZC, and 0.043 s^{-1} for RPB.

In a rotating packed bed, the two-phase mixture navigates through the interstitial spaces while adhering to the surfaces of glass beads [7.3]. The empirical relation developed by Burns et al. [7.3] to calculate the film thickness in RPB suggest the thickness would decrease on increasing rotational speed. This reduces the diffusional resistance in the liquid film. The increasing intensity of impact with the packing at high rotational speed promote mixing of the solute in the two phases that again helps to increase mass transfer rate by reducing the concentration gradient and possible increase of interfacial area. These phenomena contribute to increase of volumetric mass transfer coefficient in this contactor.

In rotating zigzag contactor, the two-phase mixture exiting the distributor initially flows as films or rivulets over the nearest baffle. It then flows over the edge of the baffle into the space between the successive baffles in the form of ligaments or droplets. Increase of the rotational speed increases the

impact velocity on the wall of the baffle further downstream leading to the increase of splash area and/or generation of secondary droplets, which further flows as rivulets/film across the baffle surface and reaches the edge of the baffle. The same phenomenon is repeated on successive baffles downstream. Increase of wetted area on the succeeding baffle wall reduces film thickness besides creating more interfacial area. The combination of thinner liquid films/filaments, higher interfacial area and intensified mixing of the phases contributes to improved mass transfer rates and higher values of $K_{oc}a$ at higher rotational speeds.

In the rotating spiral contactor, the two phases flows as two coherent liquid films along the baffle surface [7.4]. Sinkunas et al. [7.5] derived a correlation demonstrating that the film thickness on vertical surfaces depends on the Reynolds number and decreases with increasing centrifugal acceleration. The enhanced values of $K_{oc}a$ at higher rotational speeds in RSC can be related to lower diffusional resistance in the phases due to formation of thinner film at the interface.

The difference in percentage extraction and $K_{oc}a$ in the rotating contactors at the same experimental conditions is due to structural variations of the rotating contactors that affect the fluid flow pattern and the interfacial area [7.6]. The magnitude of $K_{oc}a$ is least in rotating packed bed and highest in rotating spiral contactor. The tangential dispersion of the liquid in the former equipment is restricted due to the reduced void space in the glass packing material [7.7]. This limitation leads to liquid mal-distribution which in turn prevents effective utilization of the available surface area that would have helped to reduce film thickness. Furthermore, the flow path is the least in RPB (~0.06 m) and highest in RSC (~1.9 m). So, the holdup of the solvent phase is likely to be the higher in RSC that contribute to more interfacial area for mass transfer between the phases [7.6,7.8,7.9].

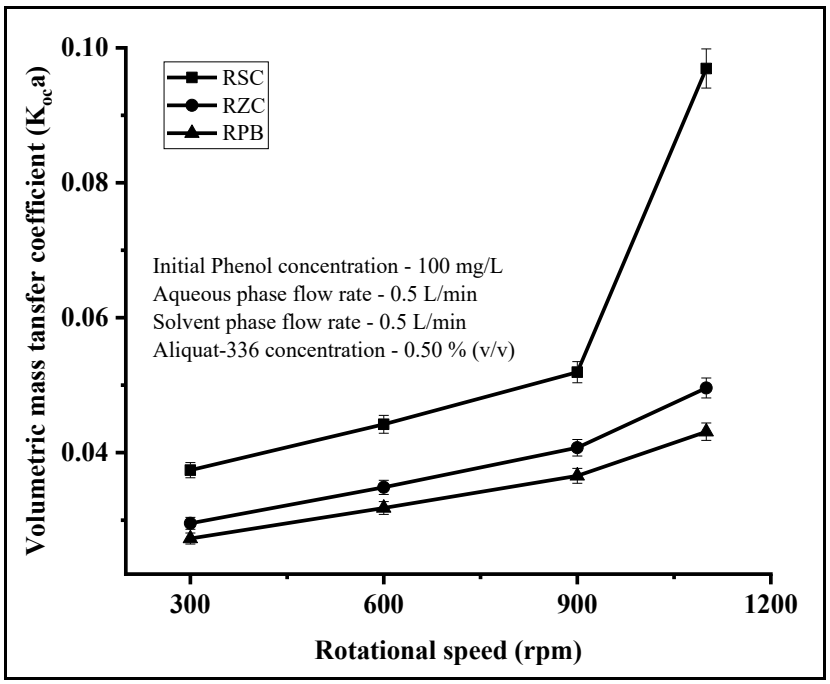

Figure 7.5: Variation of $K_{oc}a$ with rotational speed in rotating contactors

7.3.2.2 Effect of Aqueous Phase Flow Rate

Continuous experiments were performed by varying the aqueous phase flow rate from 0.5 L/min to 1.5 L/min while keeping the other variables constant (ω =1100 rpm, solvent phase flow rate = 0.5 L/min, initial phenol concentration = 100 mg/L, and Aliquat-336 concentration = 0.50% v/v).

It is seen in Figure 7.6 that increasing the aqueous phase flow rate from 0.5 L/min to 1.5 L/min resulted in a decrease in percentage extraction from 78.77% to 54.25% in the rotating spiral contactor, from 74.44% to 48.74% in the rotating zig-zag contactor, and from 72.36% to 46.46% in the rotating packed bed. Higher percentage extraction was observed in the rotating spiral contactor in comparison with the rotating zig-zag contactor and rotating packed bed. The volumetric mass transfer coefficient increased from 0.096 s^{-1} to 0.13 s^{-1} in RSC, 0.049 s^{-1} to 0.088 s^{-1} in RZC, and 0.043 s^{-1} to 0.066 s^{-1} in RPB due to increase in aqueous flow rate over the range (Figure 7.7).

The amount of phenol removed from the aqueous phase per unit time, C can be estimated from the following equation.

$$\mathrm{C} = Q_a\left(C_a^i - C_a^o\right) \tag{7.14}$$

Where C_a^o is the concentration of phenol in the aqueous phase exiting the contactor. Calculation shows that C increases with aqueous flow rate for all the contactors. For example, in RSC the value increases steadily from 40.4 mg/min to 83.5 mg/min as the flow rate is increased from 0.5 L/min to 1.5 L/min. One of the factors contributing to higher removal rate is the increased mass transfer driving force as higher flow rate brings in more phenol into the contactor thus enabling higher concentration of phenol to be maintained in the aqueous phase.

Yan et al. [7.10] noted that there is improved circumferential spreading of liquid with an increase in flow rate as a greater number of openings in the liquid distributor become operational. The two phase mixture spreads more uniformly in the rotating contactors that not only partly negates the expected increase in thickness of the liquid films/rivulets but also increasing the interfacial area as the organic phase also becomes more uniformly distributed. On the other hand, decrease of residence time with an increase in flow rate has reported in the experimental studies in RPB by Guo et al. [7.9]. This would reduce the holdup of the phases and hence interfacial area. The two opposing phenomena contribute to the observed trend of the volumetric mass transfer coefficient. The increase in $K_{oc}a$ is clearly not sufficient to remove the higher amount of phenol entering the contactor resulting in decrease in percentage extraction.

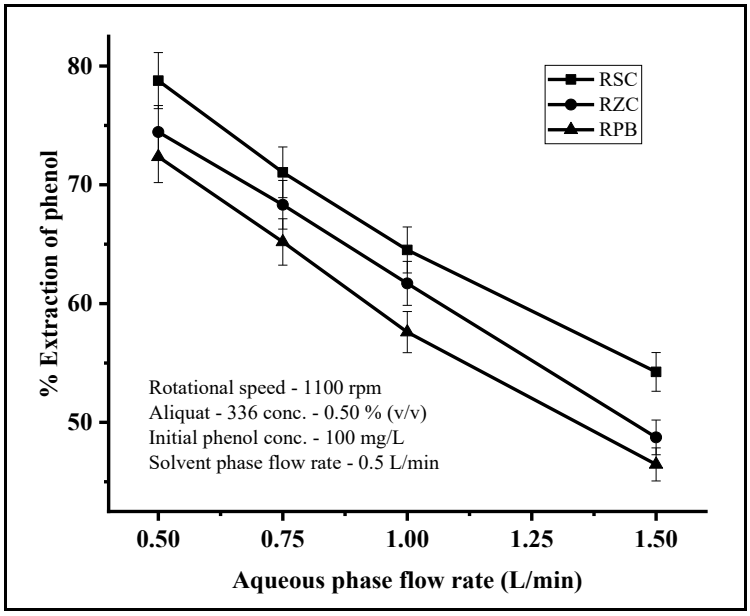

Figure 7.6: Influence of aqueous phase flow rate on % extraction in rotating contactors

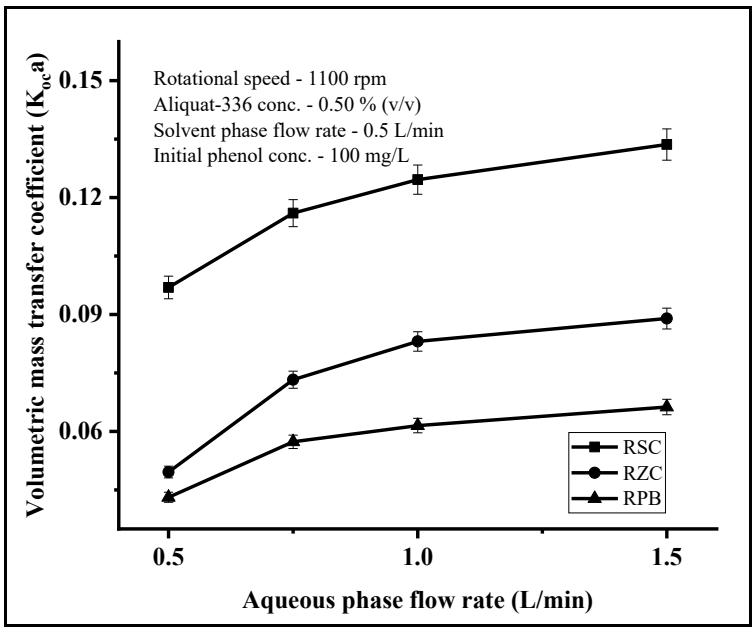

Figure 7.7: Variation of $K_{oc}a$ with aqueous phase flow rate in rotating contactors

7.3.2.3 Effect of Solvent Phase Flow Rate

The effect of solvent phase flow rate on percentage extraction was investigated by varying the solvent phase flow rate from 0.5 L/min to 1.25 L/min while keeping other variables constant. For this investigation, the aqueous phase flow rate was maintained at 1.0 L/min, rotational speed at 1100 rpm, Aliquat-336 concentration at 0.50 %(v/v), and feed concentration at 100 mg/L. Experimental results shown in Figure 7.8 indicate that increasing the solvent phase flow rate from 0.5 L/min to 1.25 L/min resulted in increase in percentage extraction in all the high-gravity contactors. Specifically, % *E* increased from 64.25% to 82.14% in the rotating spiral contactor, from 61.70% to 78.45% in the rotating zig-zag contactor, and from 59.40% to 76.92% in the rotating packed bed. The volumetric mass transfer coefficient for the rotating contactor (Figure 7.9) too increased with the solvent phase flow rate. With an increase in solvent flow rate from 0.5 mL/min to 1.25 L/min, the parameter increased from 0.11 s^{-1} to 0.19 s^{-1} in RSC, from 0.083 s^{-1} to 0.10 s^{-1} in RZC, and for RPB it increased from 0.069 s^{-1} to 0.098 s^{-1}.

The holdup of the solvent phase and interfacial area for mass transfer increases at higher solvent phase flow rate. The higher solvent phase holdup helps to reduce the concentration of extracted

phenol in the solvent phase and increase driving force for mass transfer. Furthermore, more effective liquid distribution over the contactor inner periphery at higher solvent flow rate promotes creation of more interfacial area and better mixing. All of these contribute to the increase of percentage extraction and $(K_{oc}a)$.

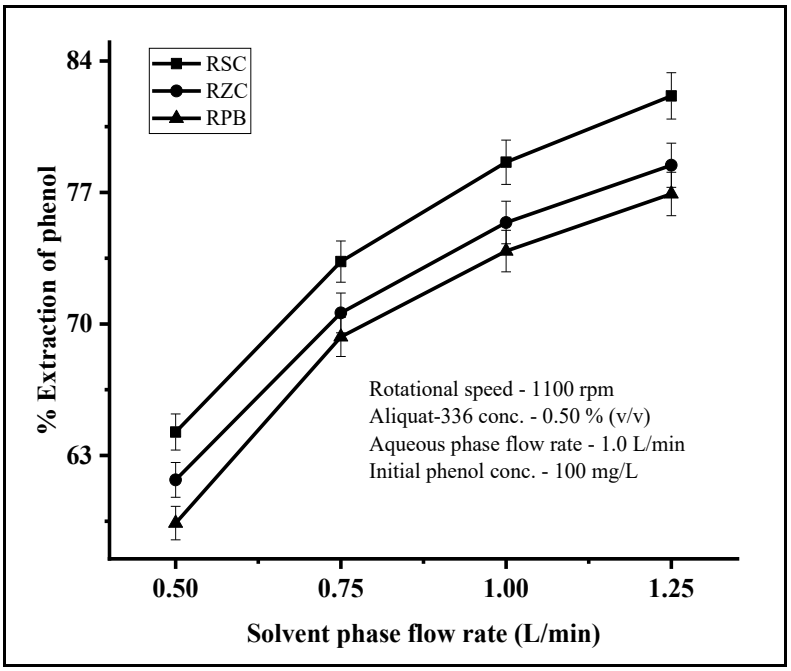

Figure 7.8: Influence of solvent phase flow rate on % extraction in rotating contactors

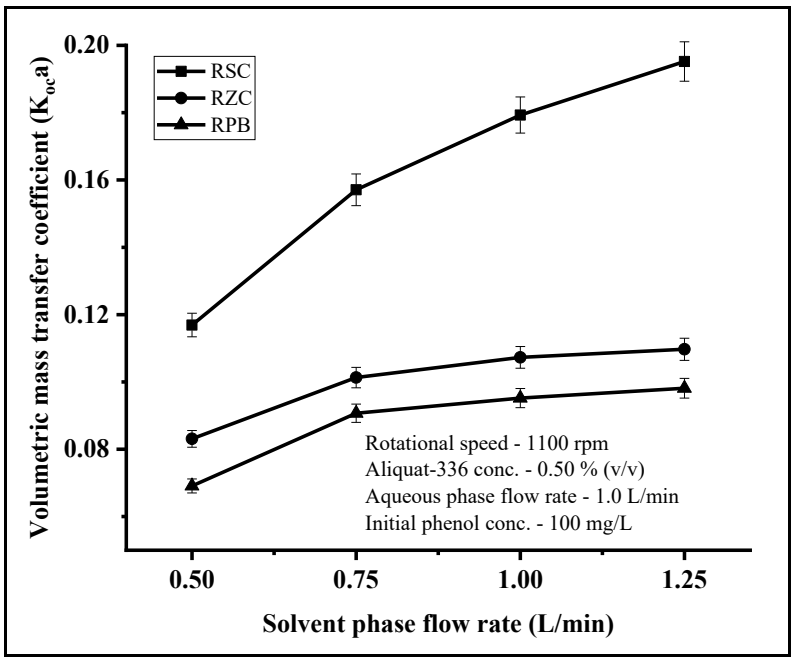

Figure 7.9: Variation of $K_{oc}a$ with solvent phase flow rate in rotating contactors

7.3.2.4 Effect of Aliquat-336 Concentration

The experimental results on variation of Aliquat-336 concentration in kerosene were carried at constant rotational speed (1100 rpm), initial phenol concentration (100 mg/L), and aqueous and solvent phase flow rate (0.5 L/min). The results are plotted in Figure 7.10. The percentage extraction of phenol increased with the concentration of Aliquat-336 from 65.05% (0.25 % v/v) to 89.11% (1.50 % v/v) in rotating spiral contactor, while in rotating zig-zag contactor and rotating packed bed, it increased from 62.12% to 84.56% and 59.41% to 80.73% respectively.

The value of the distribution ratio is 1.86 at Aliquat 336 concentration 0.25 %(v/v) increased to 8.18 at Aliquat 336 concentration 1.50 % (v/v). Increase in solubility permits more extraction into the organic phase besides lowering the mass transfer resistance in the solvent phase and higher extraction follows.

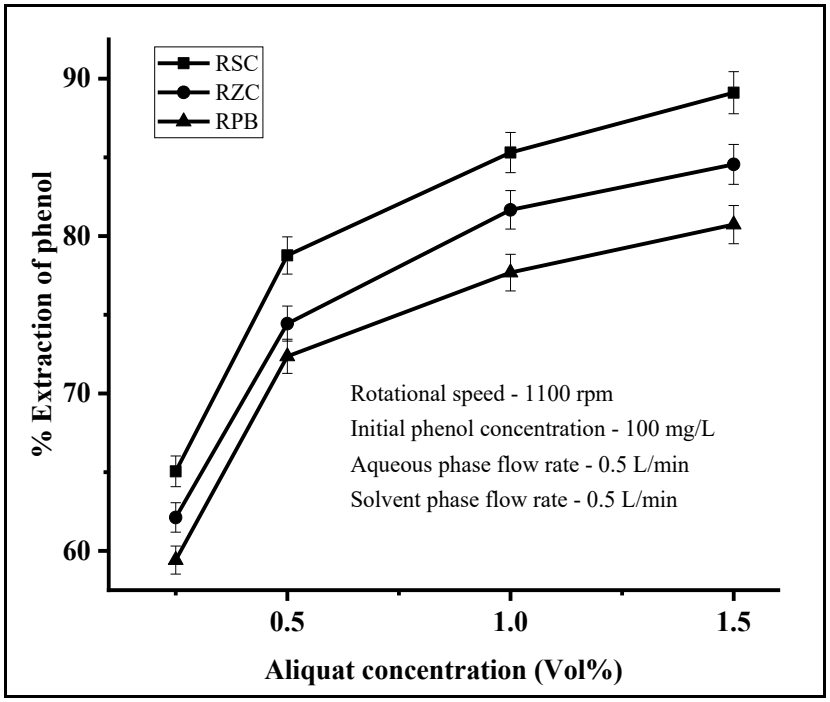

Figure 7.10: Influence of Aliquat-336 concentration on % extraction in rotating contactors

7.3.2.5 Comparison of rotating contactors with fixed bed and continuous stirred tank

The continuous mass transfer of phenol extraction was carried out in the fixed bed with the mixture of solvent phase and aqueous phase flowing up in a fixed bed column of 5.0 cm in diameter and height of 30.0 cm filled with the glass beads having an average diameter of ~ 4mm. Experiments were also carried out in a continuous stirred tank reactor under the same operating conditions (agitator speed = 1100 rpm). The volume of the packing in the fixed bed and the liquid holdup in the stirred tank reactor were maintained equal to the rotor volume of high gravity contactors. The percentage of extraction of phenol at different Aliquat-336 concentration in the extractors studies is illustrated in Figure 7.11. With increase of Aliquat-336 concentration from 0.25 % (v/v) to 1.50 % (v/v), the percentage extraction of phenol increases from 65.05% to 89.11% in the rotating spiral contactor, from 62.12% to 84.56% in the rotating zig-zag contactor, from 59.41% to 80.73% in the rotating packed bed, from 56.73% to 77.44% in the fixed bed, and from 54.32% to 74.31% in the continuous stirred tank.

The percentage extraction of phenol in the high gravity contactor and conventional reactor with solvent phase flow rate is depicted in the Figure 7.12. On increasing the solvent phase flow rate from 0.5 L/min to 1.25 L/min, the percentage extraction of phenol increases from 64.25% to 82.14% in the rotating spiral contactor, 61.70% to 78.45% in the rotating zig-zag contactor, 59.40% to 76.92% in the rotating packed bed, 56.28% to 70.43% in the fixed bed, and 51.06% to 65.75% in the continuous stirred tank.

The packing surface area of the fixed bed was ~ 210 $cm^2.cm^3$ nearly the same as in rotating spiral contactor. Thinner aqueous and organic liquid film would be developed in RSC even without accounting for liquid maldistribution in packed bed as it be amplified by the fact that the flow in the former is subjected to centrifugal acceleration nearly twenty-five times that of gravity than in the fixed bed column. These factors are responsible for higher percentage extraction in rotating spiral contactor.

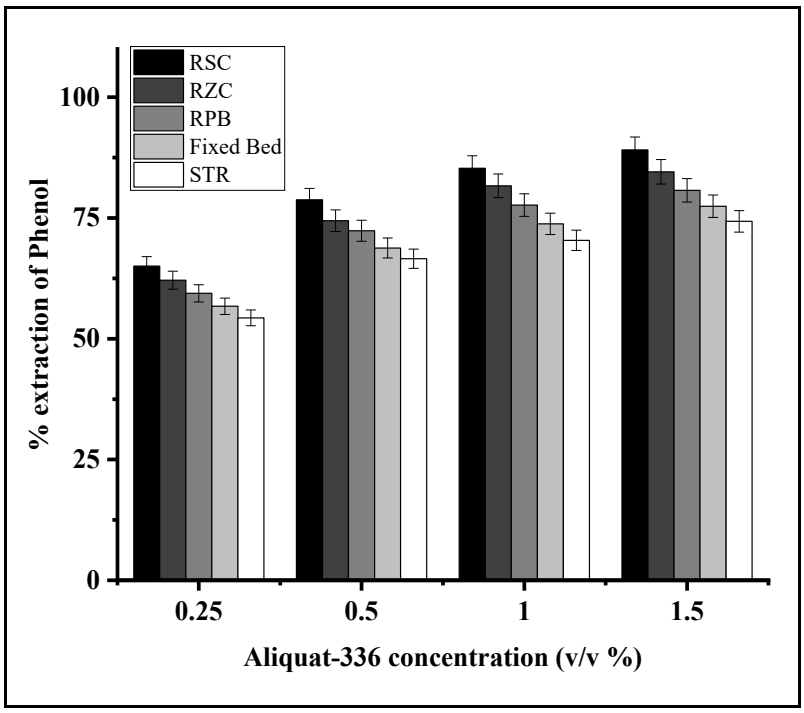

Figure 7.11: Comparison of performance of rotating contactors, fixed bed, and STR with variation in Aliquat-336 concentration

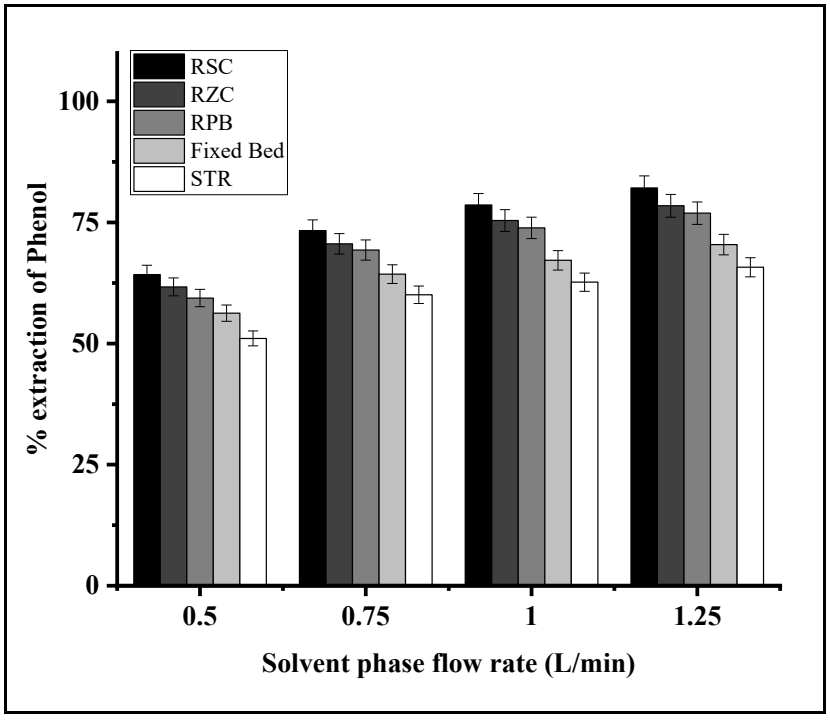

Figure 7.12: Comparison of performance of rotating contactors, fixed bed, and STR with variation in solvent phase flow rate

7.4 Conclusion

This experimental investigation compared the mass transfer performance efficiency of three high-gravity rotating contactors which are designed for the liquid-liquid extraction of phenol under centrifugal acceleration. The mass transfer performance of the rotating spiral contactor was found to be superior to that of the rotating zig-zag contactor and rotating packed bed. The results indicated that traditional contactors used in industrial applications can be replaced with rotating contactors to achieve better efficiency in wastewater treatment and other related fields. Data available on overall volumetric mass transfer coefficients for liquid-liquid extraction in rotating contactors is limited. Thus, this research would help in accurately designing rotors for liquid-liquid extraction.

Nomenclature

Q_a	Aqueous phase flow rate (L/min)
Q_O	Solvent phase flow rate (L/min)
C_a	Aqueous phase concentration of phenol (mg/L)
C_o	Organic phase concentration of solvent
$K_{oc}a$	Overall volumetric mass transfer coefficient (1/s)
C_a^*	Aqueous phase concentration of phenol in equilibrium
r	Radial distance of the rotor
h	Axial distance between rotating disks
D	Distribution ratio
C_a^i	Inlet concentration of phenol in aqueous phase
C_O^i	Inlet concentration of phenol in solvent phase

C	Amount of phenol removed from the aqueous phase per unit time
C_a^o	Concentration of phenol in the aqueous phase exiting the contactor

Greek Symbol

ω	Rotational speed

References:

7.1 Standard Methods for the Examination of Water and Wastewater, 14th Edition (1975), Method 510 through 510C, 574-581.

7.2 C. Zidi, R. Tayeb, M. B. Sik Ali, M. Dhahbi, Liquid–liquid extraction and transport across supported liquid membrane of phenol using tributyl phosphate, *J. Membr. Sci.,* 360 (2010) 334–340.

7.3 J. R. Burns, C. Ramshaw, Process intensification: Visual study of liquid maldistribution in rotating packed beds, *Chem. Eng. Sci.,* 51 (8) (1996) 1347-1352.

7.4 J. M. MacInnes, J. Ortiz-Osorio1, P. J. Jordan, G. H. Priestman, R. W. K. Allen, Experimental demonstration of rotating spiral microchannel distillation, *Chem. Eng. J.,* 159 (2010) 159–169.

7.5 S. Sinkunas, J. Gylys, A. Kiela, Analysis of laminar liquid film flowing down a vertical surface, Fourth International Conference on CFD in the Oil and Gas, Metallurgical & Process Industries. 2005.

7.6 H. J. Yang, G. W. Chu, Y. Xiang, J.F. Chen, Characterization of micromixing efficiency in rotating packed beds by chemical methods, *Chem. Eng. J.,* 121 (2006) 147-152.

7.7 Y. S. Chen, F. Y. Lin, C. C. Lin, C. Y. D. Tai, H. S. Liu, Packing Characteristics for Mass Transfer in a Rotating Packed Bed, *Ind. Eng. Chem. Res.,* 45(20) (2006) 6846-6853.

7.8 K. Yang, G. Chu, H. Chou, B. Sun, L. Shau, J.F. Chen, Determination of the effective interfacial area in rotating packed bed, *Chem. Eng. J.,* 168 (2011) 1377-1382.

7.9 K. Guo, F. Guo, Y. Feng, J. Chen, C. Zheng, N.C. Gardner, Synchronous visual and RTD study on liquid flow in rotating packed-bed contactor, *Chem. Eng. Sci.,* 55 (2000) 1699-1706.

7.10 Z. Yan, C. Lin, Q. Ruan, Dynamics of droplets and mass transfer in a rotating packed bed, *AIChE J.,* 60 (2014) 2705-2723.

Chapter 08

OVERALL CONCLUSION AND FUTURE SCOPE

8.1 Overall Conclusion

Fluoride contamination in drinking water is a global issue. Over-exposure to fluoride causes several health problems such as fluorosis, neurological, thyroid, osteoporosis, etc. The guideline prescribed by World Health Organization show that the concentration of fluoride in the drinking water need to be below 1.5 mg/L. Several defluoridation management techniques were suggested to address excess fluoride in drinking water. Defluoridation techniques like the Nalgonda technique and adsorption have been found to be promising to limit the fluoride concentration within the prescribed values. Phenol is also one of typically refractory pollutant in wastewater and threatens to the human's health. The removal of phenol can be efficiently carried out by liquid-liquid extraction.

Objective of this study was to employ the principles of process intensification to determine the feasibility of enhancing removal of two harmful pollutants - fluoride and phenol from wastewater using adsorption, precipitation and coagulation for the former, and liquid-liquid extraction for the latter pollutant by carrying out the waste water treatment processes in high gravity contactors.

In adsorption, commercially available powdered activated charcoal was used as an adsorbent for removal of fluoride by dispersing the adsorbent directly into the synthetic solution. The following conclusions can be made based on the results of equilibrium and contunous studies

- Maximum removal of fluoride was observed at feed solution pH of 2.
- High rotational speed and adsorbent dosage increases the percentage removal by this process.
- Higher percentage removal was attained in rotating contactors in comparison to traditional contactors. It was observed among the rotating contactors studied the maximum adsorption efficiency was achieved in rotating spiral contactor at the same operating conditions.

- High adsorbent dosage and low fluoride concentration in feed ensures high percentage removal of fluoride and maximum utilization of the adsorbent.

Removal of fluoride by precipitation and coagulation using alum and lime was studied in batch and continuous process. The main conclusions of the experimental investigation were

- Higher percentage removal was attained in continuous removal of fluoride in rotating reactors in comparison to traditional reactors. Rotating Spiral reactor gave the maximum removal among the contactors studied.
- The optimum conditions in the high gravity rotating contactors were pH 7, feed concentration below 25 mg/L, rotational speed of 1000 rpm and flow rate of 1 L/min.
- At the optimum condition, the removal obtained in Rotating Spiral reactor was nearly the same as that obtained in batch equilibrium studies.
- Deviation from the optimum condition resulted in significant lower removal than the value determined from batch equilibrium results.

Liquid-liquid extraction studies were performed for removal of phenol using aliquat-336 as the extractant dissolved in organic phase kerosene with decanol as phase modifier. The experimental observation suggested that

- The percentage extraction of phenol in rotating contactors increased at higher with rotational speed. The percentage extraction of phenol for the same operating condition was higher in the high gravity contactors than the traditional reactors.
- The overall volumetric mass transfer coefficient increased with rotational speed, aqueous phase flow rate, organic flow rate and extractant concentration.

Overall, the experimental study suggested that the traditional contactors like fixed bed and CSTR used industrially can be replaced by rotating contactors. The rotating spiral contactor is best suited among the rotating contactors (Rotating packed bed, rotating zigzag contactor, rotating spiral contactor) for all the process studied. For all the three removal techniques processes studied in

rotating contactors, amount of pollutant removed increased with rotational speed, feed flow rate and feed concentration. In slurry adsorption, higher adsorbent concentration results in better utilization of adsorbent. The overall volumetric mass transfer coefficient increased with rotational speed and flow rate for both slurry adsorption and liquid-liquid extraction.

8.2 Future Work

The success of rotating contactors for drastically reducing the concentration of pollutants in the effluent stream left a huge scope for further work. Few of these are mentioned below.

- Rotating packed bed has been widely studied. Studies in rotating zigzag contactor has mainly focused on performance for gas-liquid mass transfer operations and modelling of gas phase pressure drop. But for chemical reactions micro mixing plays a significant role. Several micro mixing studies are available in the literature for rotating packed bed but there is no such data for rotating spiral contactor and modified rotating zig zag contactor which gave better performance than rotating packed bed for all the processes studied here. So, there is a need to determine micro mixing characteristics and residence time in these two contactors. Similarly, there is also a need to evaluate solid-liquid mass transfer coefficient in these two rotating contactors.
- Slurry adsorption and liquid-liquid extraction were carried out in concurrent mode of operation. But counter current process gives higher mass transfer driving force and should be able to reduce the concentration further even when the concurrent and counter current contactors have the same volume. Therefore, the feasibility of designing novel counter current contactors need to be explored.
- It was noted that the removal of fluoride obtained in precipitation and coagulation in rotating spiral contactor which gave the maximum removal compared to other rotating contactors was far removed from that obtained in equilibrium batch studies when the operating

condition of pH and fluoride concentration was not at their optimum values. It is not possible to always operate at optimum conditions in practical situations due to several constraints in cost etc. So, the mechanism of removal needs to be determined in a more definite manner.

- In this study, the main focus was the use of high gravity contactors for intensifying removal rate compared to conventional contactors and reactors for adsorption, precipitation and coagulation, and liquid-liquid extraction. So, the experiments were carried out using synthetic solution of the pollutants as it was a feasibility study. But industrial effluents contain several other chemicals which could influence the removal efficiency through influencing equilibrium, mass transfer and reaction rate. So, there is need to evaluate the performance of this equipment with waste water from specific industries.

LIST OF FIGURES

LIST OF TABLES